Doctoral Dissertation

Development of Highly Functional $SrTiO_3$ Photocatalyst for Overall H_2O Splitting

(H_2O 分解反応のための高機能性 $SrTiO_3$ 光触媒の開発)

JIANG JUNZHE

姜 君哲

Graduate School of Sciences and Technology for Innovation

Yamaguchi University, Japan

山口大学大学院創成科学研究科物質工学系専攻

2021 年 3 月

Abstract

The energy crisis and environmental pollution are primary problems with the development of human society and civilization. Photocatalytic technology as a low-cost, efficient, and environment-friendly path is considered to be one of the best solutions to the severe energy crisis and environmental pollution problems. So far, various photocatalytic materials with activity in the water-splitting reaction have been developed. Strontium Titanate ($SrTiO_3$) as one of the typical photocatalysts has been investigated for more than thirty years. However, the efficiency of this photocatalyst for the H_2O splitting reaction is low, and a significant improvement in the efficiency is required.

In this thesis, to significantly improve the efficiency of the $SrTiO_3$ photocatalyst for overall H_2O splitting, the bulk, surface, and morphology of the $SrTiO_3$ photocatalyst were controlled, and their effects on the activity and photoconversion efficiency (AQY) of the photocatalyst were investigated. From the obtained research results, the factors for improving the efficiency of the photocatalyst for the H_2O decomposition reaction were discussed.

The major aspects of the investigations in the thesis are presented as follows:

Chapter 1: General introduction.

This chapter presents the general research background of this paper, the development and progress of photocatalysts, especially the historical background of photo energy conversion and research on H_2O decomposition reactions, and methods for improving photocatalytic efficiency.

The outline, the structure of this paper, and the purpose of the research are described.

Chapter 2: Investigation on the highly active $SrTiO_3$ photocatalyst toward overall H_2O splitting by doping Na ion

To prepare Na ion-doped $SrTiO_3$ (Na^+-$SrTiO_3$) with high photocatalytic activity for overall H_2O splitting, the polymerizable complex (PC), and solid-state reaction (SSR) methods were applied to elucidate the factors on the improvement of the activity by doping Na ions and mechanisms. Here, $Rh_{0.7}Cr_{1.3}O_3$ was used as the co-catalyst. The photocatalytic activity of the photocatalyst prepared using the high-purity raw material

was significantly improved, and it was noticed that the purity of the photocatalyst is a factor for improving the photocatalytic activity of Na^{+}-$SrTiO_3$. Co-loading $Rh_{0.7}Cr_{1.3}O_3$ for H_2 evolution reaction (HER) co-catalyst and CoOOH for O_2 evolution reaction (OER) co-catalyst further improved the photocatalytic activity and significantly extended lifetime. From the structural analysis of the photocatalyst and the measurement of the transient absorption spectrum, the improvement of the photocatalytic activity by Na ion doping was attributed to the oxygen vacancies in the $SrTiO_3$ crystal, which formed trapped sites of electrons generated by light irradiation, and separated electrons and holes.

Chapter 3: Controllable modification of metal ion-doped $SrTiO_3$ photocatalysts for photocatalytic overall H_2O splitting to almost the ultimate quantum yield

For Al ion-doped $SrTiO_3$ (Al-$SrTiO_3$ (flux)), using the flux method can prepare fine particles with a single crystal, the HER cocatalyst Rh-Cr_2O_3, and the OER cocatalyst CoOOH is loaded on the surface by the photocatalytic deposition method. As a result, we found that the apparent quantum yield (AQY, λ = 360 nm) for the H_2O splitting reaction was 96%. The crystal facet where electrons and holes generated by light irradiation appear is different due to the difference in surface energy of the photocatalyst particles whose specific crystal plane is exposed by the flux method with Al-doping. This is since the co-catalyst could be efficiently loaded on the surface. Furthermore, Mg-$SrTiO_3$ was prepared and examined using the PC method, SSR method, and flux method. When the photocatalytic activity was examined using $Rh_{0.7}Cr_{1.3}O_3$ as a co-catalyst, Mg-$SrTiO_3$ (flux) showed the highest photocatalytic activity compared to Mg-$SrTiO_3$ prepared by other methods, and its AQY (λ = 365 nm) was 55%. Therefore, the effect of the co-catalyst was examined using Mg-$SrTiO_3$ (flux). As a result, by co-loading OER co-catalyst CoOOH, AQY (= 365 nm) reached 68% at 365 nm. The HER co-catalyst Rh-Cr_2O_3 and the OER co-catalyst CoOOH are coloaded on the surface by the photocatalytic method as that of Al-$SrTiO_3$ (flux). The AQY of 94% nearly the ultimate quantum yield was achieved at 350 nm and 360 nm.

Chapter 4: Fabrication of $SrTiO_3$ doped metal ions utilizing the $SrCl_2$ flux as a medium for photocatalytic water splitting under visible light

Finally, to prepare a visible light-responsive $SrTiO_3$ photocatalyst that can be applied to the H2O splitting reaction, a metal ion-doped $SrTiO_3$ was synthesized using the flux method and its photocatalytic properties under visible light irradiation were examined. The prepared metal ion-doped $SrTiO_3$ showed a cubic morphology and light absorption in visible light. The photocatalytic performances were examined under visible light irradiation ($\lambda > 420$ nm) with HER using Pt as a cocatalyst and methanol as a sacrifice, and OER using IrO_2 as a cocatalyst and Ag^+ as sacrificing agents.

Chapter 5: Summary and outlook

In this chapter, the results presented in Chapter 2-4 were summarized, and the application and prospects of photocatalytic technology for overall H_2O splitting to produce H_2 under sunlight irradiation using a photocatalyst are discussed.

概要

エネルギー危機と環境汚染は、人間社会と文明の発展における主要な問題である。光触媒による光と H_2O から H_2 を製造する方法は、低コストで環境にやさしく次世代のエネルギーとして注目されている H_2 を直接 H2O から製造する技術であり、深刻なエネルギー危機と環境汚染問題に対する最良の解決方法の 1 つである。これまで、H_2O 分解反応に活性を示す様々な光触媒材料が開発されてきた。この中でチタン酸ストロンチウム（$SrTiO_3$）は、典型的な光触媒の 1 つとして 30 年以上にわたって研究されてきたが、この光触媒の H_2O 分解反応に対する効率は低く、大幅な効率の改善が求められている。

本論文は、$SrTiO_3$ 光触媒の H_2O 分解反応に対する大幅な効率改善を目的として、そのバルク、表面、形態を制御し、それらの、この光触媒による H2O 分解反応に対する活性と光変換効率（AQY）への影響を検討した。得られた研究結果より、H_2O 分解反応に対する光触媒の効率改善の要因を考察した。

論文の内容は次のとおりである。

第 1 章：序論

本章は本論文の一般的な研究背景、光触媒の開発と進歩、特に光触媒による光エネルギー変換と H_2O 分解反応の研究ついての歴史的背景と光触媒による H_2O 分解反応に対する光触媒効率を改善するための方法の概要、さらに、本論文の構成と研究目的について述べた。

第 2 章：Na イオンドープ $SrTiO_3$ の H_2O 分解に対する光触媒活性向上に関する検討

H_2O 分解反応に高い光触媒活性を示す Na イオンドープ $SrTiO_3$（Na+-$SrTiO_3$）について、Na イオンのドープによる活性向上要因とその機構解明を目的として、錯体重合法(PC 法)、固相法(SSR 法)を用いて Na^+-$SrTiO_3$ を調製して光触媒特性を検討した。ここでは、助触媒に $Rh_{0.7}Cr_{1.3}O_3$ を用いた。光触媒活性は高純度原料を用いて調製した光触媒の活性が著しく向上しことより、光触媒の純度が Na^+-$SrTiO_3$ の光触媒活性を向上させる要因であることが判明した。H_2 生成反応(HER)助触媒の $Rh_{0.7}Cr_{1.3}O_3$ と O_2 生成反応(OER)助触媒の CoOOH を共担持すると光触媒活性はさらに向上し、触媒寿命が著しく伸びた。光触媒の構造解析と過渡吸収スペクトル測定から光触媒活性向上は、Na イオンドープにより $SrTiO_3$ 結晶内に酸素欠陥が生じ、それが光照射で生成した電子のトラップ準位を形成させ、電子と正孔の分離を促進させることに起因することを見出した。

第 3 章：H_2O 分解反応に究極の量子収率を示す金属イオンドープ $SrTiO_3$ 光触媒の調製

単結晶微粒子が調製できるフラックス法を用いて調製した Al イオンドープ SrTiO3(Al-$SrTiO_3$(フラックス))について、HER 助触媒の Rh-Cr_2O_3 と OER 助触媒の CoOOH を光電着法で表面上に担持することで、H_2O 分解反応に対する見かけの量子収率(AQY，=360 nm)が 96 %となることを見出した。これは、Al イオンドープの効果に加え、フラックス法により特定な結晶面が露出した光触媒粒子の表面エネルギーの違いから光照射で生じた電子と正孔が出現する結晶面が異なりこれを利用して助触媒を効率的に表面に担持できたことに起因する。さらに、PC 法、SSR 法、フラックス法を用いて、$SrTiO_3$（Mg-$SrTiO_3$）を調製し検討を行った。$Rh_{0.7}Cr_{1.3}O_3$ を助触媒として光触媒活性を検討した時、Mg-SrTiO3（フラックス）は他の方法で調製した Mg-$SrTiO_3$ と比べて最高の光触媒活性を示し、その AQY(λ=365nm)は 55%であった。そこで Mg-$SrTiO_3$（フラックス）を用いて助触媒の効果を検討した。その結果、OER 助触媒 CoOOH の共担持により、AQY(□=365nm)は 68 %, Al-$SrTiO_3$(フラックス)と同様に HER 助触媒の Rh-Cr_2O_3 と OER 助触媒の CoOOH を光電着法で表面上に担持することで AQY(□=350 nm)は 94%となり、Mg-$SrTiO_3$(フラックス)は究極の AQY を示す光触媒となりえることが判明した。

第 4 章：フラックス法を利用した金属イオンドープ可視光応答 $SrTiO_3$ 光触媒の合成

最終的に H_2O 分解反応に応用できる可視光応答性の $SrTiO_3$ 光触媒の調製を目的として、フラックス法を利用して金属イオンドープ $SrTiO_3$ を合成しその可視光照射下での光触媒特性を検討した。調製された金属イオンドープ $SrTiO_3$ は立方体形態を示し可視光に光吸収を示した。光触媒特性は助触媒に Pt、メタノールを犠牲剤とした HER と助触媒に IrO_2、Ag^+を犠牲剤とした OER で、可視光照射下(λ>420 nm)で検討した。調製した光触媒の中で Rh と Ta を共ドープした $SrTiO_3$ が最も高い活性を示した。

第 5 章：総　括

本章では、第 2 章から第 4 章で得られた研究成果を総括し、光触媒を用いた太陽光照射下での H_2O から H_2 の製造に関しての光触媒技術の応用と今後の展望について考察した。

Contents

Chapter 1 General Introduction

1.1 Research background

The current global environmental and energy situations are relatively severe [1–6]. The energy industry is facing increasing pressure from economic growth, environmental protection, and social development. Among them, the accelerating industrialization process in developing countries has led to an increase in energy consumption. As a result, a continuous increase in the average global energy consumption index will accelerate the consumption of conventional fossil energy reserves. The consequences will be very serious. The earth will continue to become warm and the ecological environment will also deteriorate, and natural disasters will be caused. Therefore, it is crucial to explore fleshly clean and renewable energy to replace fossil fuels.

Solar energy is a typically clean and renewable energy source. The biggest feature of solar energy is its huge energy. The development of solar energy resources is one of the effective ways to solve the energy and environmental problems in human sustainable development [3,4,7,8]. Hydrogen energy is currently the most ideal energy source [9–11]. The final product is water and does not cause pollution. Photocatalytic overall H_2O splitting to produce hydrogen can convert and store solar energy into chemical energy [12–15]. The development of high-efficiency solar energy conversion photocatalytic material systems has become a major scientific exploration in the field of international materials to fundamentally solve energy and environmental pollution problems.

1.2 Application of photocatalysis

In 1972, A. Fujishima and K. Honda reported that a photoelectrochemical system composed of TiO_2 photoelectrodes and platinum electrodes could decompose water into hydrogen and oxygen, which opened up a new field of semiconductor photocatalysis [16]. The purpose of semiconductor photocatalysis was only to realize the conversion of photoelectrochemical solar energy at first, and then the focus of research shifted to the field of environmental photocatalysis [17,18]. The photocatalytic redox technology represented by semiconductor photocatalysts has become a promising environmental pollution control technology due to its direct use of sunlight to drive the reaction and the good stability of the catalyst [8,19–25]. A series of achievements have been made in the fields of organic pollutant degradation [6,25–28], heavy metal reduction [29–31], hydrogen and oxygen production [32–38], and organic synthesis [39–44]. The broad application prospects of photocatalytic reactions have attracted extensive attention from researchers in the fields of environment, materials, chemistry, and energy.

1.2.1 Photocatalytic overall water splitting

The photocatalytic water splitting technology started in 1972 [16]. Fujishima and Honda first reported the discovery of the phenomenon of TiO_2 single crystal electrode photo-catalytically decomposed water to produce hydrogen, thus revealing the direct decomposition of water using solar energy. The photocatalytic method for splitting water into H_2 and O_2 emerged with the conversion from electrode electrolysis of water to semiconductor photocatalytic decomposition of water to produce hydrogen. In recent decades, with the steady growth of global energy demand, exploring new energy attracts more and more attention from researchers. Hydrogen as secondary energy has generally been considered to be one of the most ideal pollution-free green energy in the new century. Therefore, the development of highly functional photocatalytic materials for overall water splitting into H_2 and O_2 was attached great importance. The continuous research made great progress for overall H_2O splitting in the synthesis and modification of photocatalysts [11,12,52–58,13,45–51].

Photocatalytic overall water splitting to produce H_2 and O_2 is a high energy barrier reaction that needs to satisfy more than the standard Gibbs free energy ($\triangle G°$ = 273 kJ/mol), converting the solar energy into chemical energy [44,59–61]. The chemical reaction formula is as follows:

$$H_2O\ (l) \rightarrow H_2\ (g) + 1/2O_2\ (g) \qquad \triangle G° = 273\ kJ/mol$$

During photocatalytic overall H_2O splitting reaction as shown in Figure 1-1A [61], the thermodynamics of decomposing water to release H_2 and O_2 requires that the conduction band potential of the semiconductor material as a photocatalytic material is slightly negative than the hydrogen electrode potential E_{H^+/H_2}, and the valence band potential should be slightly positive than the oxygen electrode potential E_{O_2/H_2O} [62–66]. In principle, as shown in Figure 1-1(B), when the absorbed energy is greater than or equal to the forbidden bandwidth of the semiconductor photocatalyst, the electrons in the semiconductor are excited to transition from the valence band to the conduction band, while the holes remain in the valence band. The electrons and holes are separated, and then reduce water to H_2 or oxidize water to oxygen at different locations in the semiconductor. As a photocatalytic water splitting material for H_2 and O_2 production, it needs to meet the properties of high stability, no photo-corrosion, and low price. Therefore, $SrTiO_3$ material is an exceedingly promising photocatalyst applying in the photocatalytic reactions [67,68].

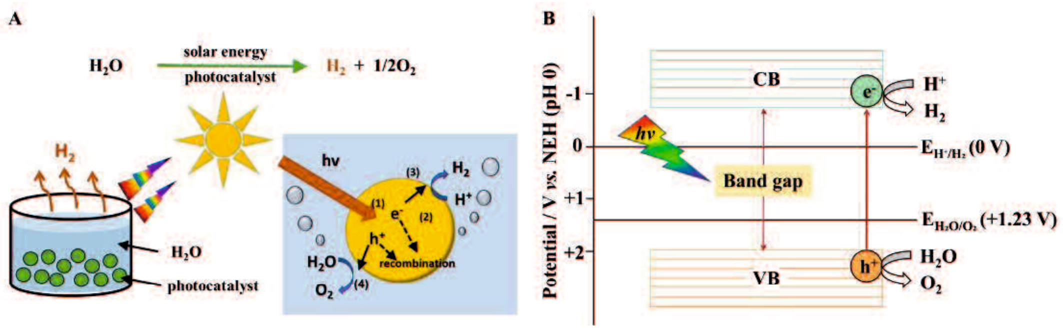

Figure 1-1. Solar water splitting using semiconductor photocatalyst. (A) Schematic illustration of the main processes during the photocatalytic overall H_2O splitting reaction; (B) Principle of water splitting using semiconductor photocatalysts. CB, Conduction Band; VB, Valance Band.

1.2.2 Photocatalytic reduction of CO_2

At present, the world's energy consumption is still dominated by fossil fuels. The greenhouse effect is caused by excessive greenhouse gases such as carbon dioxide emissions from fossil-fuel combustion [69–72]. Inspired by the photosynthesis of plants, the researchers have designed artificial photosynthesis to catalyze carbon dioxide into hydrocarbon fuels under natural environmental conditions, which not only helps reduce the concentration of CO_2 in the air but also provides high-value-added carbon-based fuels [73–77].

In the photocatalytic reduction of CO_2 reaction as shown in Figure 1-2 [73,77,78], if the energy of the absorbed photons is greater than that of the energy bandgap of the semiconductor photocatalyst, the semiconductor will be excited. The electrons that jump from the valence band will reach the conduction band, thereby generating corresponding holes in the valence band. The pairs of electrons are separated from each other and migrate to the semiconductor surface (captured by a cocatalyst if possible) for surface catalyzed redox reactions. The corresponding redox potential of the photogenerated electrons generated for reducing CO_2 should be thermodynamically lower than the conduction band energy level of the semiconductor. The products of CO_2 reduction are diverse according to the conduction band energy [79–83]. Therefore, the photocatalytic reduction of CO_2 has great application potential in synthetic industrial raw materials.

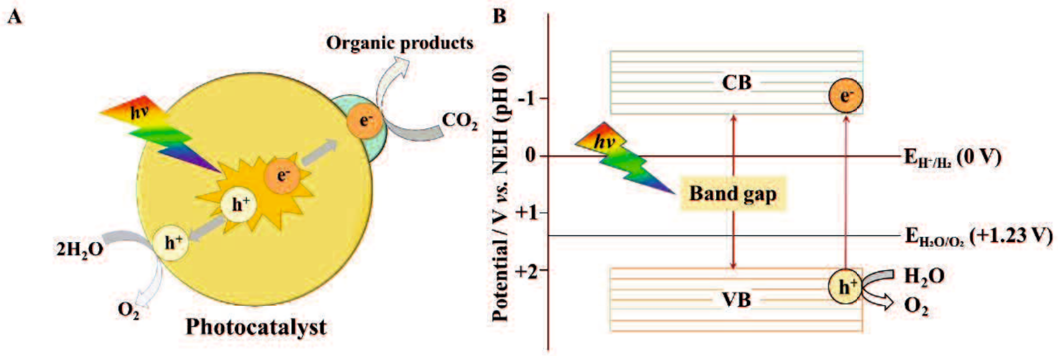

Product	Reaction	E^0_{redox} (V *vs.* NHE)
Oxygen	$H_2O/0.5O_2 + 2H^+ + 2e^-$	0.82
Methane	$CO_2 + 8H^+ + 8e^-/CH_4 + 2H_2O$	-0.24
Ethane	$2CO_2 + 14H^+ + 14e^-/C_2H_6 + 4H_2O$	-0.27
Carbon monoxide	$CO_2 + 2H^+ + 2e^-/CO + H_2O$	-0.51
Methanol	$CO_2 + 6H^+ + 6e^-/CH_3OH + H_2O$	-0.39
Ethanol	$2CO_2 + 12H^+ + 12e^-/C_2H_5OH + 3H_2O$	-0.33
1-Propanol	$3CO_2 + 18H^+ + 18e^-/CH_3CH_2CH_2OH + 5H_2O$	-0.31
2-Propanol	$3CO_2 + 18H^+ + 18e^-/CH_3CH(OH)CH_3 + 5H_2O$	-0.30
Formaldehyde	$CO_2 + 4H^+ + 4e^-/HCHO + H_2O$	-0.55
Acetaldehyde	$2CO_2 + 10H^+ + 10e^-/CH_3CHO + 3H_2O$	-0.36
Propionaldehyde	$3CO_2 + 16H^+ + 16e^-/CH_3CH_2CHO + 5H_2O$	-0.32
Acetone	$3CO_2 + 16H^+ + 16e^-/CH_3COCH_3 + 5H_2O$	-0.31
Formic acid	$CO_2 + 2H^+ + 2e^-/HCOOH$	-0.58
Acetic acid	$2CO_2 + 8H^+ + 8e^-/CH_3COOH + 2H_2O$	-0.31

Figure 1-2. Photocatalytic reduction of CO_2. (A) Schematic illustration of the main process of photocatalytic reduction of CO_2 to various organic products and (B) relative energy levels of photocatalytic reduction of CO_2 on a semiconductor photocatalyst. CB, Conduction Band; VB, Valance Band.

1.2.3 Photocatalytic degradation of organic pollution

Over-exploitation of resources has caused energy shortages and brought various pollution problems. It can be said that human beings have paid a heavy price for their temporary greed. Overuse of fossil fuels such as coal and petroleum has not only caused a series of environmental pollution but also caused the depletion of non-renewable mineral resources [2,69,70,84]. The content of organic pollutants in wastewater from various industries has been continuously increasing. These organic pollutants include a wide range of persistent organic compounds, such as drugs, toxic metal ions, dyes, and various antibiotics. This toxic pollution has a serious effect on human health. Photocatalysis is a promising wastewater treatment technology [7,18,24–26,30,85–88].

In recent years, various methods have been used to remove dissolved organic pollutants in water, for instance, the photocatalytic oxidation method [89–94], absorption [95,96], microbial decomposition method [97], and molecular sieve [98,99]. These methods are high-cost and the pollutants can't be eliminated. Compared to the traditional approach, photocatalytic oxidation degradation of organic pollutants in wastewater has outstanding advantages such as low energy consumption, simple operation, mild reaction conditions, and reduction of secondary pollution, so it has attracted increasing attention.

In the process of photocatalytic degradation of pollutants in Figure 1-3, ·OH, $\cdot O_2^-$ free radicals, and h^+ are generated [100–102]. Organic pollutant molecules combine with these free radicals and are oxidized and degraded. $\cdot O_2^-$ is obtained by the reduction of O_2 dissolved in water by photogenerated electrons. The potential at the bottom of the conduction band (CB) must be more negative than -0.33 V ($O_2/\cdot O_2^-$ = -0.33 V *vs.* NHE), and ·OH free radicals are the products of the oxidation of H_2O by the photogenerated holes [103]. The potential at the top of the valence band (VB) must be located at a more positive than 2.72 V (·OH, H^+/H_2O = 2.72 V *vs.* NHE) [102]. Due to the highly active free radicals generated during the photocatalytic reaction process, most organic pollutants can be completely oxidized and mineralized to non-toxic inorganic small molecules, H_2O, and CO_2 [102].

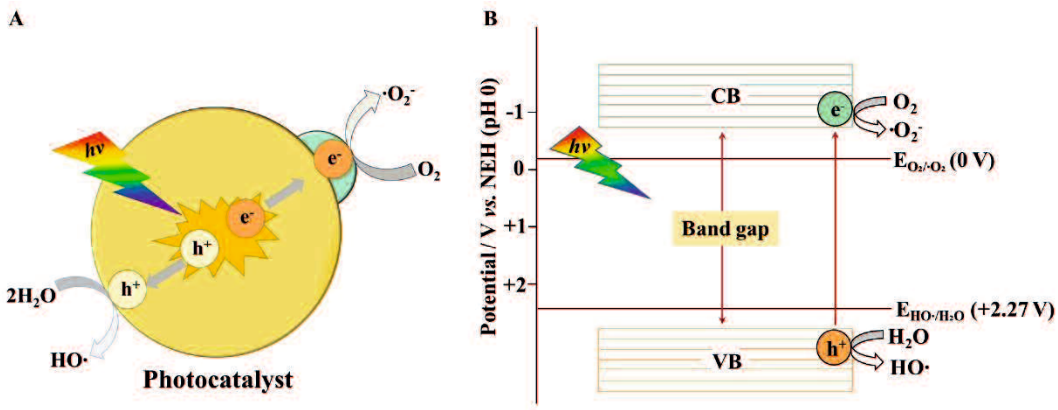

Figure 1-3. Photocatalytic degradation of organic pollution. (A) Schematic illustration of the main process of photocatalytic degradation of organic pollution and (B) relative energy levels of photocatalytic degradation of organic pollution on a semiconductor photocatalyst. CB, Conduction Band; VB, Valance Band.

1.2.4 Other applications

The above listed are the most extensive areas of photocatalysis research in recent years. Moreover, photocatalysis also has great application prospects in organic synthesis and nitrogen fixation [58,104].

1.3 Typical photocatalytic materials for overall H_2O splitting

The report of the photocatalytic water splitting TiO_2 photoelectrode opened the novel field of photocatalysis research. After the development for more than 40 years, photocatalysis has made significant progress in energy and environmental fields, especially water splitting to produce hydrogen, CO_2 fixation, environment purification, organic synthesis, and chemical reactions. However, the efficiency of most photocatalytic systems has not yet reached the level of practical application. The development of high-performance photocatalysts is still the main research topic in the field of photocatalysis. The following are some typical photocatalysts with great development potential.

Metal oxide particulate photocatalyst Metal oxide photocatalysts have received extensive attention in recent years [105]. At first, the metal oxide of TiO_2 photocatalyst was the widely studied photocatalytic material because of its strong oxidation ability, stable chemical properties, and non-toxicity [21]. Subsequently, the other photocatalysts such as perovskite $SrTiO_3$ materials, $NaTaO_3$, WO_3, Ga_2O_3 constantly emerged [106–110]. These photocatalysts have broad application prospects in the fields of water splitting into H_2 and O_2, degradation of organic pollutants, and reduction of titanium dioxide. The performances of the photocatalysts have achieved great progress, especially the decomposition of water into H_2 and O_2 under Ultraviolet (UV) light irradiation. La ion-doped $NaTaO_3$ with NiO as a co-catalyst was the first to be reported as a relatively high photocatalytic overall H_2O splitting activity under (UV) irradiation, achieving an AQY of 56% at 270 mm [109]. Also, Zn (3 mol%)-Ga_2O_3 prepared with de-ionized water and dilute $CaCl_2$ ultra-pure water solution (0.001 mol L^{-1}) has been reported to show an AQY of 71% at 254 nm [106]. After long-term continuous modification and optimization, Rh (0.1 wt%)/ Cr (0.05 wt%)/Co (0.05 wt%) loaded-$SrTiO_3$: Al photocatalyst achieved photocatalytic overall water splitting with an apparent quantum efficiency almost unity [50]. However, most of these catalysts have very low efficiency in the use of sunlight limited by the wide bandgap. Therefore, these catalysts are still faced with great challenges in future development and efficient utilization.

(Oxy)nitrides and (oxy)sulfides photocatalysts The absorption bands of (oxy)nitrides and (oxy)sulfides photocatalysts are at 500-750 nm and have narrow bandgap energies of 1.7 - 2.5 eV [111]. In the presence of a sacrificial electron donor or acceptor, most of the photocatalysts have the capability of water splitting into H_2 or O_2 under visible light irradiation ($\lambda \geq 420$ nm), respectively. It has been reported that the TaON oxynitride photocatalyst achieved a quantum yield of 34% upon visible light irradiation [112]. Although this material has the potential for overall H_2O splitting to produce H_2 and O_2, it has not been realized. Recently, Domen'group used $KTaO_3$ as the matrix, single-crystal Ta_3N_5 without grain boundaries was synthesized after a short period of nitrogen treatment [113]. This single crystal Ta_3N_5 with Rh/Cr_2O_3 as a cocatalyst was applied to split H_2O into H_2 and O_2 at a stoichiometric ratio for the first time. Subsequently, the overall water splitting over $Y_2Ti_2O_5S_2$ oxysulfide photocatalyst was also demonstrated, and simultaneous production of hydrogen and oxygen at a stoichiometric ratio was realized under visible light irradiation [52]. However, the efficiencies of overall H_2O splitting were extremely low and most photocatalysts have not accomplished the overall H_2O splitting reaction, probably due to the defect densities in these photocatalysts. Therefore, continuous optimization and modification need to be made to improve photocatalytic water-splitting efficiency.

Metal-free photocatalyst Graphite phase carbon nitride ($g-C_3N_4$,), BN, and other metal-free photocatalysts have been extensively studied in the photocatalytic overall water splitting to produce hydrogen [114,115]. As a typical non-metallic photocatalyst, $g-C_3N_4$ has attracted widespread attention due to its high thermal/chemical stability, low cost, and non-toxic properties. Xinchen Wang's group realized the direct overall H_2O splitting over graphitic carbon nitride ($g-C_3N_4$) loaded with Pt, PtO_x, and CoO_x cocatalysts under visible light irradiation. This photocatalyst shows a great application prospect [116].

Solid-solution photocatalyst The solid-solution method can be applied to adjust the bandgap and band edge position, expanding the spectral response of photocatalytic materials. Therefore, solid solution photocatalysts are promising visible light-responsive photocatalyst [117,118]. The typical solid-solution photocatalyst was GaN: ZnO [119]. This photocatalyst has accomplished photocatalytic overall H_2O splitting into stoichiometric amounts of H_2 and O_2 stably by modifying with redox co-catalysts under visible irradiation [120–125].

1.4 $SrTiO_3$ photocatalyst

Traditional semiconductor materials $SrTiO_3$ have the characteristics of low cost, high chemical stability, non-toxicity, and can decompose water to produce H_2 and O_2 under sunlight. The photocatalyst has a strong ability to photooxidation and degradation of organic pollutants. This typical photocatalytic material has attracted considerable attention.

1.4.1 Property of $SrTiO_3$ material

Strontium titanate ($SrTiO_3$) has a typical perovskite-type structure with a high dielectric constant, low dielectric loss, and good thermal stability [126]. At the same time, as a functional material, strontium titanate has the properties of excellent photocatalytic activity, and unique electromagnetic properties, and redox catalytic activity. It can be used in the photocatalytic decomposition of water to produce H_2 and O_2, degradation of organic pollutants, and photochemical cells.

1.4.2 Strategy of developing highly functional $SrTiO_3$ for overall water splitting

The wide forbidden bandwidth (3.2 eV), rich defects, and rapid recombination of photo-generated electron-hole pairs of $SrTiO_3$ lead to low photocatalytic efficiency, especially visible light hydrogen production efficiency. To improve the efficiency of photocatalytic hydrogen production, it is usually necessary to modify the photocatalyst, effectively adjust the energy band structure, reduce the recombination rate of electron-hole pairs, and improve the stability. The modification of $SrTiO_3$ photocatalysts mainly includes the following methods.

Modifying the surface of photocatalyst with co-catalyst Loading co-catalyst has been extensively studied as an effective surface modification technology, which can be as active sites, reducing the recombination rate of photogenerated electrons and holes and activation energy, enhancing the stability of the catalyst, and promoting surface reactions. The typical co-catalysts include noble metal (Pt, Au, Ru, Pb, Ag, and Rh) [50,125,127], noble metal oxide (RuO_2, NiO, Cr_2O_3, CoO_x, IrO_2, MoO_x, and $Rh_yCr_{2-y}O_3$) [50,54,132,133,55,122,124,125,128–131]. The pure $SrTiO_3$ shows no photocatalytic activity due to the rapid recombination of photogenerated electrons and holes. Modifying the photocatalyst with hydrogen evolution cocatalyst (Pt, NiO, and $Rh_yCr_{2-y}O_3$), $SrTiO_3$ can be applied to overall H_2O splitting [128,134,135]. Following co-loading oxygen evolution cocatalyst (RuO_2, IrO_2, and CoO_x) [34,52,54,56,131,136], the photocatalytic activity and stability are both remarkably improved.

Ion-doping There is two main aspects of ion-doping into $SrTiO_3$. (1) The photocatalytic reaction is carried out under UV irradiation. The pristine $SrTiO_3$ has abundant defects in the bulk, which act as the recombination centers, reducing the photocatalytic reaction. Doping the aliovalent metal cations with a valence lower than that of the parent cation, can reduce the density of defects, and introducing the oxygen vacancy [48,50,129,137–139]. The doped $SrTiO_3$ modifying suitable cocatalyst can remarkably improve the photocatalysts. (2) The photocatalytic reaction is performed under visible light irradiation. The pure $SrTiO_3$ does not respond to the visible light due to the large bandgap. Doping appropriate noble metal ions (Rh, Ru, Cr, Mn, Fe, and Ni) can make forbidden bandwidth narrow and then realize photocatalytic reaction under visible irradiation [130,140–145].

Modification of the morphology Some excellent properties such as larger reactive surface area and more active sites by preparing the photocatalyst with special morphology. The special morphologies included nanorods, nanosheets, mesoporous structure, core-shell structure, and cubes, which fabricate the separation of reduction and oxidation active sites [50,93,153,139,146–152]. Following selectively depositing the redox cocatalysts, the photogenerated electrons and holes rapidly transfer to corresponding actives sites and then realize the separation of the charge carriers. Domen's group synthesized the $SrTiO_3$ with cubic morphology achieving an AQY of 30% at 360 nm [139]. At the same time, an anisotropic facets 18-facet $SrTiO_3$ with anisotropic facets were prepared facets using a nanocrystal morphology tailoring strategy. The modified $SrTiO_3$ achieved a fivefold enhancement of AQY for overall H_2O splitting combining with modifying the surface using the redox cocatalysts reported by Li’s group [150]. Furthermore, Domen’s group achieved photocatalytic overall water splitting with a quantum efficiency of almost unity by using $SrTiO_3$ with special morphology combing modify the redox cocatalysts [50].

Fabrication of Z-scheme heterojunction Z-scheme heterojunction is a charge transfer method inspired by the light reaction stage of photosynthesis in natural plants [15,154]. Two kinds of semiconductors with different energy band structures (O_2 evolution photocatalyst and H_2 evolution photocatalyst) may form a heterostructure after connection. The electron holes in the two semiconductors are retained to participate in the redox reaction. The use of this system can not only realize the spatial separation of redox sites but also ensure that the photocatalyst can maintain a proper valence band position, thereby maintaining a strong redox reaction ability. Bard, for the first time, put forward the Z-scheme system of photocatalysis [155]. The Z-scheme system has been continuously improved after years of research. Domen's group has achieved a solar-to-hydrogen (STH) energy conversion efficiency exceeding 1% by fabricating a Z-scheme system of $SrTiO_3$: La, Rh/Au/$BiVO_4$: Mo sheet [156].

1.5 Contents and research significance of this thesis

Hydrogen energy is regarded as ideal alternative energy for the development of human society. The preparation of clean energy hydrogen by photocatalytic H_2O splitting technology can effectively realize the conversion of solar energy to chemical energy, which has important research significance for the development of clean energy and the reduction of environmental pollution.

In this thesis, the investigations on the development of highly active metal ions doped -$SrTiO_3$ photocatalysts for overall H_2O splitting were preceded. The research contents mainly included the effects of preparation methods, the property of starting materials used for preparing the photocatalyst, the morphology, and cocatalysts on the photocatalytic activity for overall H_2O splitting. The photocatalytic performances of $SrTiO_3$ photocatalyst were investigated by doping the various metal ions with different preparation methods by modifying the morphology, surface active sites, and optical property. The optimal Na doped-$SrTiO_3$ photocatalyst with modifying the $Rh_yCr_{2-y}O_3$ and CoO_x co-catalysts achieved an AQY of 30 % at 365 nm. Even more, the optimal Mg (Al) doped-$SrTiO_3$ prepared by the flux method with modifying Rh, Cr_2O_3, and CoOOH cocatalysts through sequential the photo-deposition method showed almost the ultimate quantum yield for photocatalytic H_2O splitting.

As all known, ultraviolet light only accounts for 4%~5% of sunlight while visible light accounts for 45~50%. Even though the quantum efficiency of $SrTiO_3$ photocatalyst reached almost the ultimate value under UV irradiation, the solar-to-hydrogen efficiency conversation was still quite low and cannot satisfy the application of photocatalytic H_2O splitting in practical production. To improve the utilization efficiency of sunlight, the electronic structure was tuned by flux-mediated co-doping of various noble metal ions to respond to visible light as well as modifying the morphology of $SrTiO_3$. The modified $SrTiO_3$ photocatalysts by the flux method showed cubic or tailoring cubic morphology and were employed for sacrificial H_2 or O_2 evolution under visible irradiation ($\lambda > 420$ nm).

Furthermore, the mechanisms of the various factors affecting the photocatalytic performances were discussed by the analysis of X-ray diffractometer (XRD), Electron microscopies (SEM, TEM), TEM-EDS elemental mapping images, EDS spectrum, UV-vis absorption spectra, Raman spectroscopy, Transient Absorption Spectra.

1.6 References

[1] M.S. Anjum, S.M. Ali, M. Imad-ud-din, M.A. Subhani, M.N. Anwar, A.S. Nizami, U. Ashraf, M.F. Khokhar, An emerged challenge of air pollution and ever-increasing particulate matter in pakistan; A Critical Review, J. Hazard. Mater. 402 (2021) 123943.

[2] M.S. Sthel, J.G.R. Tostes, J.R. Tavares, Current energy crisis and its economic and environmental consequences: Intense human cooperation, Nat. Sci. 05 (2013) 244–252.

[3] P.O. Ukaogo, U. Ewuzie, C. V. Onwuka, Environmental pollution: causes, effects, and the remedies, Microorg. Sustain. Environ. Heal. (2020) 419–429.

[4] A.M. Nasir, J. Jaafar, F. Aziz, N. Yusof, W.N.W. Salleh, A.F. Ismail, M. Aziz, A review on floating nanocomposite photocatalyst: Fabrication and applications for wastewater treatment, J. Water Process Eng. 36 (2020) 101300.

[5] L.G.A. Barboza, A. Cózar, B.C.G. Gimenez, T.L. Barros, P.J. Kershaw, L. Guilhermino, Chapter 17 - Macroplastics Pollution in the Marine Environment, World Seas An Environ. Eval. Vol. III Ecol. Issues Environ. Impacts, 2019: pp. 305–328.

[6] J.L. Martinez, Environmental pollution by antibiotics and by antibiotic resistance determinants, Environ. Pollut. 157 (2009) 2893–2902.

[7] P.A.K. Reddy, P.V.L. Reddy, E. Kwon, K.H. Kim, T. Akter, S. Kalagara, Recent advances in photocatalytic treatment of pollutants in aqueous media, Environ. Int. 91 (2016) 94–103.

[8] M.R. Hoffmann, S.T. Martin, W. Choi, D.W. Bahnemann, Environmental applications of semiconductor photocatalysis, Chem. Rev. 95 (1995) 69–96.

[9] H.T. Arat, M.K. Baltacioglu, B. Tanç, M.G. Sürer, I. Dincer, A perspective on hydrogen energy research, development and innovation activities in Turkey, Int. J. Energy Res. 44 (2020) 588–593.

[10] F. Dawood, M. Anda, G.M. Shafiullah, Hydrogen production for energy: An overview, Int. J. Hydrogen Energy. 45 (2020) 3847–3869.

[11] A. Pareek, R. Dom, J. Gupta, J. Chandran, V. Adepu, P.H. Borse, Insights into

renewable hydrogen energy: Recent advances and prospects, Mater. Sci. Energy Technol. 3 (2020) 319–327.

[12] Q. Wang, K. Domen, Particulate photocatalysts for light-driven water splitting: Mechanisms, challenges, and design strategies, Chem. Rev. 120 (2020) 919–985.

[13] T. Takata, K. Domen, Particulate photocatalysts for water splitting: Recent advances and future prospects, ACS Energy Lett. 4 (2019) 542–549.

[14] S. Chen, T. Takata, K. Domen, Particulate photocatalysts for overall water splitting, Nat. Rev. Mater. 2 (2017) 1–17.

[15] J. Low, J. Yu, M. Jaroniec, S. Wageh, A.A. Al-Ghamdi, Heterojunction photocatalysts, Adv. Mater. 29 (2017) 1601694.

[16] A. Fujishima, K. Honda, Electrochemical photolysis of water at a semiconductor electrode, Nature 238 (1972) 37–38.

[17] A.J. Nozik, p-n photoelectrolysis cells, Appl. Phys. Lett. 29 (1976) 150–153.

[18] S.N. Frank, A.J. Bard, Semiconductor electrodes. II. Electrochemistry at n-type TiO_2 electrodes in acetonitrile solutions, J. Am. Chem. Soc. 97 (1975) 7427–7433.

[19] Y. Boyjoo, H. Sun, J. Liu, V.K. Pareek, S. Wang, A review on photocatalysis for air treatment: From catalyst development to reactor design, Chem. Eng. J. 310 (2017) 537–559.

[20] H. Park, Y. Park, W. Kim, W. Choi, Surface modification of TiO_2 photocatalyst for environmental applications, J. Photochem. Photobiol. C Photochem. Rev. 15 (2013) 1–20.

[21] K.R. Reddy, M. Hassan, V.G. Gomes, Hybrid nanostructures based on titanium dioxide for enhanced photocatalysis, Appl. Catal. A Gen. 489 (2015) 1–16.

[22] G. Huang, Z. Xiao, W. Zhen, Y. Fan, C. Zeng, C. Li, S. Liu, P.K. Wong, Hydrogen production from natural organic matter via cascading oxic-anoxic photocatalytic processes: An energy recovering water purification technology, Water Res. 175 (2020) 115684.

[23] V.H. Nguyen, B.S. Nguyen, C.W. Huang, T.T. Le, C.C. Nguyen, T.T. Nhi Le, D. Heo, Q.V. Ly, Q.T. Trinh, M. Shokouhimehr, C. Xia, S.S. Lam, D.V.N. Vo, S.Y. Kim, Q. Van Le, Photocatalytic NO_x abatement: Recent advances and emerging

trends in the development of photocatalysts, J. Clean. Prod. 270 (2020) 121912.

[24] D. Chen, Y. Cheng, N. Zhou, P. Chen, Y. Wang, K. Li, S. Huo, P. Cheng, P. Peng, R. Zhang, L. Wang, H. Liu, Y. Liu, R. Ruan, Photocatalytic degradation of organic pollutants using TiO_2-based photocatalysts: A review, J. Clean. Prod. 268 (2020) 121725.

[25] M.M. Mahlambi, C.J. Ngila, B.B. Mamba, Recent developments in environmental photocatalytic degradation of organic pollutants: The case of titanium dioxide nanoparticles-A review, J. Nanomater. 2015 (2015) 790173.

[26] D.S. Bhatkhande, V.G. Pangarkar, A.A.C.M. Beenackers, Photocatalytic degradation for environmental applications - A review, J. Chem. Technol. Biotechnol. 77 (2002) 102–116.

[27] X. Li, J. Xie, C. Jiang, J. Yu, P. Zhang, Review on design and evaluation of environmental photocatalysts, Front. Environ. Sci. Eng. 12 (2018).

[28] N.S. Alharbi, B. Hu, T. Hayat, S.O. Rabah, A. Alsaedi, L. Zhuang, X. Wang, Efficient elimination of environmental pollutants through sorption-reduction and photocatalytic degradation using nanomaterials, Front. Chem. Sci. Eng. 14 (2020) 1124–1135.

[29] Z. Zhao, H. An, J. Lin, M. Feng, V. Murugadoss, T. Ding, H. Liu, Q. Shao, X. Mai, N. Wang, H. Gu, S. Angaiah, Z. Guo, Progress on the photocatalytic reduction removal of chromium contamination, Chem. Rec. 19 (2019) 873–882.

[30] M.B. Tahir, H. Kiran, T. Iqbal, The detoxification of heavy metals from aqueous environment using nano-photocatalysis approach: a review, Environ. Sci. Pollut. Res. 26 (2019) 10515–10528.

[31] C.C. Wang, X.D. Du, J. Li, X.X. Guo, P. Wang, J. Zhang, Photocatalytic Cr(VI) reduction in metal-organic frameworks: A mini-review, Appl. Catal. B Environ. 193 (2016) 198–216.

[32] Y. Zhang, Y.J. Heo, J.W. Lee, J.H. Lee, J. Bajgai, K.J. Lee, S.J. Park, Photocatalytic hydrogen evolution via water splitting: A short review, Catalysts 8 (2018) 655.

[33] V.Preethi, S.Kanmani, Photocatalytic Hydrogen Production, Mater. Sci. Semicond. Process. 16 (2013) 561–575.

[34] K. Maeda, A. Xiong, T. Yoshinaga, T. Ikeda, N. Sakamoto, T. Hisatomi, M. Takashima, D. Lu, M. Kanehara, T. Setoyama, T. Teranishi, K. Domen, Photocatalytic overall water splitting promoted by two different cocatalysts for hydrogen and oxygen evolution under visible light, Angew. Chemie - Int. Ed. 49 (2010) 4096–4099.

[35] A.A. Ismail, D.W. Bahnemann, Photochemical splitting of water for hydrogen production by photocatalysis: A review, Sol. Energy Mater. Sol. Cells 128 (2014) 85–101.

[36] G. Zhang, Z.A. Lan, X. Wang, Surface engineering of graphitic carbon nitride polymers with cocatalysts for photocatalytic overall water splitting, Chem. Sci. 8 (2017) 5261–5274.

[37] J. Sarkar, S. Bhattacharyya, Application of graphene and graphene-based materials in clean energy-related devices Minghui, Arch. Thermodyn. 33 (2012) 23–40.

[38] H. Ahmad, S.K. Kamarudin, L.J. Minggu, M. Kassim, Hydrogen from photo-catalytic water splitting process: A review, Renew. Sustain. Energy Rev. 43 (2015) 599–610.

[39] B. König, Photocatalysis in organic synthesis – Past, present, and future, European J. Org. Chem. 2017 (2017) 1979–1981.

[40] T. Hering, A.U. Meyer, B. König, Photocatalytic anion oxidation and applications in organic synthesis, J. Org. Chem. 81 (2016) 6927–6936.

[41] C. Michelin, N. Hoffmann, Photosensitization and photocatalysis - Perspectives in organic synthesis, ACS Catal. 8 (2018) 12046–12055.

[42] D.M. Schultz, T.P. Yoon, Solar synthesis: Prospects in visible light photocatalysis, Science 343 (2014) 1239176.

[43] J. Chen, J. Cen, X. Xu, X. Li, The application of heterogeneous visible light photocatalysts in organic synthesis, Catal. Sci. Technol. 6 (2016) 349–362.

[44] D. Friedmann, A. Hakki, H. Kim, W. Choi, D. Bahnemann, Heterogeneous photocatalytic organic synthesis: State-of-the-art and future perspectives, Green Chem. 18 (2016) 5391–5411.

[45] S. Suzuki, A. Iwase, A. Kudo, Long wavelength visible light-responsive $SrTiO_3$

photocatalysts doped with valence-controlled Ru for sacrificial H_2 and O_2 evolution, Catal. Sci. Technol. 10 (2020) 4912–4916.

[46] J. Wang, M. Kuo, P. Zeng, L. Xu, S. Chen, T. Peng, Few-layer $BiVO_4$ nanosheets decorated with $SrTiO_3$: Rh nanoparticles for highly efficient visible-light-driven overall water splitting, Appl. Catal. B Environ. 279 (2020) 119377.

[47] S. Pokrant, An almost perfectly efficient light-activated catalyst for producing hydrogen from water, Nature. 581 (2020) 386–388.

[48] J. Jiang, K. Kato, H. Fujimori, A. Yamakata, Y. Sakata, Investigation on the highly active $SrTiO_3$ photocatalyst toward overall H_2O splitting by doping Na ion, J. Catal. 390 (2020) 81–89.

[49] R. Acharya, K. Parida, A review on TiO_2/g-C_3N_4 visible-light-responsive photocatalysts for sustainable energy generation and environmental remediation, J. Environ. Chem. Eng. 8 (2020) 103896.

[50] T. Takata, J. Jiang, Y. Sakata, M. Nakabayashi, N. Shibata, V. Nandal, K. Seki, T. Hisatomi, K. Domen, Photocatalytic water splitting with a quantum efficiency of almost unity, Nature. 581 (2020) 411–414.

[51] A. Kudo, S. Yoshino, T. Tsuchiya, Y. Udagawa, Y. Takahashi, M. Yamaguchi, I. Ogasawara, H. Matsumoto, A. Iwase, Z-scheme photocatalyst systems employing Rh- and Ir-doped metal oxide materials for water splitting under visible light irradiation, Faraday Discuss 215 (2019) 313–328.

[52] Q. Wang, M. Nakabayashi, T. Hisatomi, S. Sun, S. Akiyama, Z. Wang, Z. Pan, X. Xiao, T. Watanabe, T. Yamada, N. Shibata, T. Takata, K. Domen, Oxysulfide photocatalyst for visible-light-driven overall water splitting, Nat. Mater. 18 (2019) 827–832.

[53] X. Wang, T. Hisatomi, Z. Wang, J. Song, J. Qu, T. Takata, K. Domen, Core–Shell-Structured $LaTaON_2$ Transformed from $LaKNaTaO_5$ Plates for Enhanced Photocatalytic H_2 Evolution, Angew. Chemie - Int. Ed. 58 (2019) 10666–10670.

[54] H. Lyu, T. Hisatomi, Y. Goto, M. Yoshida, T. Higashi, M. Katayama, T. Takata, T. Minegishi, H. Nishiyama, T. Yamada, Y. Sakata, K. Asakura, K. Domen, An Al-doped $SrTiO_3$ photocatalyst maintaining sunlight-driven overall water splitting activity for over 1000 h of constant illumination, Chem. Sci. 10 (2019)

3196–3201.
[55] T.H. Chiang, H. Lyu, T. Hisatomi, Y. Goto, T. Takata, M. Katayama, T. Minegishi, K. Domen, Efficient photocatalytic water splitting using Al-doped $SrTiO_3$ coloaded with molybdenum oxide and rhodium-chromium oxide, ACS Catal. 8 (2018) 2782–2788.
[56] Y. Goto, T. Hisatomi, Q. Wang, T. Higashi, K. Ishikiriyama, T. Maeda, Y. Sakata, S. Okunaka, H. Tokudome, M. Katayama, S. Akiyama, H. Nishiyama, Y. Inoue, T. Takewaki, T. Setoyama, T. Minegishi, T. Takata, T. Yamada, K. Domen, A particulate photocatalyst water-splitting panel for large-scale solar hydrogen heneration, Joule 2 (2018) 509–520.
[57] J. Qi, W. Zhang, R. Cao, Solar-to-hydrogen energy conversion based on water splitting, Adv. Energy Mater. 8 (2018) 1–16.
[58] T. Yamada, K. Domen, Development of sunlight driven water splitting devices towards future artificial photosynthetic Industry, ChemEngineering 2 (2018) 36.
[59] S. Ye, C. Ding, M. Liu, A. Wang, Q. Huang, C. Li, Water oxidation catalysts for artificial photosynthesis, Adv. Mater. 31 (2019) 1902069.
[60] L. Nicholson, Energy conversion, Apollo. 191 (2020) 148–153.
[61] R. Abe, Recent progress on photocatalytic and photoelectrochemical water splitting under visible light irradiation, J. Photochem. Photobiol. C Photochem. Rev. 11 (2010) 179–209.
[62] A. Kudo, Y. Miseki, Heterogeneous photocatalyst materials for water splitting, Chem. Soc. Rev. 38 (2009) 253–278.
[63] S. Zhu, D. Wang, Photocatalysis: Basic principles, diverse forms of implementations and emerging scientific opportunities, Adv. Energy Mater. 7 (2017) 1700841.
[64] S. V. Eliseeva, J.C.G. Bünzli, Rare earths: Jewels for functional materials of the future, New J. Chem., 35 (2011) 1165–1176.
[65] A.-L. Linsebigler, G. Lu, J.-T. Yates, Jr., Photocatalysis on TiO_2 surfaces: principles, mechanisms, and selected results, Chem. Rev. 95 (1995) 735-758.
[66] R. Li, C. Li, Photocatalytic water splitting on semiconductor-based photocatalysts, Adv. Catal. 60 (2014) 1–6.

[67] Y.-Y. Pai, A. Tylan-Tyler, P. Irvin, J. Levy, Physics of $SrTiO_3$-based heterostructures and nanostructures: A review, Reports Prog. Phys. 81 (2018) 036503.

[68] H. Yan, Z. Zhang, S. Wang, K. Jin, Review of photoresponsive properties at $SrTiO_3$-based heterointerfaces, Chinese Phys. B. 27 (2018) 117804.

[69] D.J. Wuebbles, A.K. Jain, Concerns about climate change and the role of fossil fuel use, Fuel Process. Technol. 71 (2001) 99–119.

[70] S.H. Schneider, The greenhouse effect - Science and policy, Indian J. Environ. Prot. 9 (1989) 789–792.

[71] A.F. Bouwman, The role of soils and land use in the greenhouse effect, Neth. J. Agric. Sci. 37 (1989) 13–19.

[72] R.J. Andres, T.A. Boden, F.M. Bréon, P. Ciais, S. Davis, D. Erickson, J.S. Gregg, A. Jacobson, G. Marland, J. Miller, T. Oda, J.G.J. Olivier, M.R. Raupach, P. Rayner, K. Treanton, A synthesis of carbon dioxide emissions from fossil-fuel combustion, Biogeosciences 9 (2012) 1845–1871.

[73] J. Hong, W. Zhang, J. Ren, R. Xu, Photocatalytic reduction of CO_2: A brief review on product analysis and systematic methods, Anal. Methods. 5 (2013) 1086.

[74] J. Yu, J. Low, W. Xiao, P. Zhou, M. Jaroniec, Enhanced photocatalytic CO_2-reduction activity of anatase TiO_2 by coexposed {001} and {101} facets, J. Am. Chem. Soc. 136 (2014) 8839–8842.

[75] M. Marszewski, S. Cao, J. Yu, M. Jaroniec, Semiconductor-based photocatalytic CO_2 conversion, Mater. Horizons 2 (2015) 261–278.

[76] A.D. Handoko, K. Li, J. Tang, Recent progress in artificial photosynthesis: CO_2 photoreduction to valuable chemicals in a heterogeneous system, Curr. Opin. Chem. Eng. 2 (2013) 200–206.

[77] C. Peng, G. Reid, H. Wang, P. Hu, Perspective: Photocatalytic reduction of CO_2 to solar fuels over semiconductors, J. Chem. Phys. 147 (2017) 030901.

[78] L. Liu, Y. Li, Understanding the reaction mechanism of photocatalytic reduction of CO_2 with H_2O on TiO_2-based photocatalysts: A review, Aerosol Air Qual. Res. 14 (2014) 453–469.

[79] C.C. Wang, Y.Q. Zhang, J. Li, P. Wang, Photocatalytic CO_2 reduction in metal-organic frameworks: A mini review, J. Mol. Struct. 1083 (2015) 127–136.
[80] M. Anpo, H. Yamashita, Y. Ichihashi, S. Ehara, Photocatalytic reduction of CO_2 with H_2O on various titanium oxide catalysts, J. Electroanal. Chem. 396 (1995) 21–26.
[81] S.N. Habisreutinger, L. Schmidt-Mende, J.K. Stolarczyk, Photocatalytic reduction of CO_2 on TiO_2 and other semiconductors, Angew. Chemie Int. Ed. 52 (2013) 7372–7408.
[82] N.N. Vu, S. Kaliaguine, T.O. Do, Critical aspects and recent advances in structural engineering of photocatalysts for sunlight-driven photocatalytic reduction of CO_2 into fuels, Adv. Funct. Mater. 29 (2019) 1901825.
[83] O. Ola, M.M. Maroto-Valer, Review of material design and reactor engineering on TiO_2 photocatalysis for CO_2 reduction, J. Photochem. Photobiol. C Photochem. Rev. 24 (2015) 16–42.
[84] H.S. Auta, C.U. Emenike, S.H. Fauziah, Distribution and importance of microplastics in the marine environment: A review of the sources, fate, effects, and potential solutions, Environ. Int. 102 (2017) 165–176.
[85] M.R.D. Khaki, M.S. Shafeeyan, A.A.A. Raman, W.M.A.W. Daud, Application of doped photocatalysts for organic pollutant degradation - A review, J. Environ. Manage. 198 (2017) 78–94.
[86] T. Aarthi, G. Madras, Photocatalytic degradation of rhodamine dyes with nano-TiO_2, Ind. Eng. Chem. Res. 46 (2007) 7–14.
[87] L. Cui, X. Ding, Y. Wang, H. Shi, L. Huang, Y. Zuo, S. Kang, Applied surface science facile preparation of Z-scheme WO_3/g-C_3N_4 composite photocatalyst with enhanced photocatalytic performance under visible light, Appl. Surf. Sci. 391 (2017) 202–210.
[88] C. Annabi, F. Fourcade, I. Soutrel, F. Geneste, D. Floner, N. Bellakhal, A. Amrane, Degradation of enoxacin antibiotic by the electro-Fenton process: Optimization, biodegradability improvement and degradation mechanism, J. Environ. Manage. 165 (2016) 96–105.
[89] Y. Fu, L. Peng, Q. Zeng, Y. Yang, H. Song, J. Shao, S. Liu, J. Gu, High efficient

removal of tetracycline from solution by degradation and flocculation with nanoscale zerovalent iron, Chem. Eng. J. 270 (2015) 631–640.

[90] H. Wang, D. Zhang, S. Mou, W. Song, F.A. Al-Misned, M.G. Mortuza, X. Pan, Simultaneous removal of tetracycline hydrochloride and As(III) using poorly-crystalline manganese dioxide, Chemosphere 136 (2015) 102–110.

[91] L. Zhang, W. Tian, Y. Chen, J. Chen, H. Teng, J. Zhou, J. Shi, Y. Sun, Light-driven removal of rhodamine B over $SrTiO_3$ modified Bi_2WO_6 composites, RSC Adv. 6 (2016) 83471–83481.

[92] X. Wang, J. Jia, Y. Wang, Combination of photocatalysis with hydrodynamic cavitation for degradation of tetracycline, Chem. Eng. J. 315 (2017) 274–282.

[93] X. Liu, Y. Zhang, Y. Jia, J. Jiang, Y. Wang, X. Chen, T. Gui, Visible light-responsive carbon-decorated p-type semiconductor $CaFe_2O_4$ nanorod photocatalyst for efficient remediation of organic pollutants, Chinese J. Catal. 38 (2017) 1770–1779.

[94] J. Jiang, Y. Jia, Y. Wang, R. Chong, L. Xu, X. Liu, Insight into efficient photocatalytic elimination of tetracycline over $SrTiO_3$(La,Cr)under visible-light irradiation: The relationship of doping and performance, Appl. Surf. Sci. 486 (2019) 93–101.

[95] J. Mohanraj, D. Durgalakshmi, S. Balakumar, P. Aruna, S. Ganesan, S. Rajendran, M. Naushad, Low cost and quick time absorption of organic dye pollutants under ambient condition using partially exfoliated graphite, J. Water Process Eng. 34 (2020) 101078.

[96] I. Ali, M. Asim, T.A. Khan, Low cost adsorbents for the removal of organic pollutants from wastewater, J. Environ. Manage. 113 (2012) 170–183.

[97] L.X. Zhou, J.W.C. Wong, Microbial decomposition of dissolved organic matter and its control during a sorption experiment, J. Environ. Qual. 29 (2000) 1852–1856.

[98] Y. Dai, L. Yin, S. Wang, Y. Song, Shape-selective adsorption mechanism of CS-Z1 microporous molecular sieve for organic pollutants, J. Hazard. Mater. 392 (2020) 122314.

[99] S. Luo, L. Duan, B. Sun, M. Wei, X. Li, A. Xu, Manganese oxide octahedral

molecular sieve (OMS-2) as an effective catalyst for degradation of organic dyes in aqueous solutions in the presence of peroxymonosulfate, Appl. Catal. B Environ. 164 (2015) 92–99.

[100] C.M. Teh, A.R. Mohamed, Roles of titanium dioxide and ion-doped titanium dioxide on photocatalytic degradation of organic pollutants (phenolic compounds and dyes) in aqueous solutions: A review, J. Alloys Compd. 509 (2011) 1648–1660.

[101] D. Zhu, Q. Zhou, Action and mechanism of semiconductor photocatalysis on degradation of organic pollutants in water treatment: A review, Environ. Nanotechnology, Monit. Manag. 12 (2019) 100255.

[102] I.G. Umar, A.A. Halim, Heterogeneous photocatalytic degradation of organic contaminants over titanium dioxide: A review of fundamentals, progress and problems, J. Photochem. Photobiol. C Photochem. Rev. 9 (2007) 1–12.

[103] X. Liu, J. Jiang, Y. Jia, J. Qiu, T. Xia, Y. Zhang, Y. Li, X. Chen, Insight into synergistically enhanced adsorption and visible light photocatalytic performance of Z-scheme heterojunction of $SrTiO_3$ (La,Cr)-decorated WO_3 nanosheets, Appl. Surf. Sci. 412 (2017) 279–289.

[104] M. Cheng, C. Xiao, Y. Xie, Photocatalytic nitrogen fixation: The role of defects in photocatalysts, J. Mater. Chem. A 7 (2019) 19616–19633.

[105] C.V. Reddy, K.R. Reddy, N.P. Shetti, J. Shim, T.M. Aminabhavi, D.D. Dionysiou, Hetero-nanostructured metal oxide-based hybrid photocatalysts for enhanced photoelectrochemical water splitting – A review, Int. J. Hydrogen Energy 45 (2020) 18331–18347.

[106] Y. Sakata, T. Hayashi, R. Yasunaga, N. Yanaga, H. Imamura, Remarkably high apparent quantum yield of the overall photocatalytic H_2O splitting achieved by utilizing Zn ion added Ga_2O_3 prepared using dilute $CaCl_2$ solution, Chem. Commun. 51 (2015) 12935-12938.

[107] Y. Sakata, T. Nakagawa, Y. Nagamatsu, Y. Matsuda, R. Yasunaga, E. Nakao, H. Imamura, Photocatalytic properties of gallium oxides prepared by precipitation methods toward the overall splitting of H_2O, J. Catal. 310 (2014) 45–50.

[108] X. Wang, H. Zhang, L. Liu, W. Li, P. Cao, Controlled morphologies and growth

direction of WO_3 nanostructures hydrothermally synthesized with citric acid, Mater. Lett. 130 (2014) 248–251.

[109] H. Kato, K. Asakura, A. Kudo, Highly efficient water splitting into H_2 and O_2 over lanthanum-doped $NaTaO_3$ photocatalysts with high crystallinity and surface nanostructure, J. Am. Chem. Soc. 125 (2003) 3082–3089.

[110] L.P. E. García-López, G. Marcì, B. Megna, F. Parisi, L. Armelao, A. Trovarelli, M. Boaro, $SrTiO_3$-based perovskites Preparation, characterization and photocatalytic activity in the gas-solid regime under simulated solar irradiation, J. Catal. 321 (2005) 13–22.

[111] K. Maeda, K. Domen, Chapter 12 Nano-particulate photocatalysts for overall water splitting under visible light, Theor. Comput. Chem. 18 (2007) 301–315.

[112] G. Hitoki, T. Takata, J.N. Kondo, M. Hara, H. Kobayashi, K. Domen, An oxynitride, TaON, as an efficient water oxidation photocatalyst under visible light irradiation ($\lambda \leq 500$ nm), Chem. Commun. 2 (2002) 1698–1699.

[113] Z. Wang, Y. Inoue, T. Hisatomi, R. Ishikawa, Q. Wang, T. Takata, S. Chen, N. Shibata, Y. Ikuhara, K. Domen, Overall water splitting by Ta_3N_5 nanorod single crystals grown on the edges of $KTaO_3$ particles, Nat. Catal. 1 (2018) 756–763.

[114] W.-J. Ong, L.-L. Tan, Y.H. Ng, S.-T. Yong, S.-P. Chai, Graphitic carbon nitride (g-C_3N_4)-based photocatalysts for artificial photosynthesis and environmental remediation: Are we a step closer to achieving sustainability? Chem. Rev. 116 (2016) 7159–7329.

[115] M.Z. Rahman, M.G. Kibria, C.B. Mullins, Metal-free photocatalysts for hydrogen evolution, Chem. Soc. Rev. 49 (2020) 1887–1931.

[116] G. Zhang, Z.A. Lan, L. Lin, S. Lin, X. Wang, Overall water splitting by Pt/g-C_3N_4 photocatalysts without using sacrificial agents, Chem. Sci. 7 (2016) 3062–3066.

[117] K. Teramura, K. Maeda, T. Saito, T. Takata, N. Saito, Y. Inoue, K. Domen, Characterization of ruthenium oxide nanocluster as a cocatalyst with $(Ga_{1-x}Zn_x)(N_{1-x}O_x)$ for photocatalytic overall water splitting, J. Phys. Chem. B 109 (2005) 21915–21921.

[118] B. Liu, J. Li, W. Yang, X. Zhang, X. Jiang, Y. Bando, Semiconductor solid-

solution nanostructures: Synthesis, property tailoring, and applications, Small 13 (2017) 1701998.

[119] K. Maeda, T. Takata, M. Hara, N. Saito, Y. Inoue, H. Kobayashi, K. Domen, GaN:ZnO solid solution as a photocatalyst for visible-light-driven overall water splitting, J. Am. Chem. Soc. 127 (2005) 8286–8287.

[120] K. Maeda, K. Teramura, T. Takata, M. Hara, N. Saito, K. Toda, Y. Inoue, H. Kobayashi, K. Domen, Overall water splitting on $(Ga_{1-x}Zn_x)(N_{1-x}O_x)$ solid solution photocatalyst: Relationship between physical properties and photocatalytic activity, J. Phys. Chem. B 109 (2005) 20504–20510.

[121] K. Maeda, K. Teramura, D. Lu, T. Takata, N. Saito, Photocatalyst releasing hydrogen from water water splitting, Nature 440 (2006) 9.

[122] K. Maeda, K. Teramura, D. Lu, N. Saito, Y. Inoue, K. Domen, Noble-metal/Cr_2O_3 core/shell nanoparticles as a cocatalyst for photocatalytic overall water splitting, Angew. Chemie - Int. Ed. 45 (2006) 7806–7809.

[123] K. Maeda, K. Teramura, N. Saito, Y. Inoue, K. Domen, Improvement of photocatalytic activity of $(Ga_{1-x}Zn_x)(N_{1-x}O_x)$ solid solution for overall water splitting by co-loading Cr and another transition metal, J. Catal. 243 (2006) 303–308.

[124] K. Maeda, K. Teramura, K. Domen, Development of cocatalysts for photocatalytic overall water splitting on $(Ga_{1-x}Zn_x)(N_{1-x}O_x)$ solid solution, Catal. Surv. from Asia. 11 (2007) 145–157.

[125] K. Maeda, N. Sakamoto, T. Ikeda, H. Ohtsuka, A. Xiong, D. Lu, M. Kanehara, T. Teranishi, K. Domen, Preparation of core-shell-structured nanoparticles (with a noble-metal or metal oxide core and a chromia shell) and their application in water splitting by means of visible light, Chem. - A Eur. J. 16 (2010) 7750–7759.

[126] E. García-López, G. Marcì, B. Megna, F. Parisi, L. Armelao, A. Trovarelli, M. Boaro, L. Palmisano, $SrTiO_3$-based perovskites: Preparation, characterization and photocatalytic activity in gas-solid regime under simulated solar irradiation, J. Catal. 321 (2015) 13–22.

[127] S. Wang, K. Teramura, T. Hisatomi, K. Domen, H. Asakura, S. Hosokawa, T. Tanaka, Effective driving of Ag-loaded and Al-doped $SrTiO_3$ under irradiation at

$\lambda > 300$ nm for the photocatalytic conversion of CO_2 by H_2O, ACS Appl. Energy Mater. 3 (2020) 1468–1475.

[128] K. Maeda, D. Lu, K. Teramura, K. Domen, Direct deposition of nanoparticulate rhodium-chromium mixed-oxides on a semiconductor powder by band-gap irradiation, J. Mater. Chem. 18 (2008) 3539–3542.

[129] K. Kato, J. Jiang, Y. Sakata, A. Yamakata, Effect of Na-doping on electron decay kinetics in $SrTiO_3$ photocatalyst, ChemCatChem 11 (2019) 6349–6354.

[130] R. Asai, H. Nemoto, Q. Jia, K. Saito, A. Iwase, A. Kudo, A visible light responsive rhodium and antimony-codoped $SrTiO_3$ powdered photocatalyst loaded with an IrO_2 cocatalyst for solar water splitting, Chem. Commun. 50 (2014) 2543–2546.

[131] S. Suzuki, H. Matsumoto, A. Iwase, A. Kudo, Enhanced H_2 evolution over an Ir-doped $SrTiO_3$ photocatalyst by loading of an Ir cocatalyst using visible light up to 800 nm, Chem. Commun. 54 (2018) 10606–10609.

[132] D.A. Tenne, I.E. Gonenli, A. Soukiassian, D.G. Schlom, S.M. Nakhmanson, K.M. Rabe, X.X. Xi, Raman study of oxygen reduced and re-oxidized strontium titanate, Phys. Rev. B - Condens. Matter Mater. Phys. 76 (2007) 1–7.

[133] T. Hisatomi, K. Maeda, K. Takanabe, J. Kubota, K. Domen, Aspects of the water splitting mechanism on $(Ga_{1-x}Zn_x)(N_{1-x}O_x)$ photocatalyst modified with $Rh_{2-y}Cr_yO_3$ Cocatalyst, J. Phys. Chem. C 113 (2009) 21458–21466.

[134] K. Domen, S. Naito, T. Onishi, K. Tamaru, M. Soma, Study of the photocatalytic decomposition of water vapor over a nickel(II) oxide-strontium titanate ($SrTiO_3$) catalyst, J. Phys. Chem. 86 (1982) 3657–3661.

[135] K. Domen, S. Naito, T. Onishi, K. Tamaru, Photocatalytic decomposition of liquid water on a NiO-$SrTiO_3$ catalyst, Chem. Phys. Lett. 92 (1982) 433–434.

[136] Y. Hiramachi, H. Fujimori, A. Yamakata, Y. Sakata, Achievement of high photocatalytic performance to $BaTi_4O_9$ toward overall H_2O splitting, ChemCatChem 11 (2019) 6213–6217.

[137] T. Takata, K. Domen, Defect engineering of photocatalysts by doping of aliovalent metal cations for efficient water splitting, J. Phys. Chem. C 113 (2009) 19386–19388.

[138] Y. Sakata, Y. Miyoshi, T. Maeda, K. Ishikiriyama, Y. Yamazaki, H. Imamura, Y. Ham, T. Hisatomi, J. Kubota, A. Yamakata, K. Domen, Photocatalytic property of metal ion added $SrTiO_3$ to overall H_2O splitting, Appl. Catal. A Gen. 521 (2016) 227–232.

[139] Y. Ham, T. Hisatomi, Y. Goto, Y. Moriya, Y. Sakata, A. Yamakata, J. Kubota, K. Domen, Flux-mediated doping of $SrTiO_3$ photocatalysts for efficient overall water splitting, J. Mater. Chem. A 4 (2016) 3027–3033.

[140] D. Wang, J. Ye, T. Kako, T. Kimura, Photophysical and photocatalytic properties of $SrTiO_3$ doped with Cr cations on different sites, J. Phys. Chem. B 110 (2006) 15824–15830.

[141] J. Wang, T. Fang, S. Yan, Z. Li, T. Yu, Z. Zou, Highly efficient visible light photocatalytic activity of Cr-La codoped $SrTiO_3$ with surface alkalinization: An insight from DFT calculation, Comput. Mater. Sci. 79 (2013) 87–94.

[142] H. Yu, J. Wang, S. Yan, T. Yu, Z. Zou, Elements doping to expand the light response of $SrTiO_3$, J. Photochem. Photobiol. A Chem. 275 (2014) 65–71.

[143] E. Grabowska, M. Marchelek, T. Klimczuk, W. Lisowski, A. Zaleska-Medynska, TiO_2/$SrTiO_3$ and $SrTiO_3$ microspheres decorated with Rh, Ru or Pt nanoparticles: Highly UV–vis responsible photoactivity and mechanism, J. Catal. 350 (2017) 159–173.

[144] K. Iwashina, A. Kudo, Rh-doped $SrTiO_3$ photocatalyst electrode showing cathodic photocurrent for water splitting under visible-light irradiation, J. Am. Chem. Soc. 133 (2011) 13272–13275.

[145] R. Konta, T. Ishii, H. Kato, A. Kudo, Photocatalytic activities of noble metal ion doped $SrTiO_3$ under visible light irradiation, J. Phys. Chem. B 108 (2004) 8992–8995.

[146] T. Hirakawa, P. V. Kamat, Charge separation and catalytic activity of Ag@TiO_2 core-shell composite clusters under UV-irradiation, J. Am. Chem. Soc. 127 (2005) 3928–3934.

[147] H. Kato, M. Kobayashi, M. Hara, M. Kakihana, Fabrication of $SrTiO_3$ exposing characteristic facets using molten salt flux and improvement of photocatalytic activity for water splitting, Catal. Sci. Technol. 3 (2013) 1733–1738.

[148] N. Cheng, J. Tian, Q. Liu, C. Ge, A.H. Qusti, A.M. Asiri, A.O. Al-Youbi, X. Sun, Au-nanoparticle-loaded graphitic carbon nitride nanosheets: Green photocatalytic synthesis and application toward the degradation of organic pollutants, ACS Appl. Mater. Interfaces. 5 (2013) 6815–6819.

[149] P.L. Hsieh, G. Naresh, Y.S. Huang, C.W. Tsao, Y.J. Hsu, L.J. Chen, M.H. Huang, Shape-tunable $SrTiO_3$ crystals revealing facet-dependent optical and photocatalytic properties, J. Phys. Chem. C 123 (2019) 13664–13671.

[150] L. Mu, Y. Zhao, A. Li, S. Wang, Z. Wang, J. Yang, Y. Wang, T. Liu, R. Chen, J. Zhu, F. Fan, R. Li, C. Li, Enhancing charge separation on high symmetry $SrTiO_3$ exposed with anisotropic facets for photocatalytic water splitting, Energy Environ. Sci. 9 (2016) 2463–2469.

[151] R.C. Pawar, S. Kang, J.H. Park, J. Kim, S. Ahn, C.S. Lee, Room-temperature synthesis of nanoporous 1D microrods of graphitic carbon nitride (g-C_3N_4) with highly enhanced photocatalytic activity and stability, Nat. Publ. Gr. (2016) 1–14.

[152] S. Okunaka, H. Tokudome, R. Abe, Structure-controlled porous films of nanoparticulate Rh-doped $SrTiO_3$ photocatalyst toward efficient H_2 evolution under visible light irradiation, Catal. Sci. Technol. 6 (2016) 254–260.

[153] L. Gan, L. Xu, K. Qian, Preparation of core-shell structured $CoFe_2O_4$ incorporated Ag_3PO_4 nanocomposites for photocatalytic degradation of organic dyes, Mater. Des. 109 (2016) 354–360.

[154] J. Low, C. Jiang, B. Cheng, S. Wageh, A.A. Al-Ghamdi, J. Yu, A review of direct Z-scheme photocatalysts, Small Methods 1 (2017) 1700080.

[155] A.J. Bard, Photoelectrochemistry and heterogeneous photo-catalysis at semiconductors, J. Photochem. 10 (1979) 59–75.

[156] Q. Wang, T. Hisatomi, Q. Jia, H. Tokudome, M. Zhong, C. Wang, Z. Pan, T. Takata, M. Nakabayashi, N. Shibata, Y. Li, I.D. Sharp, A. Kudo, T. Yamada, K. Domen, Scalable water splitting on particulate photocatalyst sheets with a solar-to-hydrogen energy conversion efficiency exceeding 1%, Nat. Mater. 15 (2016) 611–615.

Chapter 2 Investigation on the Highly Active $SrTiO_3$ Photocatalyst toward Overall H_2O Splitting by Doping Na Ion

2.1 Introduction

Photocatalytic overall H_2O splitting is regarded as one of the effective techniques for the production of H_2 from H_2O. If the photocatalytic reaction proceeds under solar irradiation efficiently, this technique will become attractive for the sustainable and large-scale production of H_2 from H_2O. Therefore, a large number of investigations have been performed to develop photocatalysts that exhibit sufficient photocatalytic performance for overall H_2O splitting [1–5]. Among the investigations, a remarkable improvement of the photocatalytic activity for overall water splitting was reported by the doping of metal ions and the combination of effective co-catalyst, such as $Rh_{2-y}Cr_yO_3$ with the photocatalysts under the deep-ultraviolet (UV) irradiation [6–12]. However, few photocatalysts showed sufficient performance for the photocatalytic reactions under solar irradiation [7,13–18].

$SrTiO_3$ is one of the promising photocatalysts for overall water splitting under near-UV light irradiation since the band-gap of this photocatalyst is 3.2 eV and has been widely studied due to its high dielectric constant, low loss, good thermal stability, and excellent

photocatalytic activity [6,15–17,19–23]. Takata et al reported the photocatalytic activity of $SrTiO_3$ could be improved by doping aliovalent metal cations originated with the concept of defect engineering, which greatly promotes the development of $SrTiO_3$ used in photocatalysis under near-UV light irradiation [15]. Moreover, in recent studies, the photocatalytic activity of $SrTiO_3$ was further improved by applying a flux method for the preparation as well as doping aliovalent metal ions with the valence lower than that of the parent cation in $SrTiO_3$ [3,15,20,24,25]. Particularly, Al ion-doped $SrTiO_3$ was prepared using $SrCl_2$ flux treatments. Great achievements have also been achieved in the photocatalytic activity and durability of the photocatalysts by co-loading suitable dual co-catalysts [20,24,25]. Furthermore, this photocatalyst was reported to apply to a panel-type reactor and the photocatalytic overall water splitting under sunlight irradiation has been demonstrated [3].

In our previous work, the photocatalytic properties of $SrTiO_3$ by adding various metal ions using an impregnation method were studied [16]. In the study, adding various aliovalent ions with the lower valence than the parent cation of $SrTiO_3$ was further confirmed to be a remarkable approach to enhance the photocatalytic activity. Among the aliovalent metal cations, the Na ion was confirmed to be one of the effective additives. Na ion (Na^+) which valence is lower than the parent cation of Sr^{2+} adding into $SrTiO_3$ exhibited better activity than that of other low valance metal ions added $SrTiO_3$ using the impregnation method, showing good application prospect and development space. Moreover, the study demonstrated the states of the original $SrTiO_3$ for metal ions incorporation had a significant impact on the photocatalytic performance. Nevertheless, the detailed effects of the preparation methods and preparation conditions of metal ion-doped $SrTiO_3$ on the water-splitting reaction have not been investigated in the previous reports. There is also little evidence to support the exact doping position of the metal ions and the existence of defect structure. Considering the effective preparation of metal ion-doped $SrTiO_3$ photocatalysts, various problems are still existing.

In this study, we further investigate the photocatalytic properties of Na^+-$SrTiO_3$ toward the overall H_2O splitting to develop highly active $SrTiO_3$ photocatalysis. Here, we report the effective preparation conditions and states of photocatalyst as well as the effects of Na-doping in $SrTiO_3$ on the improvement of the photocatalytic activity. The contribution of doped Na ion to the improvement of the photocatalytic activity is discussed on the basis of the investigations of structure and individual behavior of photogenerated charge carriers by Raman and transient absorption spectroscopy.

2.2 Experimental section

2.2.1 Preparation of Na ion-doped $SrTiO_3$ photocatalyst

Na ion-doped $SrTiO_3$ powder was prepared by the polymerizable complex (PC) method and solid-state reaction (SSR) method. The details of the preparation process used are described in the previous report [16]. The Sr, Na, and Ti citrate-ethylene glycol mixed solution with the molar ratio of 1-x: x: 1 (x represents the number of Na atoms) was prepared by dissolving the raw materials, Titanium isopropoxide, citric acid (Wako pure chemical, 98%), $SrCO_3$ (Wako pure chemical, 99.99%), and Na_2CO_3 (Asahi Glass Co. Ltd., 99.98%) in ethylene glycol (Wako pure chemical, 95%). The polymer precursor was formed after the polymerization was carried out at 458 K for 2 h under reflux. The polymer precursor was calcined in an alumina crucible at the specified temperature for 20 h to obtain the final different amount of Na ion-doped $SrTiO_3$ samples (Denoted as Na^+(x mol%)-$SrTiO_3$ (PC)).

For the SSR method, the starting materials $SrCO_3$, TiO_2, and Na_2CO_3 were mixed in the necessary ratios and mechanically grinding in an agate mortar to obtain the precursor of Sr: Na: Ti = 1-x: x: 1 (x represents the number of Na atoms). Next, the prepared mixtures were put in the alumina crucible and calcined at a prescribed temperature for 20 h to obtain the different amounts of Na ion-doped $SrTiO_3$ photocatalyst. Four kinds of TiO_2 materials with different purity (TiO_2 (A), 98%; TiO_2 (B), 99%; TiO_2 (C), 99.9%; TiO_2 (D), 99.99%) were applied. The detailed information about these TiO_2 materials is presented in Table 2-1. The obtained samples were denoted as Na^+(x mol%)-$SrTiO_3$ (SSR).

Table 2-1 Information of TiO_2 materials used for preparing Na^+-$SrTiO_3$ by the SSR method.

TiO_2 materials	**Manufacture**	**Crystal form**	**BET surface areas/ m^2 g^{-1}**	**Purity**
TiO_2 (A)	High purity chemicals	anatase	9.5196	98%
TiO_2 (B)	High purity chemicals	anatase	6.1187	99%
TiO_2 (C)	Wako pure chemicals	rutile	2.3568	99.9%
TiO_2 (D)	High purity chemicals	rutile	11.393	99.99%

2.2.2 Loading of co-catalysts

A mixed oxide of rhodium and chromium, $Rh_{0.7}Cr_{1.3}O_3$ (Rh: 0.3 wt%) was applied as a co-catalyst [9,26]. The loading of co-catalyst was carried out by an impregnation method, where the as-prepared sample was suspended in an $RhCl_3$ and $Cr(NO_3)_3$ mixed solution in which Rh and Cr ion were contained in the prescribed amount. The suspension was evaporated and then calcined at 623 K for 2 h in air.

The second co-catalyst Co species was loaded onto $Rh_{0.7}Cr_{1.3}O_3/Na^+$-$SrTiO_3$ by a photo-deposition method [20,27]. A prescribed amount of $Co(NO_3)_2$ aqueous solution was contained in the reaction solution before performing the photocatalytic reaction. The CoO_x was loaded during the overall water splitting reaction.

2.2.3 Photocatalytic overall H_2O splitting reaction

Photocatalytic overall water splitting was carried out in an inner-irradiation type photoreaction cell as shown in Figure 2-1. The cell was connected with an iso-volumetric system equipped with a gas chromatography sample inlet and vacuum line. Photocatalyst (1 g) was suspended in well-outgassed H_2O (600 mL) in the cell and then photoirradiation started. Photo-irradiation was performed from 450 W high-pressure Hg-lamp (USHIO UM-452, detailed power spectrum in Fig 2-2) through a water-cooling jacket made of quartz glass. The evolved gases were collected in the sampling tube and analyzed by gas chromatography (Shimadzu GC-8A). For measuring the durability of the photocatalyst, the system was open if the pressure in the system reached atmospheric pressure and the photocatalytic activity was evaluated by the amount of produced gases measured by a soap-film flow meter, where the composition of the produced gases was also measured by gas chromatography.

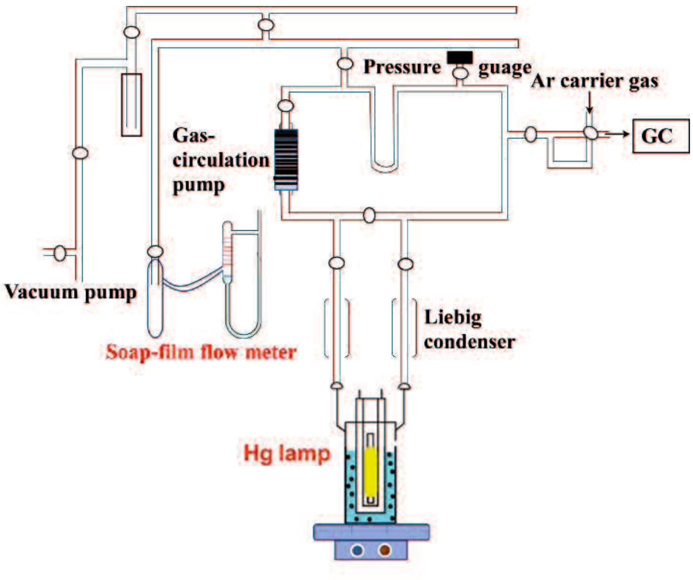

Figure 2-1. Apparatus for photocatalytic overall water splitting reaction.

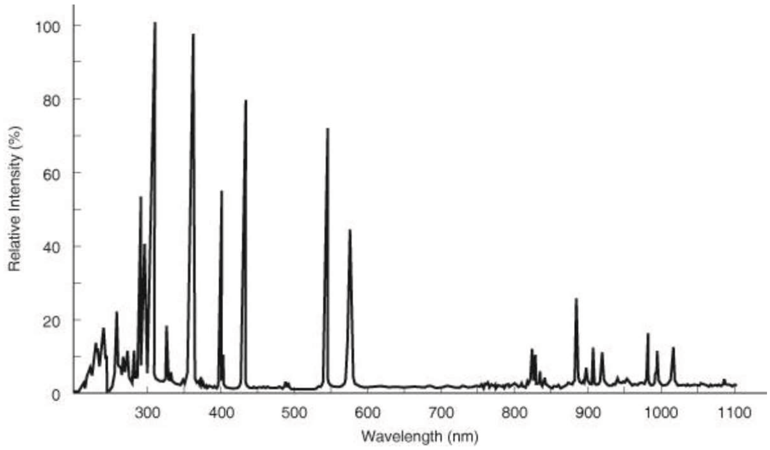

Figure 2-2. Power spectrum of the 450 W high-pressure Hg lamp in this study.

The apparent quantum yield (AQY) of overall water splitting was evaluated from the photocatalytic reaction by using a top-irradiation type photoreaction cell connected with the isovolumetric system written above as shown in Figure 2-3. The detailed procedures were reported in our previous publication [16,25,28]. Photo-irradiation was carried out from a 500 W Deep UV lamp (USHIO). The irradiation of monochromatic light was performed by inserting a band-pass filter (= 365 nm, Edmond Optics) in the light path. The light intensity dependence of overall water splitting was also performed. The light intensity was changed by attaching the corresponding neutral density (ND = 0, 0.3, 0.5, 1.0 and 2.0) filters. The number of photons concerning the photocatalytic reaction was evaluated from the H_2 production rate. The number of incident photons was evaluated from the photocurrent by using a calibrated Si-photodiode (Hamamatsu Photonics) under nearly the same condition as the photocatalytic reaction. The AQY was evaluated by the equation as follows:

AQY% = ((Number of electrons concerning photocatalytic reaction)/(Number of incident photons)) × 100

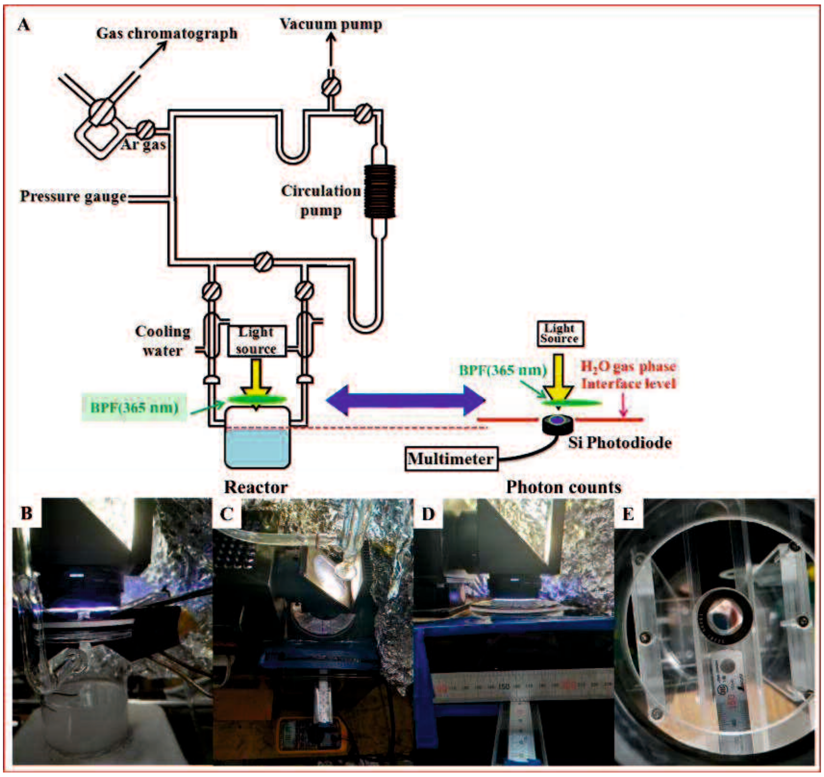

Figure 2-3. (A) Photographs of the devices used in the measurement. (B) side view of the measurement system. (C) top view of the measurement system. (D) arrangement of the lamp and reactor. (E) arrangement of the Si photodiode.

2.2.4 Characterization

The crystal structures of the as-prepared photocatalysts were determined by a powder X-ray diffraction (XRD) using Cu Kα radiation (Rigaku Smart lab 9/SWXD). The morphology of as-prepared samples was observed by field-emission scanning electron microscopy (SEM, JEOL, JSM 6335F). The specific surface areas (BET) were determined by measuring N_2 adsorption (Bel-sorp mini II) at 77 K. The UV-vis diffuse reflectance spectroscopy (Jasco. V-550DS) was applied to analyze the absorption spectra of samples equipped with an integrating sphere. The composition of the photocatalysts was confirmed by the measurement of transmission electron microscopy and energy dispersive X-ray emission spectrum (STEM-EDS, JEOL JEM-2100 for Figure 2-8 and JEM-ARM200F for Figure 2-9).

2.2.5 Raman spectroscopy

Raman measurements were performed using a continuous wave (CW) Raman spectroscopic system (JUPITER PDPT640-FJM, Photon Design Corporation, Japan) based on 2nd/3rd YAG lasers (532/355 nm), macro/micro-sample compartments (laser spot size: 100/1 μm), a two-dimensional front-illuminated open electrode charge-coupled device (CCD) detector (PIXIS 256OE, Princeton Instruments), and a single monochromator (modified HR 640, Jobin Yvon - Spex)/conjunct with a pre-monochromator (triple monochromator). A spatial filter is placed at an imaging point of the sample located between each sample compartment and the incident slit of the spectrometer (rigorously confocal optical system). The laser wavelength of 532 nm (2nd-YAG) was selected for visible excitation. The laser power at the laser oscillator was set at 150 mW. The laser spot size was about 100 μm in diameter at the sample point (macro). The single monochromator mode was chosen with a highly efficient edge filter. The entrance slit width at the spectrometer was set at 100 μm. A Hg line was used for Raman-shift calibration for each measurement. No artificial smoothing was used on the acquired Raman spectra.

2.2.6 Transient absorption spectroscopy

The transient absorption spectra of photogenerated charge carriers were measured with the spectrometers described previously [29]. Briefly, samples were excited by the third harmonics of a Nd:YAG laser (Continuum, Surelite II; 355 nm wavelength, 6 ns duration, 0.5 mJ pulse energy, 5 Hz repetition rate). As a probe light, the light from a halogen lamp was used in the visible (25,000-10,000 cm^{-1}) and near IR (10,000-6000 cm^{-1}) regions,

while that from a $MoSi_2$ coil was used in the mid-IR region (6000-1000 cm^{-1}). The transmitted or diffuse reflected probe light was monochromated by a spectrometer, and then detected by a Si, InGaAs, and MCT detector in the visible, near IR and mid-IR region, respectively. For the detailed analysis of the decay kinetics of photogenerated charge carriers, femtosecond transient absorption measurements were conducted by using a femtosecond Ti:sapphire laser system (Spectra-Physics, Solstice & TOPAS Prime; 90 fs duration; 1 kHz repetition rate). The 355 nm pulses (6 μJ $pulse^{-1}$) were used to excite the samples. As the probe light, the 24,000 cm^{-1}, 12,000 cm^{-1}, and 2000 cm^{-1} pulses were used, which are detected by a photomultiplier tube, InGaAs, and MCT detector, respectively.

2.3 Results and discussion

2.3.1 Characterization of photocatalysts

Figure 2-4 shows the XRD patterns of Na^+-$SrTiO_3$ (SSR, TiO_2 (D)) prepared using various amounts of doped Na ion, where the amounts of doped Na ion are 0 mol%, 2 mol%, 4 mol%, 5 mol%, and 6 mol%, respectively. Figure 2-4(a) shows the diffraction patterns at the range of 2θ from 10 ° to 80 ° and Figure 2-4(b) shows the diffraction peak attributed to [110] reflection in the range of 2θ from 31 ° to 33 ° using NaCl (200) peak as the standard for the diffracted angle. As shown in Figure 2-4(a), the diffraction peaks of Na^+-$SrTiO_3$ (SSR) are attributable to $SrTiO_3$ and the peaks are sharp and intense, indicating their high crystalline nature. No impurity peaks and no significant differences are observed among the XRD patterns if the content of doped Na ion was varied. This also suggests that the added Na ion disperses homogeneously in the bulk of $SrTiO_3$. Accordingly, the detailed examination of diffraction peak was carried out to know the state of Na^+-$SrTiO_3$ and the results are shown in Figure 2-4(b).

As shown in Figure 2-4(b), the diffraction peak attributed to [110] reflection of $SrTiO_3$ is noticed to systematically shift to a higher angle as well as there is a slight contraction of d-spacing in Table 2-2 when the amount of Na doping is more than 4 mol%. The reason for the slight contraction of d-spacing is that the radius of Na^+ (139 pm) is slightly smaller than that of Sr^{2+}(144 pm), confirming that Na^+ is incorporated into the Sr^{2+}-site in $SrTiO_3$ lattice [30,31]. The tolerance-values of the samples shown in Table 2-3 as a function of the amount of doped Na^+ are the normally allowed t-values ($0.75 < t < 1.0$) shown in Table 2-2.

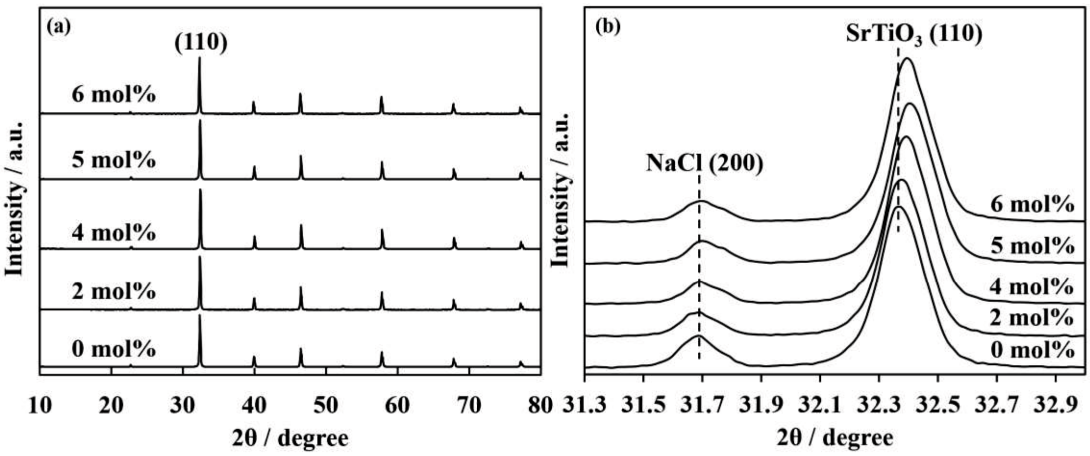

Figure 2-4. (a) XRD patterns of Na^+-$SrTiO_3$ (SSR, TiO_2 (D), preparation temperature: 1273 K) at the various amount of doped Na ion (a) diffraction pattern at the 2θ range between 10 ° and 80 ° and (b) diffraction peak [110] of $SrTiO_3$ (SSR, TiO_2 (D)) doped a series of Na^+ corrected by NaCl (200) as a standard of 2θ angle.

Table 2-2. The lattice space and t-values of Na^+-$SrTiO_3$ as a function of the amount of doped Na^+.

Amount of doped Na^+ / mol%	2θ / degree	d-spacing / nm	t (tolerance factor)
0	32.372	0.2763	0.9988
2	32.372	0.2763	0.9985
4	32.392	0.2762	0.9981
5	32.412	0.276	0.998
6	32.392	0.2762	0.9978

Bragg equation $\boldsymbol{d} = \frac{n\lambda}{2sin\theta}$ (n=1, λ = 0.15406 nm, θ is the angle between the incident ray and the reflecting surface)

tolerance factor $\boldsymbol{t} = (r_A + r_O))/\sqrt{2}(r_B + r_O)$ (r_A = 144 pm, r_{Na^+} = 139 pm, r_B = 60.5 pm and r_O=142 pm are the empirical ionic radii at room temperature) as defined by Goldschmidt for maintaining the ABO_3 perovskite structure.

To know the influences of Na^+ doping on the photo-absorption property of $SrTiO_3$. The visible-light absorption property and crystalline structure of Na ion-doped $SrTiO_3$ samples prepared by the SSR method were analyzed by UV–vis absorption spectra and X-ray diffraction patterns. The UV–Vis absorption edges of $SrTiO_3$ and Na^+-$SrTiO_3$ prepared by the two methods were displayed in Figure 2-5. The results show that the band structure of Na^+-$SrTiO_3$ substantially the same as that of $SrTiO_3$, suggesting the improvement of the photocatalytic activity was not caused by the photoresponse.

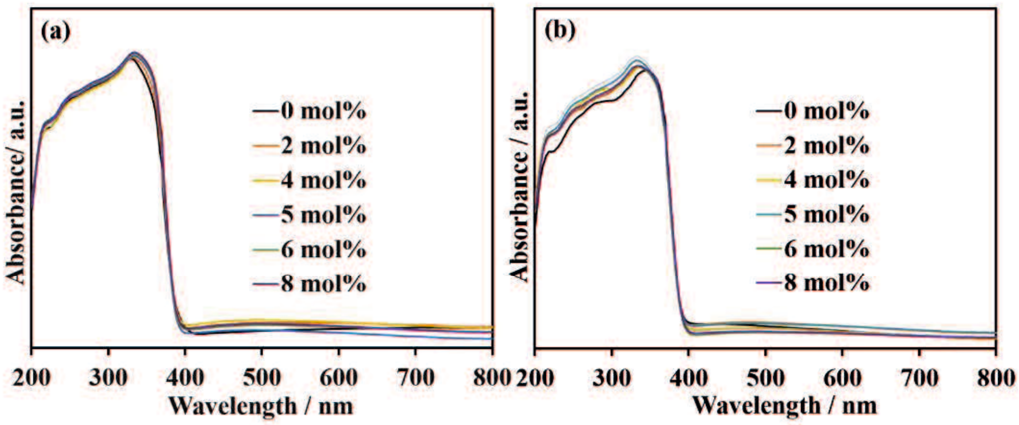

Figure 2-5. UV-Vis absorbance spectra of (a) Na^+-$SrTiO_3$ (SSR, TiO_2 (D), preparation temperature: 1273 K), (b) Na^+-$SrTiO_3$ (PC, preparation temperature: 1273 K).

According to the report of Takata et al., Na^+-doping could introduce oxygen vacancies (Vo), inhibiting the formation of Ti^{3+} which is the recombination center of photogenerated electrons and holes [23]. Nonetheless, little evidence supported the relation according to the report of Takata et al., Na^+-doping could introduce oxygen vacancies (Vo), inhibiting the formation of Ti^{3+} which is the recombination center of photogenerated electrons and holes [23]. Nonetheless, little evidence supported the relation besides the improvement of photocatalytic activity for overall H_2O splitting. The results in this study can be confirmed the preferable state of the Na^+-$SrTiO_3$ photocatalyst for overall H_2O splitting as doping of Na^+ to perovskite $SrTiO_3$ structure. The detailed influences of Na^+-doping to the bulk leading the improvement of photocatalytic activity is unclear. Then further examination was carried out to study the influences of Na^+-doping.

Here, aiming to know the influences of Na^+-doping in the structure of $SrTiO_3$, Raman spectroscopic investigations of $SrTiO_3$ and Na^+(5 mol%)-$SrTiO_3$ (SSR, TiO_2 (D)) were carried out. The results are shown in Figure 2-6. The spectra in Figure 2-6 are separated into three spectral regions as Figure 2-6(a) (0-700 cm^{-1}), Figure 2-6 (b) (170-770 cm^{-1}) and Figure 2-6(c) (690-960 cm^{-1}) by changing the excitation wavelength at (a) 360 nm, (b) 480 nm, and (c) 980 nm to clearly show the difference between the spectrum of $SrTiO_3$ and that of Na^+(5 mol%)-$SrTiO_3$. The spectrum of $SrTiO_3$ in Figure 2-6 is in agreement with that reported previously [32–37]. Therefore, the bands in the spectrum can be assigned based on the previous report. The bands are attributable to the TO_2 mode (O-Sr-O bending mode, at 81 cm^{-1}), TO_2 mode (O-Sr-O bending mode, at 176 cm^{-1}), TO_3 mode (O-Sr-O bending mode, between 248 and 348 cm^{-1}), LO mode (Ti-O-Ti bending mode, between 610 and 750 cm^{-1}) and LO_4 (Ti-O mode at 796 cm^{-1}) (The assignment of the Raman bands in $SrTiO_3$ is summarized in Table 2-4).

On the other hand, the spectrum of Na^+(5 mol%)-$SrTiO_3$ is observed to be substantially the same as that of $SrTiO_3$ while the relative intensity among the band modes and the shapes of the bands are noticed to be varied as shown in Figure 2-16. In particular, the bands at 81 cm^{-1} attributed to TO_1, 248 cm^{-1} attributed to TO_3, and bands attributed to LO_4 (610, 680, and 718 cm^{-1}) are broader, while the band at 176 cm^{-1} attributed to TO_2 is sharper. These changes in the shapes and the relative intensities in the Raman bands indicate the distortion of the perovskite lattice generated by replacing Sr ion with Na ion [38–42]. According to the report of perovskite $NaTaO_3$, K-doping resulted in a slightly distorted perovskite structure and promoting the photocatalytic activity [43]. Therefore, from the above results, the distortion of the $SrTiO_3$ lattice by doping Na^+ is also probably one of the reasons why the photocatalytic activity improves in this case. On the other hand, the relative intensities of the Raman peaks between 248 and 348 cm^{-1} of Na^+-$SrTiO_3$ reduced, which is also due to the influences of the occupied Sr^{2+}-site. Moreover, the new band that appeared at 796 cm^{-1} implied the appearance of defect vacancies, which was caused by the unbalanced charge due to the doped aliovalent Na ions. According to the previous reports, on the lower valence cation doped $SrTiO_3$ photocatalyst, the reduction of n-type semi-conductive properties, induced from the formation of vacancies by the doping of lower valence cation, was regarded as the factor for the improvement of the photocatalytic activity of overall water splitting. However, the detailed influences of changes in the states of the $SrTiO_3$ bulk by doping Na^+ to the remarkable improvement of the photocatalytic activity are still unclear.

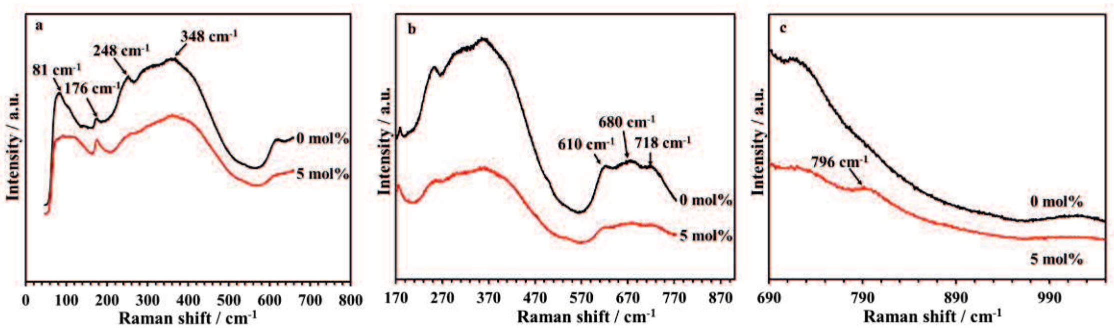

Figure 2-6. Raman spectra of $SrTiO_3$ (SSR, TiO_2 (D)) and Na^+-$SrTiO_3$ (SSR, TiO_2 (D), preparation temperature: 1273 K) at an excitation wavelength of (a) 360 nm, (b) 480 nm, and (c) 980 nm.

Table 2-3. Photo branch and band mode assignments for the Raman spectra of $SrTiO_3$ (SSR) and Na^+-$SrTiO_3$ (SSR, TiO_2(D), preparation temperature:1273 K)

Raman shift / cm^{-1}	Photon branch	Band mode
81	TO_1	O-Sr-O
176	TO_2	O-Sr-O
248-348	TO_3	O-Sr-O
610-750	LO	Ti-O-Ti
796	LO_4	Ti-O

The morphologies of the typical Na^+-$SrTiO_3$ photocatalysts prepared by the PC method and the SSR method using the different purity of TiO_2 materials (TiO_2 (B) and TiO_2 (D)) in this study are observed by scanning electron microscopy (SEM) and the results are shown in Figure 2-7. The Na^+-$SrTiO_3$ prepared by the PC method exhibited a uniform multi-faceted crystal, tending to be spherical, with a size around 100 nm is observed as shown in Figure 2-7(a). On the other hand, the morphologies of the photocatalysts prepared by the SSR method using TiO_2 (B) and TiO_2 (D) are similar, where the shapes of the observed particles are disordered with 100 nm to several hundred nanometers in diameter as shown in Figure 2-7(b and c). The similar specific surface areas (BET) of Na^+-$SrTiO_3$ prepared by the SSR method using different TiO_2 materials and the PC method are provided in Table 2-3. These results indicate that the states of Na doped $SrTiO_3$ originated with the nature of starting materials are the crucial factors rather than the morphologies originated with the preparation method and conditions in the enhancement of photocatalytic performance in this study. Then the states of Na^+-$SrTiO_3$ prepared by the SSR method by using TiO_2 (D) are further examined.

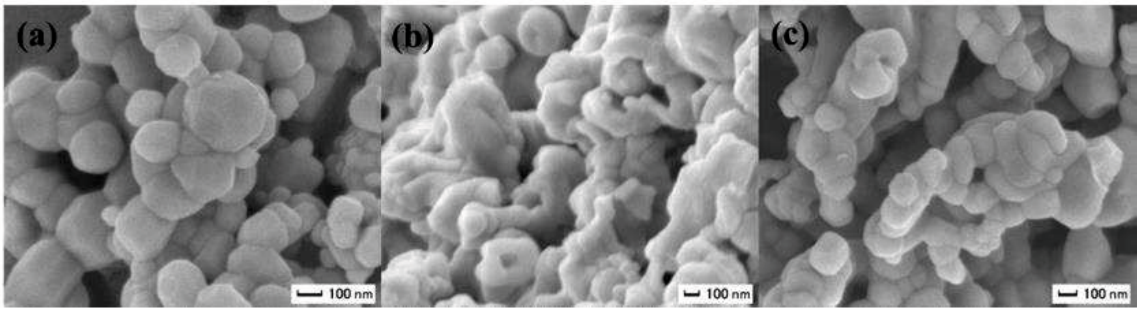

Figure 2-7. SEM images of (a) Na^+(4 mol%)-$SrTiO_3$ (PC, preparation temperature: 1273 K), (b) Na^+(5 mol%)-$SrTiO_3$ (SSR, TiO_2 (B), preparation temperature: 1273 K) and (c) Na^+(5 mol%)-$SrTiO_3$ (SSR, TiO_2 (D), preparation temperature: 1273 K).

Table 2-4. The specific surface areas (BET) of Na^{+}-$SrTiO_3$ samples were prepared by the SSR method using various TiO_2 materials and the PC method.

Photocatalyst	Preparation method	BET surface areas / m^2 g^{-1}
Na^{+}(5 mol%)-$SrTiO_3$	SSR method (TiO_2(A))	1.87
Na^{+}(5 mol%)-$SrTiO_3$	SSR method (TiO_2(B))	2.42
Na^{+}(5 mol%)-$SrTiO_3$	SSR method (TiO_2(C))	1.87
Na^{+}(5 mol%)-$SrTiO_3$	SSR method (TiO_2(D))	2.70
Na^{+}(4 mol%)-$SrTiO_3$	PC method	2.56

Figure 2-8 shows the scanning transmission electron microscopy (STEM) images, energy-dispersive X-ray spectroscopy (EDS) data, and elemental mapping images of Na^{+}(5 mol%)-$SrTiO_3$ (SSR, TiO_2 (D)). The elements of Sr, O, Na, Ti are all observed in the EDS spectrum as shown in Figure 2-8(b), indicating the presence of the elements in the sample and the unmarked signals are related to the background from the TEM support.

Figure 2-8(c–f) is the distribution of Sr, O, Na, and Ti, respectively. From the results in Figure 2-8, the elements of Sr, O, Na, and Ti are uniformly distributed in Na^{+}-$SrTiO_3$. This indicates that the Na^{+} is homogeneously doped in $SrTiO_3$. The cocatalysts were deposited cover all over the surface of the photocatalyst observed from the elemental mapping images in Figure 2-9.

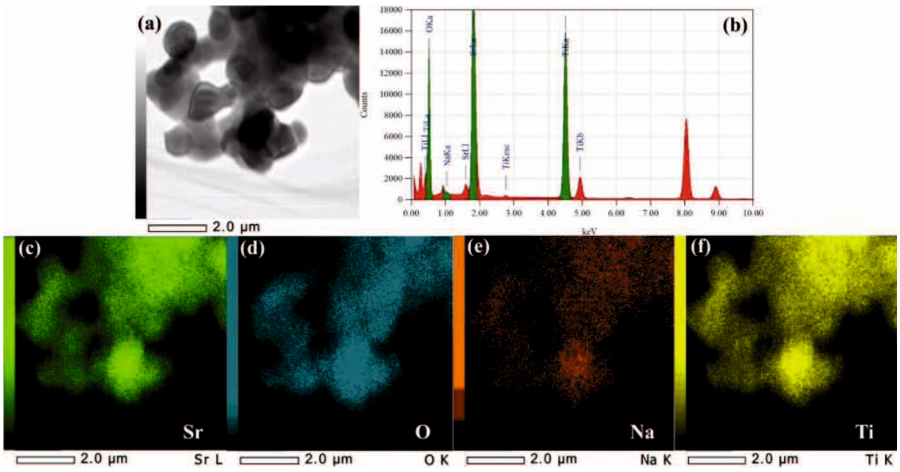

Figure 2-8. (a) STEM images, (b) EDS analysis of (5 mol%)-$SrTiO_3$ (SSR, TiO_2 (D), (preparation temperature: 1273 K), and the elemental mapping images of (c) Sr, (d) O, (e) Na, (f) Ti.

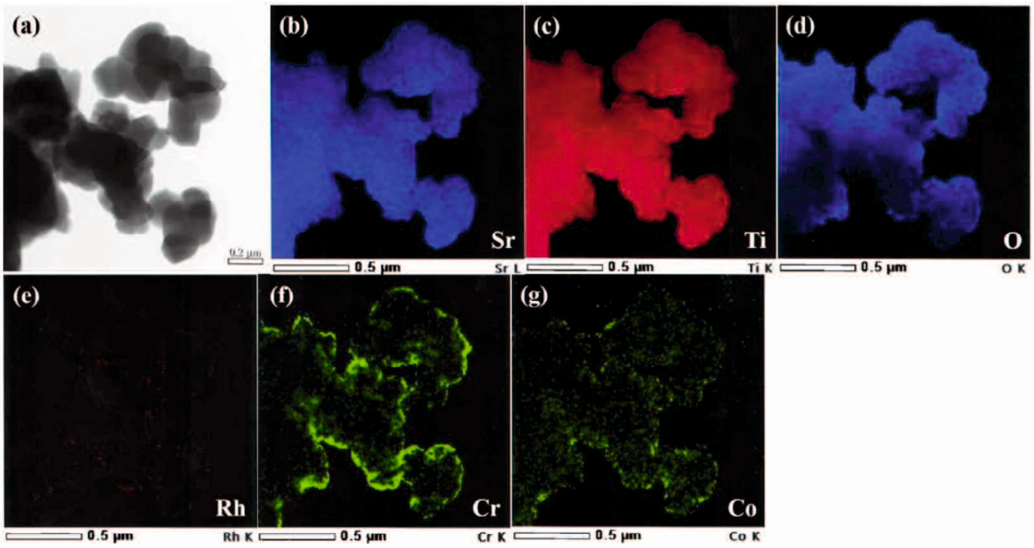

Figure 2-9 (a) STEM image of $Rh_{0.7}Cr_{1.3}O_3$/Na^+(5 mol%)-$SrTiO_3$/CoO_x (Co: 0.05 wt%), and elemental mapping images of (b) Sr, (c) Ti, (d) O, (e) Rh, (f) Cr, and (g) Co.

2.3.2 Photocatalytic activity

The prepared Na^+-$SrTiO_3$ with $Rh_{0.7}Cr_{1.3}O_3$ co-catalyst showed relatively high photocatalytic performance for overall H_2O splitting. The constant production of H_2 and O_2 in the stoichiometric ratio (2:1) was observed from the initial stage of the photocatalytic overall H_2O reaction over $Rh_{0.7}Cr_{1.3}O_3$/Na^+-$SrTiO_3$ photocatalysts as shown in Figure 2-10.

The photocatalytic activity was defined as the amount of produced H_2 and O_2 per hour (as mmol h^{-1}) in the steady-state. The photocatalytic activity of Na^+-$SrTiO_3$ prepared by the PC method is similar to that prepared by the SSR method using TiO_2 (B).

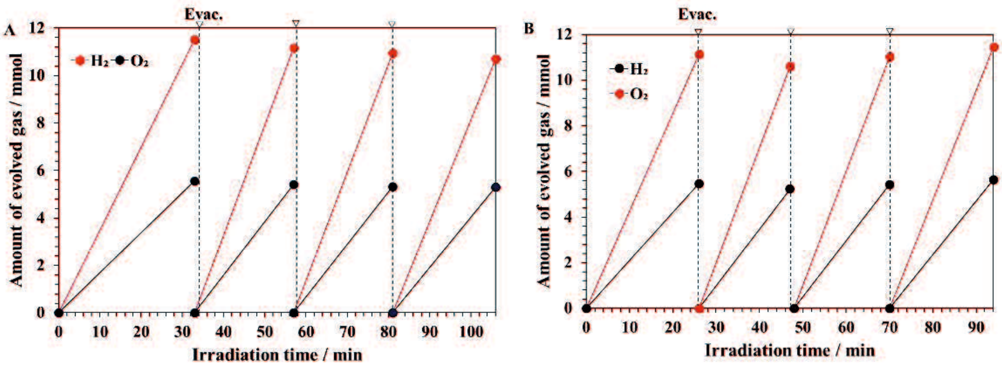

Figure 2-10. Gas evolution during the overall water splitting reaction over the photocatalysts (a) Na^+(4 mol%)-$SrTiO_3$ (PC, preparation temperature: 1273 K) and (b) Na^+(5 mol%)-$SrTiO_3$ (SSR, TiO_2 (B), preparation temperature: 1273 K). Reaction conditions: photocatalyst, 1.0 g; cocatalyst, $Rh_{0.7}Cr_{1.3}O_3$; reaction solution, 600 mL; light source, 450 W high-pressure Hg lamp ($\lambda > 300$ nm).

Figure 2-11 shows the effects of the preparation parameters of Na^+-$SrTiO_3$ prepared by the SSR method using TiO_2 (B) as a starting material. Figure 2-11(A) shows the photocatalytic activity as a function of the amount of doped Na ion where the Na^+-$SrTiO_3$ is prepared by calcining the precursors at 1273 K. As shown in Fig. 2-11a, the photocatalytic activity of pure $SrTiO_3$ is near 0 mmol h^{-1}. When Na ion is doped in $SrTiO_3$, the activity is markedly improved with the increase of the amount of doped Na ion. The $SrTiO_3$ doped with 5 mol% of Na^+ shows the maximum photocatalytic activity. When the amount of doped Na ion to $SrTiO_3$ is more than 5 mol%, the photocatalytic activity decreases. On the basis of the results in Figure 2-11(A), the influence of calcination temperature on the photocatalytic activity was examined using Na^+(5 mol%)-$SrTiO_3$ (SSR), and the results are shown in Figure 2-11(B).

Figure 2-11(B) shows the photocatalytic activity of Na^+(5 mol%)-$SrTiO_3$ (SSR) for H_2O splitting as a function of preparation temperature. The photocatalytic activity is improved with increasing the preparation temperature from 1073 K and shows the maximum activity at 1273 K. Then the activity noticeably decreases when the calcination temperature is above 1273 K. The results in Figure 2-11 show that the addition of Na ion in the raw material of $SrTiO_3$ is indispensable for generating high photocatalytic activity for overall H_2O splitting. From the results in Figure 2-11, for the preferable photocatalyst, photocatalytic activity is 25 mmol h^{-1} for H_2 evolution and 13 mmol h^{-1} for O_2 evolution, respectively, where Na^+-$SrTiO_3$ is prepared at 1273 K with 5 mol% of Na.

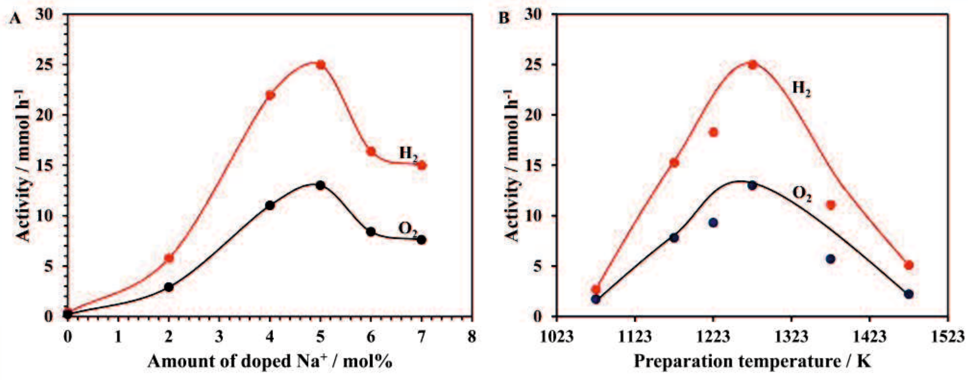

Figure 2-11. The photocatalytic overall H_2O splitting activity of (a) Na^+-$SrTiO_3$ (SSR, TiO_2 (B), preparation temperature: 1273 K) as a function of the amount of doped Na^+. (b) Na^+(5 mol%)-$SrTiO_3$ (SSR, TiO_2 (B)) as a function of preparation temperature. Reaction conditions: photocatalyst, 1.0 g; cocatalyst, $Rh_{0.7}Cr_{1.3}O_3$; reaction solution, 600 mL; light source, 450 W high-pressure Hg lamp.

Nearly the same results were obtained for the Na^+-$SrTiO_3$ photocatalysts prepared by the PC method in Figure 2-12. The preferable preparation conditions of Na^+-$SrTiO_3$ prepared by the PC method was also confirmed that the amount of doped Na^+ is 4 mol% and the preparation temperature is 1273 K, respectively.

The photocatalytic activity is 28 mmol h^{-1} for H_2 and 14 mmol h^{-1} for O_2 production, respectively. The photocatalytic activity of Na^+-$SrTiO_3$ (PC) prepared under the preferable conditions is slightly higher than that prepared by the SSR method using TiO_2 (B). This means that the influence of the difference of preparation methods between the SSR and PC methods on the photocatalytic performance of Na^+-$SrTiO_3$ is not significant in this case.

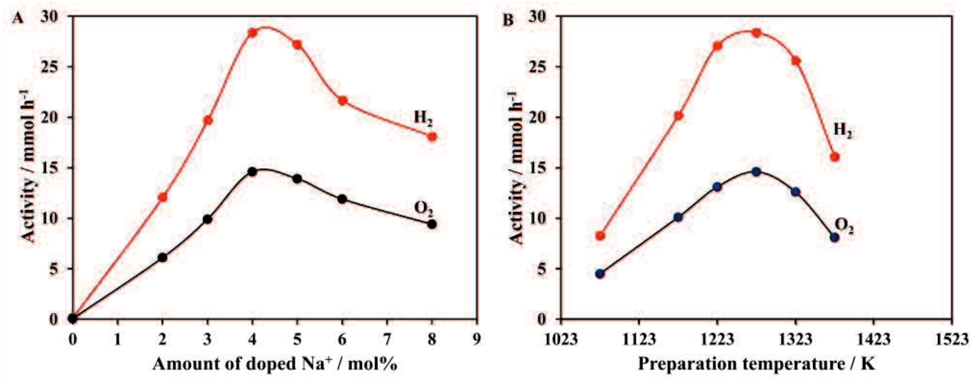

Figure 2-12. The photocatalytic overall H_2O splitting activity of (a) Na^+-$SrTiO_3$ (SSR, TiO_2 (B), preparation temperature: 1273 K) as a function of the amount of doped Na^+. (b) Na^+(5 mol%)-$SrTiO_3$ (SSR, TiO_2 (B)) as a function of preparation temperature. Reaction conditions: photocatalyst, 1.0 g; cocatalyst, $Rh_{0.7}Cr_{1.3}O_3$; reaction solution, 600 mL; light source, 450 W high-pressure Hg lamp.

On the other hand, our previous report showed that the activity of Na^+-$SrTiO_3$ photocatalyst prepared by the impregnation method for H_2O splitting was strongly influenced by the nature of $SrTiO_3$ materials [16]. Therefore, the effect of the raw material used for preparing Na^+-$SrTiO_3$ on the overall H_2O splitting activity is further examined. Here, the Na^+-$SrTiO_3$ photocatalyst was prepared using various types of TiO_2 materials by the SSR method under the preferable conditions evaluated above. The results are summarized in Figure 2-13.

Figure 2-13 shows the photocatalytic activity and of $Rh_{0.7}Cr_{1.3}O_3$/Na^+(5 mol%)-$SrTiO_3$ prepared at a preparation temperature of 1273 K by the SSR method by using various kinds of TiO_2 materials for overall H_2O splitting. As shown in Figure 2-13, the photocatalytic activity noticeably depends on the kind of TiO_2 as the starting material for preparing the Na^+-$SrTiO_3$ photocatalyst. Particularly, it is noticed that the Na^+-$SrTiO_3$ photocatalyst prepared using higher purity of TiO_2 (D) material shows higher activity.

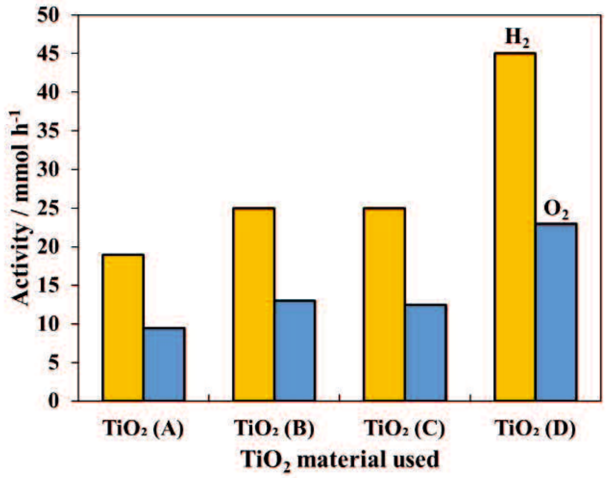

Figure 2-13. Dependence of photocatalytic activity of the overall H_2O splitting over Na^+(5 mol%)-$SrTiO_3$ (SSR, preparation temperature, 1273 K) on the purity of TiO_2 materials used, dark column: H_2, white column: O_2. Reaction conditions: photocatalyst, 1.0 g; cocatalyst, $Rh_{0.7}Cr_{1.3}O_3$; reaction solution, 600 mL; light source, 450 W high-pressure Hg lamp.

According to the previous report, co-doping of higher valent ions, such as Ta^{5+} ion, to compensate for the charge valance made the photocatalytic activity decrease [23]. This suggests that the impurities in the raw material probably influence the photocatalytic activity of Na^+-$SrTiO_3$. Therefore, the raw materials with high purity should be necessary for preparing Na^+-$SrTiO_3$ exhibiting high photocatalytic activity.

Particularly, when Na^+(5 mol%)-$SrTiO_3$ (SSR) is prepared using TiO_2 (D) (purity, 99.99%), the photocatalytic activity of $Rh_{0.7}Cr_{1.3}O_3$/ Na^+(5 mol%)-$SrTiO_3$ is further improved to 45 mmol h^{-1} for H_2 and 23 mmol h^{-1} for O_2 production, respectively. Then, the apparent quantum yield (AQY) of the H_2O splitting under the irradiation of monochromatic light at 365 nm was evaluated over Na^+-$SrTiO_3$ prepared by the SSR and PC methods under the preferable conditions in this study.

The evaluated AQY of water splitting over Na^+(5 mol%)-$SrTiO_3$ (SSR) prepared using TiO_2 (D) was 28%, while that over Na^+(4 mol%)-$SrTiO_3$ (PC) was 17.4%. The AQY of H_2O splitting over the photocatalyst prepared by the SSR method under the preferable conditions in this study is further improved relative to that of Na^+ added $SrTiO_3$ prepared by the impregnation method which achieved an AQY of 16% at 360 nm reported in our previous investigation as well as is nearly the same as the value of Al ion-doped $SrTiO_3$ prepared used flux method reported by Ham et al.

2.3.3 Effects of Na^+-doping on the dependence of photocatalytic overall H_2O splitting on light intensity

To make clear the action of doped Na^+ in $SrTiO_3$ on the photocatalytic activity, the light intensity dependence of the photocatalytic activity was carried out. The results are shown in Figure 2-14. As shown in Figure 2-14, the rates of H_2 and O_2 evolution are not stoichiometric under low light intensity during overall water splitting reaction over $Rh_{0.7}Cr_{1.3}O_3/Na^+$ $SrTiO_3$. The ratio of O_2 evolution rate and H_2 evolution rate is lower than 0.5, suggesting there is little O_2 produced under low light intensity. However, the evolution of O_2 remarkably decreases with decreasing light-intensity by the ND filter, which probably suggests the generated h^+ would supply the locations where the positive charges are not enough due to the doping of Na ion before it transfers to the active sites, so it will be less or no oxygen produced at first for a large amount of Na ions doped $SrTiO_3$ samples. Particularly, when the amount of doped Na^+ increased, this trend is more obvious. The results suggest the doped Na^+ probably acts as hole-trapping sites in the photocatalysts. The photo-generated holes are trapped in the bulk of $SrTiO_3$. However, the trapped holes will promote the separation of photoexcited charge carriers and further improve the photocatalytic overall water splitting activity under high light intensity. According to the photocatalytic activity, the preferable amount of doped Na^+ is 5 mol%. Meanwhile, the excess Na ion could form the recombination centers of charge carriers. The holes will be consumed by the recombination with electrons and trapped in the bulk, therefore, the oxygen produced is further decreased even under high light intensity as shown in Figure 2-14 (C).

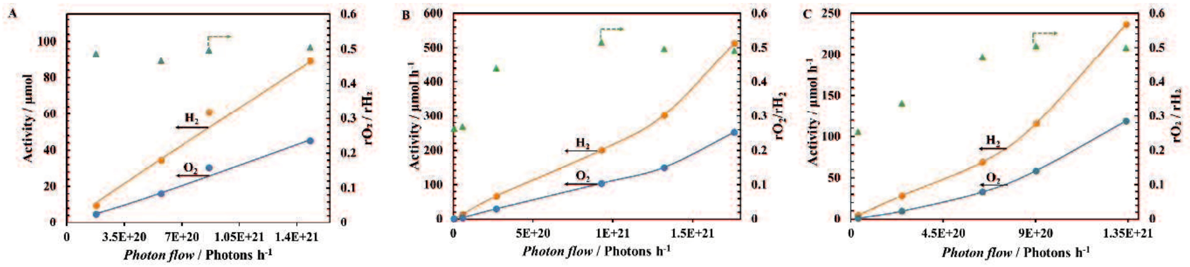

Figure 2-14. Dependence of the ratio of O_2 and H_2 evolution rates (triangle), photocatalytic activity (H_2: yellow circles, O_2: blue circles) on light intensity over (A) $Rh_{0.7}Cr_{1.3}O_3$/Na^+(2 mol%)-$SrTiO_3$, (B) $Rh_{0.7}Cr_{1.3}O_3$/Na^+(5 mol%)-$SrTiO_3$ and (C) $Rh_{0.7}Cr_{1.3}O_3$/Na^+(8 mol%)-$SrTiO_3$ prepared by the SSR method.

2.3.4 Influence of the states of HER and OER sites on the photocatalytic performance

The effective separation of hydrogen evolution reaction (HER) sites and oxygen evolution reaction (OER) sites over the photocatalyst surface is one of the important factors for the further improvement of the photocatalytic performances, not only the activity but also the durability of the photocatalyst. According to the previous studies, in the photocatalyst loaded with a $Rh_{0.7}Cr_{1.3}O_3$ co-catalyst, the photocatalytic activity for H_2O splitting was observed to reduce with passing time [7,20]. The reduction of photocatalytic activity was concluded to be originated with the degradation of the $Rh_{0.7}Cr_{1.3}O_3$ compound by the oxidation of Cr ion in the co-catalyst with the oxygenates produced under the photocatalytic oxidation of H_2O. In order to suppress the reduction of the photocatalytic activity with time, the combination of a CoO_x co-catalyst for oxygen evolution reaction (OER) was carried out to control the O_2 evolution process and confirmed the stable progress of photocatalytic overall H_2O splitting for a relatively long time in the previous studies. Here, based on the previous studies, the influences of the introduction of the CoO_x as a co-catalyst for OER on the photocatalytic activity and the durability were examined. The results are shown in Figure 2-15.

Figure 2-15 shows the time courses of photocatalytic water splitting over $Rh_{0.7}Cr_{1.3}O_3$/Na^+(5 mol%)-$SrTiO_3$/CoO_x as a function of the amount of Co species. As see in Figure 2-15, the optimal amount of Co species was 0.05 wt%. Then, a longer measurement to investigate the stability of the photocatalyst was carried out.

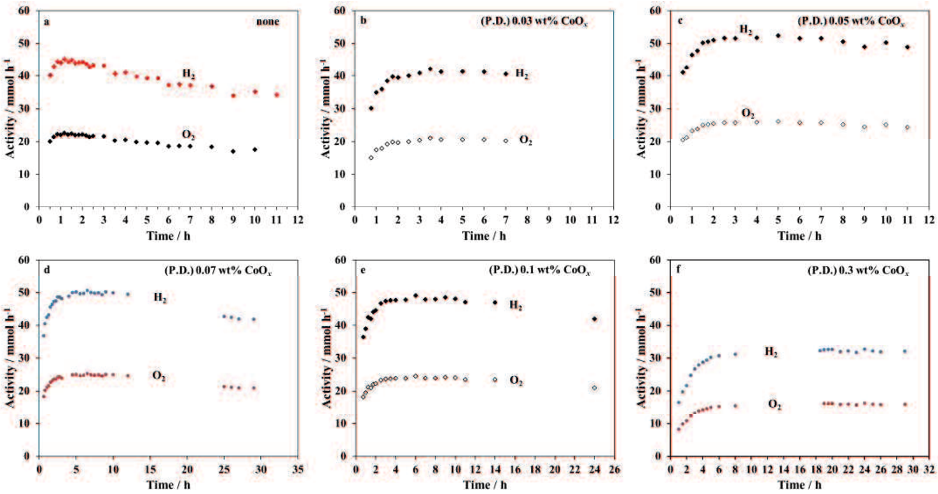

Figure 2-15. Time courses of water-splitting activity of Na^+(5 mol%)-$SrTiO_3$ (SSR) loaded with (a) $Rh_yCr_{2-y}O_3$ and CoO_x by *in situ* photo-deposition method at Co concentrations of (a) 0, (b) 0.03, (c) 0.05, (d) 0.07, (e) 0.1, and (f) 0.3 wt%. Reaction conditions: photocatalyst, 1.0 g; reaction solution, 600 mL distilled water; light source, 450 W high-pressure Hg lamp.

Figure 2-16(a) shows the photocatalytic activity of H_2O splitting as a function of irradiation time over $Rh_{0.7}Cr_{1.3}O_3$/Na^+(5 mol%)-$SrTiO_3$ and Figure 2-16(b) shows that over $Rh_{0.7}Cr_{1.3}O_3$/Na^+(5 mol%)-$SrTiO_3$/CoO_x (0.05 wt% as Co).

As shown in Figure 2-16(A), it is noticed that if the Na^+(5 mol%)-$SrTiO_3$ photocatalyst only loaded $Rh_{0.7}Cr_{1.3}O_3$ co-catalyst, its photocatalytic activity would be rapidly reduced after 10 h, while the photocatalytic activity of this photocatalyst remained 86% of the initial maximum for more than 50 h by co-loading a Co species as a co-catalyst for OER by a photo-deposition method as shown in Figure 2-16(b). Moreover, the photocatalytic activity is noticeably improved and the AQY value is increased from 28% to 30% at 365 nm by co-loading the co-catalyst. These results show that co-loading a CoO_x co-catalyst to control the OER in photocatalytic H_2O splitting over $Rh_{0.7}Cr_{1.3}O_3$/Na^+(5 mol%)-$SrTiO_3$ is significant for not only the improvement of photocatalytic activity but also the improvement of the stability of the photocatalyst and the photocatalytic reaction. The distribution of co-catalysts over the photocatalyst evaluated by STEM-EDS is shown in Figure 2-9.

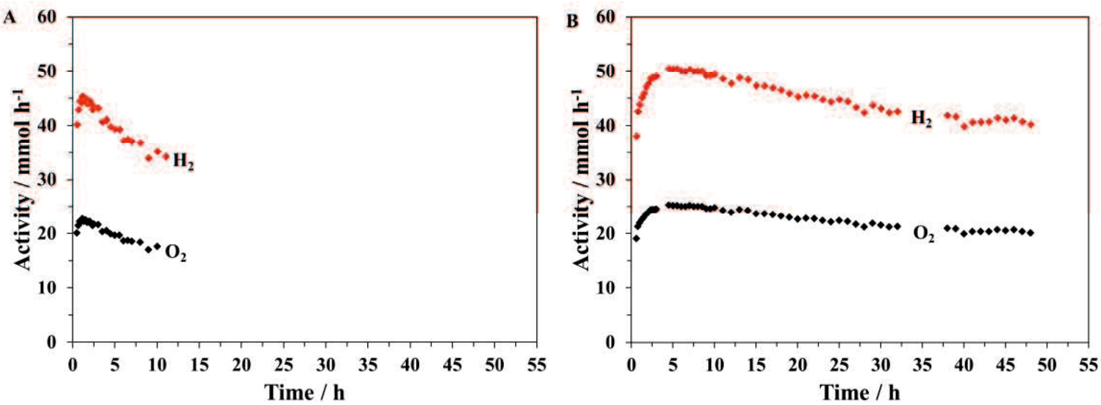

Figure 2-16. Time courses of overall H_2O splitting activity over Na^+(5 mol%)-$SrTiO_3$ (SSR, TiO_2 (D), preparation temperature, 1273 K) loaded with (a) $Rh_{0.7}Cr_{1.3}O_3$ and (b) $Rh_{0.7}Cr_{1.3}O_3$ and CoO_x (Co: 0.05 wt%). Reaction conditions: photocatalyst, 1.0 g; reaction solution, 600 mL; light source, 450 W high-pressure Hg lamp.

On basis of the above study on the structure, morphologies, and surface areas, the states of Na doped $SrTiO_3$ originated from the nature of starting materials are the crucial factors rather than the morphologies originated with the preparation method and conditions in the enhancement of photocatalytic performance in this study.

The detailed influences of Na^+-doping to the bulk leading the improvement of photocatalytic activity is unclear. Further examination was carried out to study the influences of Na^+-doping.

Then, the behavior of photogenerated charge carriers in the photocatalysts was examined by observing the decay kinetics using transient absorption spectroscopy.

Figure 2-17 shows the decay curves of free electrons giving absorption at 2,000 cm^{-1} (5000 nm) and trapped electrons giving absorption at 12,000 cm^{-1} (833 nm) produced by the irradiation of UV laser pulse [44]. This result shows that the number of surviving free electrons slightly decreased, but that of trapped electrons much increased by Na^+-doping, where they become ~80% and ~200% at 1000 ps, respectively. Figure 2-18 shows the transient absorption spectra of (a) Na^+(0 mol%)-$SrTiO_3$, (b) Na^+(5 mol%)-

$SrTiO_3$, and decay curves of transient absorptions by $Rh_{0.7}Cr_{1.3}O_3$-loaded and unloaded Na^+(5 mol%)-$SrTiO_3$ probed at (c) 2,000 (5,000 nm) and (d) 12,000 cm^{-1} (833 nm) measured in vacuum. The transient absorption at 25,000-20,000, 15,000-6000, < 4000 cm^{-1} are assigned to trapped holes, trapped electrons, and free and/or shallowly trapped electrons, respectively [45–47]. By loading $Rh_{0.7}Cr_{1.3}O_3$ co-catalysts on $SrTiO_3$, the decay of free electrons and trapped electrons are accelerated. This acceleration is ascribed to the electron transfer from $SrTiO_3$ to $Rh_{0.7}Cr_{1.3}O_3$ co-catalysts as reported in our previous works [44]. In principle, the trapped electrons should have lower reactivity than free electrons for H_2 evolution, but these trapped electrons still keep reactivity since they can transfer to loaded $Rh_{0.7}Cr_{1.3}O_3$ co-catalysts as shown in Figure 2-18(c and d). These results further confirm that the vacancies formed by the Na^+-doping, which is identified by Raman spectra, can suppress the recombination and then elongate the lifetime of photogenerated charge carriers. These would be the reason why the photocatalytic activity was enhanced by doing Na^+.

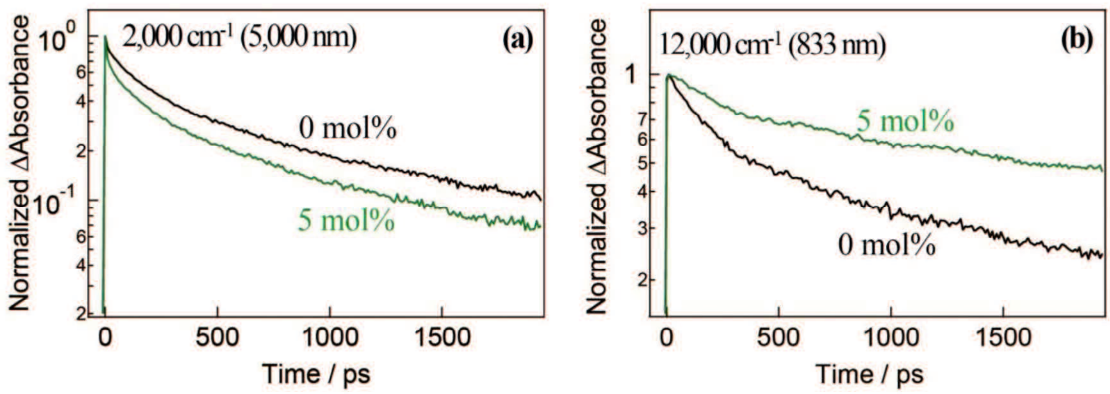

Figure 2-17. Decay curves of transient absorptions by $SrTiO_3$ (SSR, TiO_2 (D), preparation temperature: 1273 K) and Na^+ (5 mol%)-$SrTiO_3$ (SSR, TiO_2 (D), preparation temperature: 1273 K) probed at (a) 2000 (5,000), (b) 12,000 cm^{-1} (833 nm) measured in a vacuum.

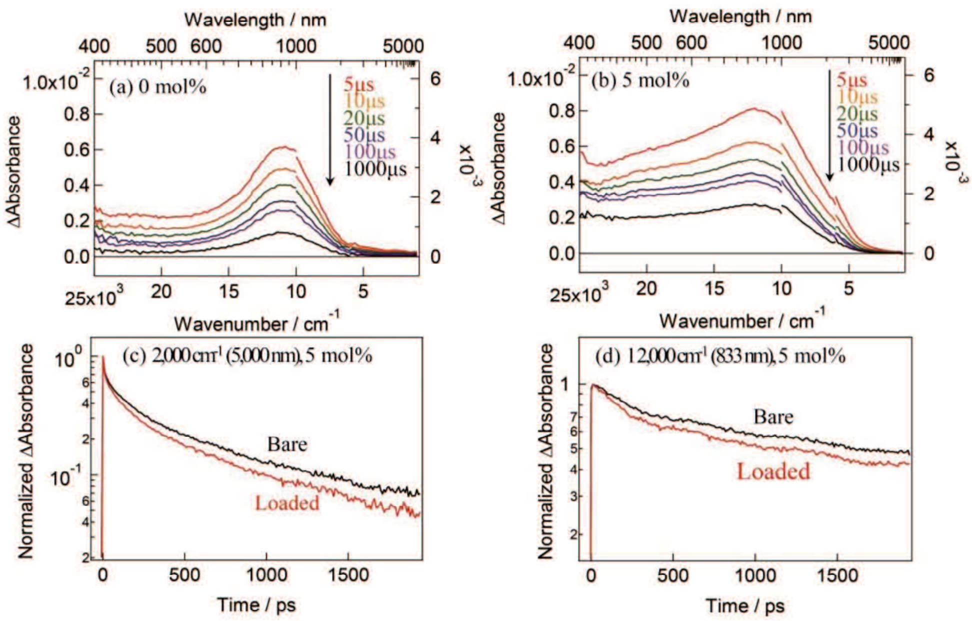

Figure 2-18. The transient absorption spectra of (a) Na^+(0 mol%)-$SrTiO_3$ (SSR, TiO_2 (D), preparation temperature: 1273 K), (b) Na^+(5 mol%)-$SrTiO_3$ (SSR, TiO_2 (D)), preparation temperature: 1273 K, and decay curves of transient absorptions by $Rh_{0.7}Cr_{1.3}O_3$-loaded and unloaded Na^+(5 mol%)-$SrTiO_3$ probed at (c) 2,000 (5,000 nm) and (d) 12,000 cm^{-1} (833 nm) measured in vacuum.

A schematic illustration of photogenerated electrons and holes recombined quickly ($SrTiO_3$) and slowly (Na^+-$SrTiO_3$) influenced by the trapping sites on powder $SrTiO_3$ is shown in Figure 2-19. As demonstrated in Figure 2-19, the large portion of photogenerated electrons and holes recombined quickly in the $SrTiO_3$ bulk, restricting its activity for water splitting. In contrast, the photogenerated electrons were quickly trapped by vacancies but still keep reactivity on Na^+-$SrTiO_3$ and transferred to the co-catalysts, resulting in the slow recombination of charge carriers and improved the photocatalytic activity for overall water splitting.

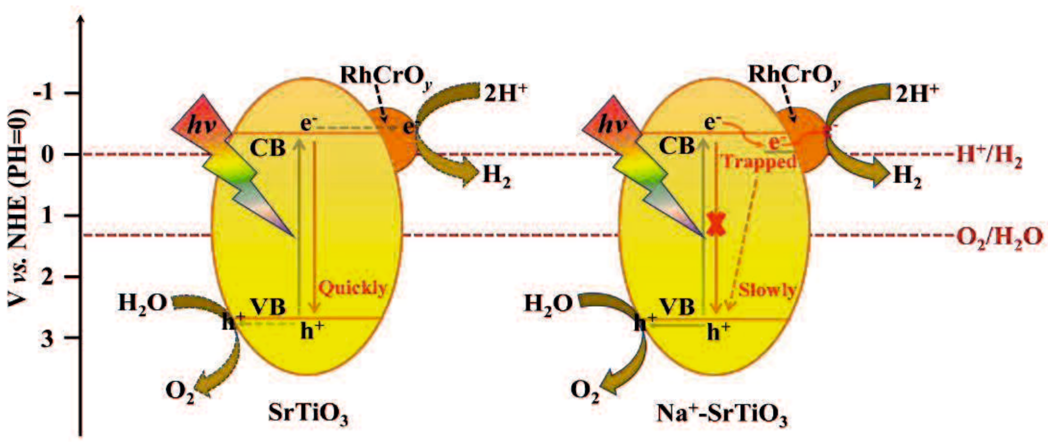

Figure 2-19. Schematic illustration of photogenerated electrons and holes recombined quickly ($SrTiO_3$) and slowly (Na^+-$SrTiO_3$) influenced by the trapping sites on powder $SrTiO_3$.

2.4 Conclusions

The photocatalytic properties of Na^+-$SrTiO_3$ loaded with a $Rh_yCr_{2-y}O_3$ co-catalyst toward the overall H_2O splitting was studied for elucidating the states of the high-performance $SrTiO_3$ photocatalyst doped aliovalent metal ions which are lower valency of the parent ions. In this study, we confirmed that the photocatalytic activity remarkably improved by doping Na ion. Particularly, the purity of the raw material was crucial for preparing highly active photocatalyst rather than the states that originated with the preparation methods. The photocatalytic activity of Na^+-$SrTiO_3$ prepared under the preferable condition in this study was 45 mmol h^{-1} for H_2 and 23 mmol h^{-1} for O_2 production, respectively, and the AQY at 365 nm was 28%.

The separation of the HER site and OER sites over the photocatalyst surface were also examined by controlling the co-catalyst. The photocatalytic activity, as well as durability of the photocatalyst for overall H_2O splitting, was confirmed to improve by co-loading CoO_x co-catalyst as the OER site of the photocatalyst surface and the examination showed the possibility for further improvement of the photocatalytic performances.

From the characterization of the photocatalyst, the doped Na ion was confirmed to be dispersed homogeneously in the bulk and incorporated into Sr^{2+}-site in the $SrTiO_3$ lattice by STEM-EDS and XRD examination. Furthermore, the distortion of the crystal lattice and production of oxygen vacancies in the lattice was also confirmed by the doping of Na ion in $SrTiO_3$ by Raman spectroscopy. The results of transient absorption spectra and dependence of photocatalytic activities on light intensity show that the variation of the states of the $SrTiO_3$ bulk by the doping of Na^+ makes the lifetime of photogenerated charge carriers and thus leads to the remarkable improvement of the photocatalytic activity for overall H_2O splitting.

2.5 References

[1] A. Kudo, Y. Miseki, Heterogeneous photocatalyst materials for water splitting, Chem. Soc. Rev. 38 (2009) 253–278.

[2] T. Yamada, K. Domen, Development of sunlight driven water splitting devices towards future artificial photosynthetic Industry, ChemEngineering 2 (2018) 36.

[3] Y. Goto, T. Hisatomi, Q. Wang, T. Higashi, K. Ishikiriyama, T. Maeda, Y. Sakata, S. Okunaka, H. Tokudome, M. Katayama, S. Akiyama, H. Nishiyama, Y. Inoue, T. Takewaki, T. Setoyama, T. Minegishi, T. Takata, T. Yamada, K. Domen, A particulate photocatalyst water-splitting panel for large-scale solar hydrogen generation, Joule 2 (2018) 509–520.

[4] X. Chen, S. Shen, L. Guo, S.S. Mao, Semiconductor-based photocatalytic hydrogen generation, Chem. Rev. 110 (2010) 6503–6570.

[5] S. Chen, T. Takata, K. Domen, Particulate photocatalysts for overall water splitting, Nat. Rev. Mater. 2 (2017) 1–17.

[6] K. Domen, A. Kudo, T. Onishi, Mechanism of photocatalytic decomposition of water into H_2 and O_2 over NiO-$SrTiO_3$, J. Catal. 102 (1986) 92–98.

[7] T. Ohno, L. Bai, T. Hisatomi, K. Maeda, K. Domen, Photocatalytic water splitting using modified GaN:ZnO solid solution under visible light: Long-time operation and regeneration of activity, J. Am. Chem. Soc. 134 (2012) 8254–8259.

[8] K. Maeda, K. Teramura, N. Saito, Y. Inoue, K. Domen, Improvement of photocatalytic activity of $(Ga_{1-x}Zn_x)(N_{1-x}O_x)$ solid solution for overall water splitting by co-loading Cr and another transition metal, J. Catal. 243 (2006) 303–308.

[9] K. Maeda, K. Teramura, D. Lu, T. Takata, N. Saito, Photocatalyst releasing hydrogen from water water splitting, Nature 440 (2006) 9.

[10] K. Maeda, K. Teramura, H. Masuda, T. Takata, N. Saito, Y. Inoue, K. Domen, Efficient overall water splitting under visible-light irradiation on $(Ga_{1-x}Zn_x)(N_{1-x}O_x)$ dispersed with Rh-Cr mixed-oxide nanoparticles: Effect of reaction conditions on photocatalytic, J. Phys. Chem. B 110 (2006) 13107–13112.

[11] K. Maeda, K. Teramura, D. Lu, N. Saito, Y. Inoue, K. Domen, Noble-

metal/Cr_2O_3 core/shell nanoparticles as a cocatalyst for photocatalytic overall water splitting, Angew. Chemie - Int. Ed. 45 (2006) 7806–7809.

[12] K. Maeda, K. Teramura, D. Lu, N. Saito, Y. Inoue, K. Domen, Roles of Rh/Cr_2O_3 (core/shell) nanoparticles photodeposited on visible-light-responsive $(Ga_{1-x}Zn_x)(N_{1-x}O_x)$ solid solutions in photocatalytic overall water splitting, J. Phys. Chem. C 111 (2007) 7554–7560.

[13] G. Colón, Towards the hydrogen production by photocatalysis, Appl. Catal. A Gen. 518 (2016) 48–59.

[14] H. Kato, K. Asakura, A. Kudo, Highly efficient water splitting into H_2 and O_2 over lanthanum-doped $NaTaO_3$ photocatalysts with high crystallinity and surface nanostructure, J. Am. Chem. Soc. 125 (2003) 3082–3089.

[15] Y. Ham, T. Hisatomi, Y. Goto, Y. Moriya, Y. Sakata, A. Yamakata, J. Kubota, K. Domen, Flux-mediated doping of $SrTiO_3$ photocatalysts for efficient overall water splitting, J. Mater. Chem. A 4 (2016) 3027–3033.

[16] Y. Sakata, Y. Miyoshi, T. Maeda, K. Ishikiriyama, Y. Yamazaki, H. Imamura, Y. Ham, T. Hisatomi, J. Kubota, A. Yamakata, K. Domen, Photocatalytic property of metal ion added $SrTiO_3$ to overall H_2O splitting, Appl. Catal. A Gen. 521 (2016) 227–232.

[17] K. Domen, S. Naito, M. Soma, T. Onishi, K. Tamaru, Photocatalytic decomposition of water vapour on a NiO-$SrTiO_3$ catalyst, J. Chem. Soc. Chem. Commun. 227 (1980) 543–544.

[18] S. Ikeda, K. Hirao, S. Ishino, M. Matsumura, B. Ohtani, Preparation of platinized strontium titanate covered with hollow silica and its activity for overall water splitting in a novel phase-boundary photocatalytic system, Catal. Today 117 (2006) 343–349.

[19] K. Domen, S. Naito, T. Onishi, K. Tamaru, Photocatalytic decomposition of liquid water on a NiO-$SrTiO_3$ catalyst, Chem. Phys. Lett. 92 (1982) 433–434.

[20] H. Lyu, T. Hisatomi, Y. Goto, M. Yoshida, T. Higashi, M. Katayama, T. Takata, T. Minegishi, H. Nishiyama, T. Yamada, Y. Sakata, K. Asakura, K. Domen, An Al-doped $SrTiO_3$ photocatalyst maintaining sunlight-driven overall water splitting activity for over 1000 h of constant illumination, Chem. Sci. 10 (2019)

3196–3201.

[21] T. Takata, K. Domen, Particulate photocatalysts for water splitting: Recent advances and future prospects, ACS Energy Lett. 4 (2019) 542–549.

[22] A. Kudo, A. Tanaka, K. Domen, T. Onishi, The effects of the calcination temperature of $SrTiO_3$ powder on photocatalytic activities, J. Catal. 111 (1988) 296–301.

[23] T. Takata, K. Domen, Defect engineering of photocatalysts by doping of aliovalent metal cations for efficient water splitting, J. Phys. Chem. C 113 (2009) 19386–19388.

[24] T.H. Chiang, H. Lyu, T. Hisatomi, Y. Goto, T. Takata, M. Katayama, T. Minegishi, K. Domen, Efficient photocatalytic water splitting using Al-doped $SrTiO_3$ coloaded with molybdenum oxide and rhodium-chromium oxide, ACS Catal. 8 (2018) 2782–2788.

[25] T. Takata, J. Jiang, Y. Sakata, M. Nakabayashi, N. Shibata, V. Nandal, K. Seki, T. Hisatomi, K. Domen, Photocatalytic water splitting with a quantum efficiency of almost unity, Nature. 581 (2020) 411–414.

[26] K. Teramura, K. Maeda, T. Saito, T. Takata, N. Saito, Y. Inoue, K. Domen Characterization of ruthenium oxide nanocluster as a cocatalyst with $(Ga_{1-x}Zn_x)(N_{1-x}O_x)$ for photocatalytic overall water splitting, J. Phys. Chem. B 109 (2005) 21915–21921.

[27] Y. Hiramachi, H. Fujimori, A. Yamakata, Y. Sakata, Achievement of High Photocatalytic performance to $BaTi_4O_9$ toward overall H_2O splitting, ChemCatChem 11 (2019) 6213–6217.

[28] Y. Sakata, T. Hayashi, R. Yasunaga, N. Yanaga, H. Imamura, Remarkably high apparent quantum yield of the overall photocatalytic H_2O splitting achieved by utilizing Zn ion added Ga_2O_3 prepared using dilute $CaCl_2$ solution, Chem. Commun. 51 (2015) 12935-12938.

[29] A. Yamakata, M. Kawaguchi, N. Nishimura, T. Minegishi, J. Kubota, K. Domen, Behavior and energy states of photogenerated charge carriers on Pt- or CoO_x-loaded $LaTiO_2N$ photocatalysts: Time-resolved visible to mid-infrared absorption study, J. Phys. Chem. C 118 (2014) 23897–23906.

[30] D. Wang, J. Ye, T. Kako, T. Kimura, Photophysical and photocatalytic properties of $SrTiO_3$ doped with Cr cations on different sites, J. Phys. Chem. B 110 (2006) 15824–15830.

[31] J.P. Zou, L.Z. Zhang, S.L. Luo, L.H. Leng, X.B. Luo, M.J. Zhang, Y. Luo, G.C. Guo, Preparation and photocatalytic activities of two new Zn-doped $SrTiO_3$ and $BaTiO_3$ photocatalysts for hydrogen production from water without cocatalysts loading, Int. J. Hydrogen Energy 37 (2012) 17068–17077.

[32] W.G. Nilsen, J.G. Skinner, Raman spectrum of strontium titanate, J. Chem. Phys. 48 (1968) 2240–2248.

[33] H. Vogt, Hyper-Raman tensors of the zone-center optical phonons in $SrTiO_3$ and $KTaO_3$, Phys. Rev. B 38 (1988) 5699–5708.

[34] R.R. and D.P. P. Ranson, R. Ouillon, J.-P. Pinan-Lucarre, Ph. Pruzan, S. K. Mishra, The various phases of the system $Sr_{1-x}Ca_xTiO_3$—A Raman scattering study, J. Raman Spectrosc. 36 (2005) 898–911.

[35] B. Ullah, W. Lei, X.Q. Song, X.H. Wang, W.Z. Lu, Crystal structure, defect chemistry and radio frequency relax or characteristics of Ce-doped $SrTiO_3$ perovskite, J. Alloys Compd. 728 (2017) 623–630.

[36] L. Gu, H. Wei, Z. Peng, H. Wu, Defects enhanced photocatalytic performances in $SrTiO_3$ using laser-melting treatment, J. Mater. Res. 32 (2017) 748–756.

[37] F.A. Rabuffetti, H.S. Kim, J.A. Enterkin, Y. Wang, C.H. Lanier, L.D. Marks, K.R. Poeppelmeier, P.C. Stair, Synthesis-dependent first-order Raman scattering in $SrTiO_3$ nanocubes at room temperature, Chem. Mater. 20 (2008) 5628–5635.

[38] R.G. M. Battabyal, P. Balasubramanian, P. M. Geethu, L. Pradipkanti, D. K Satapathy, Tailoring the optical phonon modes and dielectric properties of nanocrystalline $SrTiO_3$ via Yb doping, Mater. Res. Express 5 (2018) 046301.

[39] L.P. E. García-López, G. Marcì, B. Megna, F. Parisi, L. Armelao, A. Trovarelli, M. Boaro, $SrTiO_3$-based perovskites preparation, characterization and photocatalytic activity in the gas-solid regime under simulated solar irradiation, J. Catal. 321 (2005) 13–22.

[40] T. Šetinc, M. Spreitzer, D. Vengust, I. Jerman, D. Suvorov, Inherent defects in sol-precipitation/hydrothermally derived $SrTiO_3$ nanopowders, Ceram. Int. 39

(2013) 6727–6734.

[41] Y.G. Abreu, J.C. Soares, R.L. Moreira, A. Dias, Monitoring the Structural and Vibrational Properties in RE-doped $SrTiO_3$ Ceramic Powders, J. Phys. Chem. C 120 (2016) 16960–16968.

[42] A.D. R. L. Moreira, R. P. S. M. Lobo, G. Subodh, M. T. Sebastian, F. M. Matinaga, Optical phonon modes and dielectric behavior of $Sr_{1-3x/2}Ce_xTiO_3$ microwave ceramics, Chem. Mater. 19 (2007) 6548–6554.

[43] C.C. Hu, Y.L. Lee, H. Teng, Efficient water splitting over $Na_{1-x}K_xTaO_3$ photocatalysts with cubic perovskite structure, J. Mater. Chem. 21 (2011) 3824–3830.

[44] K. Kato, J. Jiang, Y. Sakata, A. Yamakata, Effect of Na-doping on electron decay kinetics in $SrTiO_3$ photocatalyst, ChemCatChem 11 (2019) 6349–6354.

[45] Y. Luo, S. Suzuki, Z. Wang, K. Yubuta, J.J.M. Vequizo, A. Yamakata, H. Shiiba, T. Hisatomi, K. Domen, K. Teshima, Construction of spatial charge separation facets on $BaTaO_2N$ crystals by flux growth approach for visible-light-driven H_2 production, ACS Appl. Mater. Interfaces 11 (2019) 22264–22271.

[46] A. Yamakata, J.J.M. Vequizo, M. Kawaguchi, Behavior and energy state of photogenerated charge carriers in single-crystalline and polycrystalline powder $SrTiO_3$ studied by time-resolved absorption spectroscopy in the visible to mid-infrared region, J. Phys. Chem. C 119 (2015) 1880–1885.

[47] K. Kato, A. Yamakata, Defect-induced acceleration and deceleration of photocarrier recombination in $SrTiO_3$ powders, J. Phys. Chem. C 124 (2020) 11057–11063.

Chapter 3 Controllable Modification of Mental Ion-Doped $SrTiO_3$ Photocatalyst for Overall Water Splitting to the Ultimate Quantum Efficiency

3.1 Introduction

Artificial photosynthesis has attracted much attention as a way to effectively utilize sunlight to produce environmentally-friendly, sustainable, and clean energy, especially hydrogen energy [1–6]. Photocatalytic overall water splitting as a simple and viable means to produce hydrogen has been always a top research hotspot in recent years [7–12]. The photocatalytic performances of photocatalysts are restricted by various factors, such as optical and electronic properties, charge separation, crystal defects, and so on. To achieve highly active photocatalysts for overall water splitting, various methods used to remove the obstacles have been investigated [12,13]. In the previous studies, the photocatalytic activity of $NaTaO_3$: La was remarkably improved by doping La ion, achieving an AQY of 56% at 270 nm [14]. On the other hand, a Ca and Zn doped Ca_2O_3 photocatalyst using a $Rh0.5Cr_{1.5}O_3$ cocatalyst with high photocatalytic activity was reported to show the AQY reached 71% at 254 nm [15]. Nevertheless, both of the photocatalysts can only be activated under deep ultraviolet light (UV) irradiation ($\lambda <$ 300 nm).

Strontium titanate ($SrTiO_3$) is one of the typical and promising photocatalysts for overall water splitting under near UV irradiation [16–18]. This material received much attention since it was reported to split water vapor into H_2 and O_2 stoichiometrically by loading a NiO co-catalyst [19–22]. However, the photocatalytic activity and quantum efficiency of $SrTiO_3$ were always very poor. Recently, the photocatalytic activity was remarkably improved by doping aliovalent metal ion which valence is lower than that of the substituted parent ion of $SrTiO_3$ [10,23–27], such as Na, Mg, and Al ions. Subsequently, this photocatalyst achieved much higher activity and the apparent quantum yield reached almost unity by doping Al using the flux method [28–30].

Even so, few photocatalysts could arrive at such an ultimate quantum efficiency.

Considering the Mg ion was also an effective dopant, in this presentation, Mg was also doped into $SrTiO_3$ by using the $SrCl_2$ flux as a medium. With further modification and optimization, the Mg-$SrTiO_3$ photocatalyst eventually achieved the ultimate quantum yield.

3.2 Experimental Section

3.2.1 Sample preparation

Synthesis of Mg-doped $SrTiO_3$ using the polymerizable complex (PC) method.

The Mg ion was doped into $SrTiO_3$ through the PC method. In a typical synthesis process, the Sr, Mg, and Ti citrate-ethylene glycol mixed solution with the molar ratio of 1-x: x: 1 (x represents the number of Mg atoms) was prepared by dissolving the raw materials, Titanium isopropoxide, citric acid (Wako pure chemical, 98%), $SrCO_3$ (Wako pure chemical, 99.99%), and $MgCO_3$ (Wako pure chemical) in ethylene glycol (Wako pure chemical, 95%). The polymer precursor was formed after the polymerization was carried out at 458 K for 2 h under reflux. The polymer precursor was calcined in an alumina crucible at the specified temperature for 20 h to obtain the final different amount of Mg ion-doped $SrTiO_3$ samples.

The as-prepared samples were denoted as Mg (x mol%)-$SrTiO_3$ (PC)

Synthesis of Mg-doped $SrTiO_3$ using the solid-state reaction (SSR) method

The Mg ion was doped into $SrTiO_3$ materials through a conventional SSR method. The starting materials TiO_2 (High purity Chemicals; Rutile, 99.99%), $SrCO_3$ (Wako Pure Chemicals Industries, Ltd, 99.99%), and $MgCO_3$ (Wako Pure Chemicals Industries, Ltd) were stoichiometrically mixed and then fully milled mechanically. The mixture was calcined at 1373 K for 20 h in an alumina crucible under the air atmosphere.

The as-prepared samples were denoted as Mg (x mol%)-$SrTiO_3$ (SSR)

Synthesis of Metal ion-doped $SrTiO_3$ using $SrCl_2$ flux treatment (flux)

In a typical synthesis process, the raw materials $SrTiO_3$ were prepared through a conventional solid-state reaction method (SSR). The starting materials TiO_2 (High purity Chemicals; Rutile, 99.99%), $SrCO_3$ (Wako Pure Chemicals Industries, Ltd, 99.99%) were mixed and calcined at 1373 K for 20 h using alumina crucibles in air. The as-prepared $SrTiO_3$ powders were fully mixed with MgO powder (Ga_2O_3, Al_2O_3, In_2O_3, or La_2O_3) and $SrCl_2$ flux reagent according to the nominally molar ratio of 1: x: 10 (x represents the molar ratio of the corresponding metal ion in metal oxide and $SrTiO_3$) in an agate mortar. The added amount of the $SrCl_2$ flux reagent was fixed. The mixtures were calcined at an appropriate temperature (1373 K ~ 1423 K) for 10 h in alumina crucibles. Finally, the cooled bulk was washed with hot ultrapure water several times to remove the chloride impurities and dried at a high temperature for hours. The as-prepared samples were denoted as Mg(x)-$SrTiO_3$ (flux).

As a comparison, Mg ion-doped $SrTiO_3$ was also prepared by the SSR method. The starting materials $SrCO_3$, TiO_2, and $MgCO_3$ (Wako Pure Chemicals Industries, Ltd) were stoichiometrically mixed and then fully milled mechanically. The mixture was calcined at 1373 K for 20 h in an alumina crucible under the air atmosphere.

The as-prepared sample was termed Mg -$SrTiO_3$ (SSR).

3.2.2 Modification with $Rh_{2-y}Cr_yO_3$ with co-catalyst a corundum structure

The $Rh_{2-y}Cr_yO_3$ with the corundum structure as hydrogen evolution co-catalyst (HEC) was deposited onto the surface of photocatalyst by an impregnation method (Imp.) employing $RhCl_3 \cdot 3H_2O$ (Wako Pure Chemicals Industries, Ltd, 99. 5%) and $Cr(NO_3)_3 \cdot 9H_2O$ (Sigma-Aldrich Co. LLC, 99%) as the precursors as the previous description. In a typical synthesis procedure, a certain amount of as-prepared sample powders (1.2 g) was suspended in an aqueous solution containing the necessary amount of $RhCl_3$ and $Cr(NO_3)_3$. After ultrasonic treatment for 10 min, the suspension was dried at 333 K under reduced pressure while being rotated and then heated at 623 K for 1 h.

The $Rh_{2-y}Cr_yO_3$ (Rh: 0.1 wt%, Cr: 0.1 wt%) was closely combined with the photocatalyst denoted as $Rh_{2-y}Cr_yO_3$/Mg-$SrTiO_3$ (flux).

3.2.3 Modification with Rh/Cr_2O_3 cocatalyst with a core/shell structure

Rh/Cr_2O_3 with the core/shell structure was deposited on Mg-$SrTiO_3$ (flux) according to the photo-deposition method previously reported [30–32]. The Mg-$SrTiO_3$ (flux) cubic particles (0.1g) were first dispersed in an aqueous (100 mL) containing a calculated number of $RhCl_3 \cdot 3H_2O$ solution. Then the metallic Rh nanoparticles (0.1 wt%) were loaded on Mg-$SrTiO_3$ (flux) cubic particles under irradiation (300 W Xenon lamp, full arc) for 20 min while being stirred in the air. Following, an appropriate amount of K_2CrO_4 aqueous solution (Kanto Chemical Co.) was added into the suspension under irradiation for 10 min to obtain Rh/Cr_2O_3 (Rh: 0.1 wt%, Cr: 0.05 wt%) core-shell co-catalyst as hydrogen evolution cocatalyst (HEC).

3.2.4 Modification with Co species co-catalyst

The CoO_x as cocatalysts for oxygen evolution reaction (OER) was coloaded onto the $Rh_{2-y}Cr_yO_3$/Mg-$SrTiO_3$ (flux) through both the impregnation method [33] and photo-deposition method [28,30].

In the impregnation method, the detailed deposition procedure is similar to that of loading $Rh_{2-y}Cr_yO_3$ co-catalyst, where the $Co(NO_3)_2 \cdot 6H_2O$ (Kanto Chemical Co.) solution was the precursor. The as-prepared cocatalyst was denoted as CoO_x (0.1 wt%).

In the photo-deposition method, cobalt species cocatalysts were coloaded on the surface of $Rh_{2-y}Cr_yO_3$/Mg-$SrTiO_3$ (flux) from an aqueous solution containing a certain amount of $Co(NO_3)_2 \cdot 6H_2O$ via an in-site photo-deposition method. The as-prepared cocatalyst was denoted as CoOOH (0.05 wt%) [28,30].

3.2.5 Measurement of photocatalytic activity

The photocatalytic overall water splitting reaction was performed applying a closed gas circulation connecting with an iso-volumetric system. In a typical photocatalytic experiment, 0.1 g of the prepared sample was suspended in 100 mL of distilled water in the top-irradiation type reactor. The reaction solution was thoroughly degassed by applying a vacuum and purged with argon. The full volume of the closed system is about 0.46 L. Before the reaction, the system was filled with 10 kPa argon gas. A 300 W Xenon arc lamp without cut off filters was employed to provide the incident light. The evolved gas samples were collected and analyzed using on-line gas chromatography (GC). When a large amount of sample (1.0 g) was employed to measure the photocatalytic activity, the inner-irradiation-type quartz reaction cell was employed and the photocatalyst was suspended in 600 mL of distilled water under a 450 W high-pressure mercury lamp irradiation. When the pressure in the system reached atmospheric pressure, the system was open. The photocatalytic activity was evaluated by the amount of produced gases measured by a soap-film flow meter, where the composition of the produced gases was also measured by gas chromatography (Shimadzu GC-8A).

3.2.6 Measurement of apparent quantum yield (AQY)

The detailed experimental equipment for the measurement of AQY was shown and the methods used for the quantum efficiency measurement were explained in our previous report [30]. The dependence of overall water splitting activity and AQYs on the light intensity was examined in a top-irradiation-type reactor. A certain amount of (0.2 g) sample was dispersed in the reactor and illuminated by monochromatic light from 500 W deep UV lamp through a quartz window, bandpass filter (λ = 365 nm), and a series of neutral density filters (OD = 0, 0.3, 0.5, and 1.0, Edmund Optics) with controlled intensity. The AQY at the wavelengths of 350, 360, 370, and 380 nm were also estimated by using monochromatic light from a 300 W Xenon lamp inserting corresponding bandpass filters. The photocurrent from a calibrated Si-photodiode (Hamamatsu Photonics) was employed to evaluate the number of incident photons in the same condition as the photocatalytic reaction. The AQY values were calculated according to the following equation:

AQY (%) = ((Number of evolved H_2 molecules × 2) / (Number of incident photons)) × 100

3.2.7 Characterization

The powder X-ray diffraction (XRD) using Cu Kα radiation at 0.15418 nm (Rigaku Smart lab 9/SWXD) at the scanning step of 0.02°/min was employed to determine the crystal structure of the as-prepared samples and the precise diffraction peak attributed to [110] reflection in the range from 31° to 33° using NaCl (200) peak as the standard for the diffracted angle. The field-emission scanning electron microscopy (SEM, JEOL, JSM 6335F) was applied to observe the morphology. A UV–vis spectrometer (JASCO. V-550DS) equipped with an integrating sphere was applied to obtain the absorption spectra of samples. A transmission electron microscope equipped with energy-dispersive X-ray spectroscopy (EDX) was carried out to observe the compositional distribution. Inductively coupled plasma‒atomic emission spectroscopy (ICP-AES) analyses were used to determine the actual content of the elements in the sample.

3.3 Results and discussion

3.3.1 Characterization of photocatalysts

The XRD patterns in Figure 3-1(a) shows that there are no impurities in the as-prepared samples and the diffraction patterns of Mg-$SrTiO_3$ (flux) with different Cr contents maintained an almost identified feature as the pristine $SrTiO_3$, referring to the typical cubic lattice (JCPDS. 35-0734). The typical diffraction peak at about 32.39° corresponds to the [110] plane. The Mg-doping doesn't change the crystalline phase of $SrTiO_3$. Besides, in the detailed review of XRD patterns, the calibrated diffraction peak attributed to [110] reflection (Figure 1B) using NaCl [200] peak as the standard [24,26]. The diffracted angle shifted slightly toward the lower angles and the lattice spacing (110) plane (Figure 3-1C) decreases with increasing the amount of Mg ion (>2 mol%) compared to those of purity $SrTiO_3$, suggesting the incorporation of Mg ion into the lattice of $SrTiO_3$. To the best of our knowledge, the ionic radius of the six-coordinated Mg^{2+} (0.72 Å) is slightly larger than that of Ti^{4+} (0.605 Å) and smaller than that of the twelve-coordinated Sr^{2+} (1.44 Å). According to the Goldschmidt tolerance factors ($t = (r_A+r_O)/\sqrt{2}(r_B+r_O)$) exhibiting the degree of deviation of the ideal perovskite crystal structure, the calcinated t-value (Figure 3-1C) for the substitution of Sr^{2+}-site or Ti^{4+}-site by Mg^{2+}, leading to the shift towards lower angle or higher angles are within the allowed t-values (0.75 to 1.0). Therefore, the shift of the diffraction (110) peak towards the lower angles and the decreased lattice spacing (110) plane affirms that the substitution of Ti^{4+}-site by Mg^{2+}, which is in contrast to that of Al-doping [34]. Besides, from the results of the energy-dispersive X-ray spectrum (EDS) in Figure 3-4g, no signal of Al element is observed, suggesting negligible amounts of Al-doping. However, the fixed (110) peak when the amount of doped Mg^{2+} is more than 4 mol% suggests the small additional substitution of Sr^{2+}-site or the location on the surface of the sample. The collected UV-vis absorption spectra of pristine $SrTiO_3$ and Mg-$SrTiO_3$ (flux) is shown in Figure 3-2. The same absorption edges of Mg-$SrTiO_3$ (flux) and pristine $SrTiO_3$ suggest an insignificant influence of bandgap by the introduction of Mg ion on the photocatalytic overall water splitting.

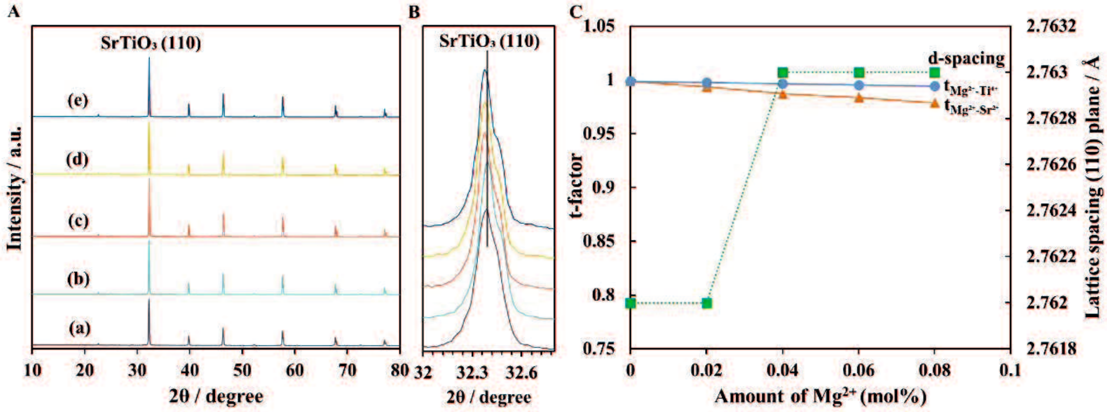

Figure 3-1. XRD patterns of the pristine $SrTiO_3$ (SSR) and Mg-$SrTiO_3$ (flux): (A, B) (a) pristine $SrTiO_3$; (b) Mg(0.02)-$SrTiO_3$; (c) Mg(0.04)-$SrTiO_3$; (d) Mg(0.06)-$SrTiO_3$; (e) Mg(0.08)-$SrTiO_3$ (C) Relationship between the amount of incorporated Mg ion and the shift in the lattice spacing of the (110) plane and tolerance factor (t-value). $t_{Mg^{2+}\text{-}Ti^{4+}}$: the substitution of the Ti^{4+}-site by Mg^{2+}; $t_{Mg^{2+}\text{-}Sr^{2+}}$: the substitution the Sr^{2+}-site by Mg^{2+}.

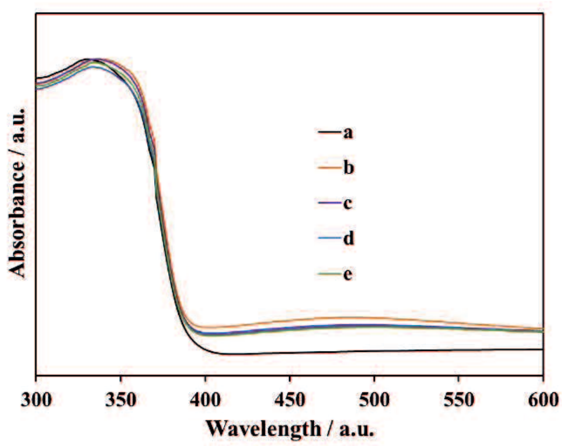

Figure 3-2. UV-Vis absorbance spectra of (a) $SrTiO_3$ (SSR), (b) Mg(0.02)- $SrTiO_3$ (flux), (c) Mg(0.04)- $SrTiO_3$ (flux), (d) Mg(0.06)- $SrTiO_3$ (flux), and (e) Mg(0.08)-$SrTiO_3$ (flux).

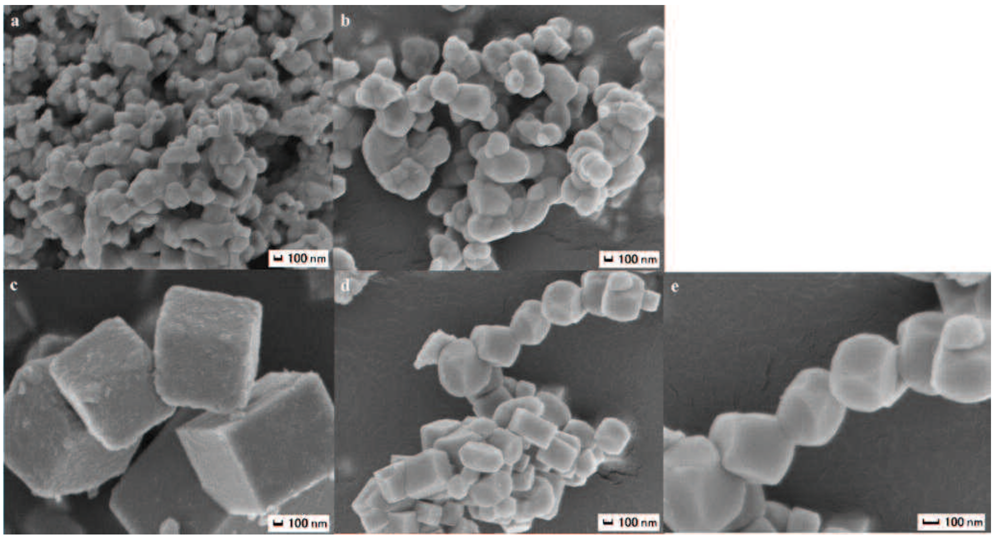

Figure 3-3. SEM images of (a) $SrTiO_3$ (SSR), (b) Mg(0.7 mol%)-$SrTiO_3$ (SSR), (c) Mg(0)-$SrTiO_3$ (flux), and (d and e) Mg(0.02)-$SrTiO_3$ (flux).

Figure 3-3 shows the SEM images of the pristine $SrTiO_3$, Mg-$SrTiO_3$ (SSR), and Mg-$SrTiO_3$ (flux) samples fabricated via the flux method. The purity $SrTiO_3$ and Mg-$SrTiO_3$ (SSR) samples prepared by the SSR method show an irregular morphology aggregated nano-particles. The Mg(0)-$SrTiO_3$ (flux) sample which was prepared by the flux method without adding MgO powder shows cubic particles with a large size and rough surface, while the Mg(0.04)-$SrTiO_3$ (flux) synthesized by the flux method with adding a small amount of MgO powder displays an irregularly polyhedral cube with exposing several different smooth crystal facets, which is conducive to the separation of the reduction and oxidation catalytic sites. Several cubic particles were also present. Simultaneously, the TEM images were investigated as well as the chemical compositions were determined by EDS-mapping. As shown in 3-4, the morphology observed from TEM images corresponds to that from the SEM image. The EDS images are shown in Figure 3-4(g) confirmed the existence of Sr, Ti, O, and Mg in the samples, and the C signal was from the TEM support grid for the powder samples. The Mg ions were homogeneously presented in the Mg-$SrTiO_3$ (flux) nano-cubes lattice from the EDS elemental mapping images in Figure 3-4(c-f), suggesting the successful doping of Mg^{2+}.

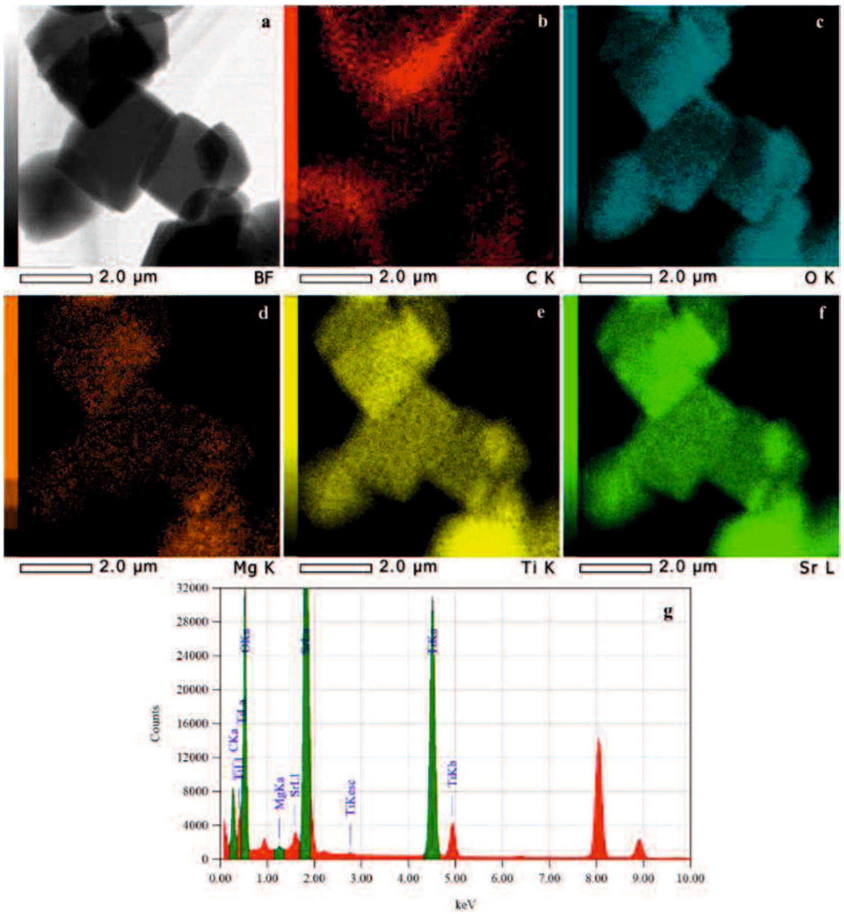

Figure 3-4. TEM image, (b-f) STEM-EDS elemental mapping images of Mg-$SrTiO_3$ (flux), and (g) EDS spectrum.

To best our knowledge, the noble metals and metal oxide were randomly dispersed on the surface of photocatalyst by the impregnation method, while they were selectively deposited by the photo-deposition method. Therefore, the STEM-EDS mapping images of the prepared samples were observed as shown in Figure 3-5 and the results are consistent with the previous report. The cocatalysts $Rh_{2-y}Cr_yO_3$ with a corundum structure [35] and CoO_x deposited by the impregnation method was evenly dispersed all over the surface of the photocatalyst, while the cocatalysts Rh/Cr_2O_3 with a core/shell structure [32] and CoOOH were selectively loaded on the separated crystal faces, which created the spatial separation of charge carriers and improved the photocatalytic activity. The detailed high-resolution images of STEM-EDS mapping are shown in Figure 3-6.

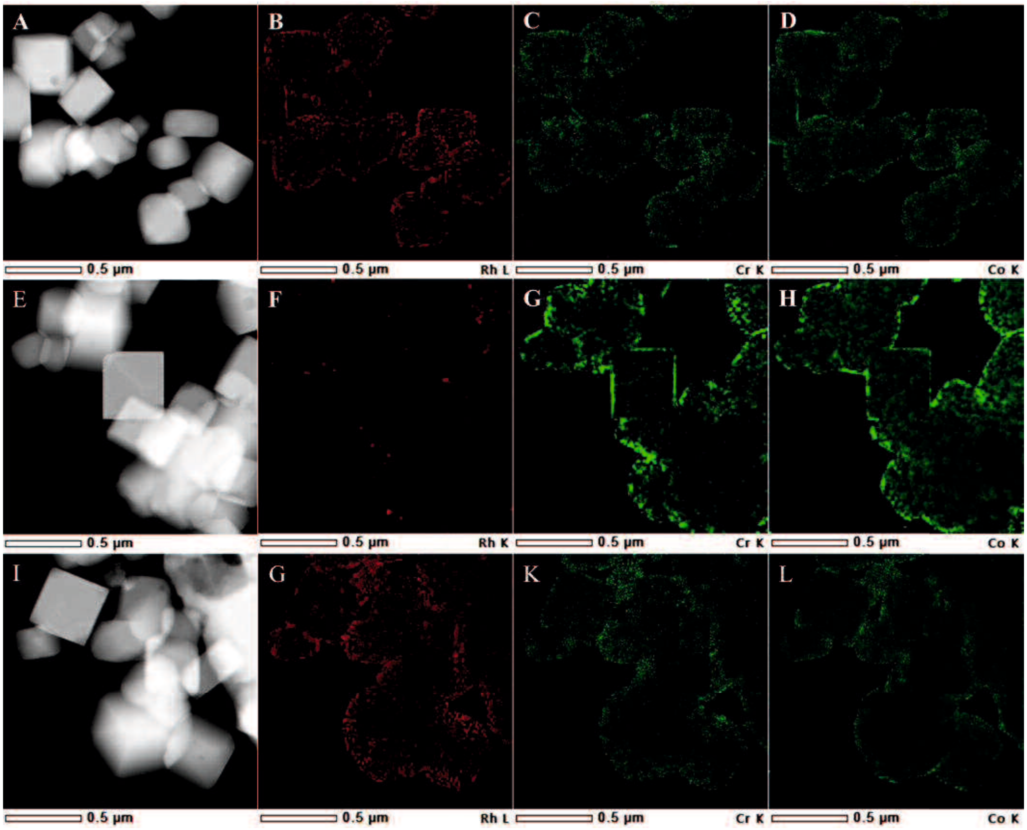

Figure 3-5. Location of cocatalysts. SEM images and STEM-EDS elemental mappings of Mg-$SrTiO_3$ (flux) loaded with various cocatalysts. (a-d) loaded with $Rh_{2-y}Cr_yO_3$ (Imp. Rh, 0.1 wt%; Cr, 0.1 wt%) and CoO_x (Imp. Co, 0.05 wt%) (e-h), $Rh_{2-y}Cr_yO_3$ (Imp. Rh, 0.1 wt%; Cr, 0.1 wt%) and CoOOH (P.D. Co, 0.1 wt%) (c) Rh (0.1 wt%)/Cr_2O_3 (0.05 wt%)/CoOOH (0.05 wt%) (i-l). (0.05 wt%)/CoOOH (0.05 wt%).

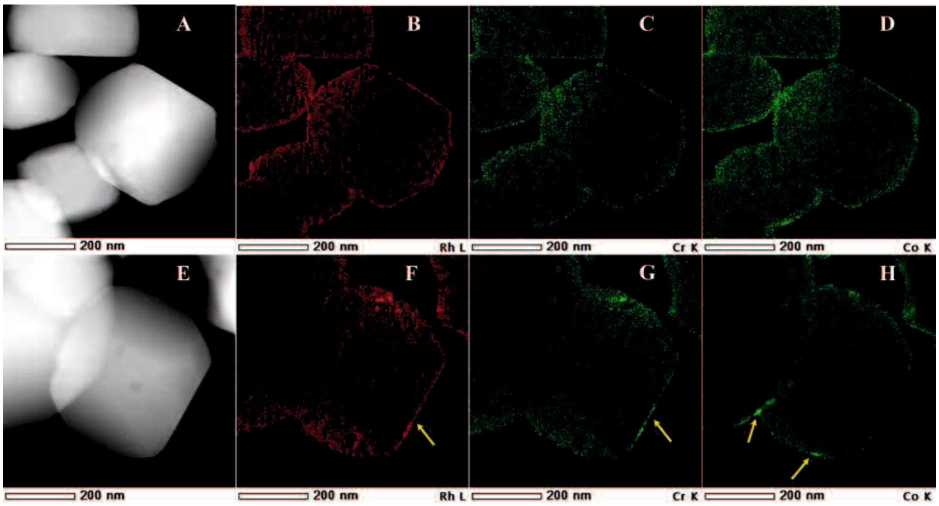

Figure 3-6. Magnified TEM images and STEM-EDS elemental mappings of Mg-$SrTiO_3$ (flux) loaded with (a-d) $Rh_{2-y}Cr_yO_3$ and CoO_x deposited by the impregnation method. (e-h) Rh/Cr_2O_3/CoOOH cocatalysts loaded by the photo-deposition method.

3.3.2 Photocatalytic activity

Dependence of the photocatalytic activity and AQY of Rh/Cr_2O_3/CoOOH loaded-Al-$SrTiO_3$ photocatalyst on light intensity and wavelength

The Rh(0.05 wt%)/Cr_2O_3 (0.05 wt%)/CoOOH(0.05 wt%)/Al-$SrTiO_3$ photocatalyst shows a remarkably high photocatalytic activity. The dependences of the water-splitting activity of the photocatalyst on light intensity and wavelength were measured. The results are shown in Figure 3-7, Figure 3-8, and Table 3-1. The AQY value was almost unchanged, suggesting the independence of the light intensity in the relevant range. The average AQY values which were measured in this series of experiments is calculated to be 91.6%. The relevant plot involved was shown in Figure 3-7. The dependence of the AQY during overall water splitting using the most optimal Rh/Cr_2O_3/CoOOH/Al-$SrTiO_3$ and the UV–vis diffuse reflectance spectrum of Al-$SrTiO_3$ were shown in Figure 3-8 and Table 3-1 gives the AQYs at the corresponding wavelength. The AQY values at 350 nm, 360 nm, and 365 nm were measured to be 95.7%, 95.9%, and 91.6%, respectively. As far as we know, these values are the highest among the reported water-splitting photocatalysts. The AQY values at 370 nm and 380 nm were decreased to 59.7% and 33.6% due to the decreased light absorption and probably the lower AQY at these wavelengths, respectively.

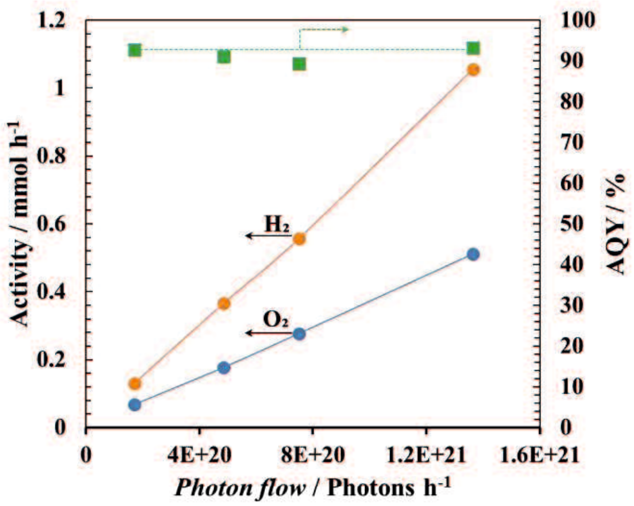

Figure 3-7. Dependence of the water splitting activity and AQY values of Rh (0.1 wt%)/Cr_2O_3 (Cr: 0.05 wt%)/CoOOH (Co: 0.05 wt%)-loaded Al-$SrTiO_3$ (flux) on the light intensity: Reaction conditions: photocatalyst, 0.1 g; reaction solution, 100 mL of distilled water; reactor, top-irradiation-type reactor; light source, 300 W Xenon lamp.

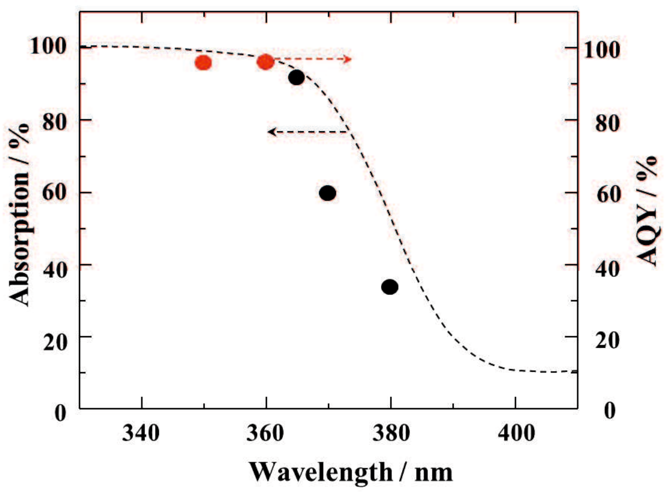

Figure 3-8. Dependence of the water-splitting activity and AQY of Rh (0.1 wt%)/Cr_2O_3 (Cr: 0.05 wt%)/CoOOH (Co: 0.05 wt%)-loaded Al-$SrTiO_3$ (flux) on wavelength: Reaction conditions: photocatalyst, 0.1 g; reaction solution, 100 mL of distilled water; reactor, top-irradiation-type reactor; light source, 300 W Xenon lamp.

Table 3-2. Results of AQY measurements over Rh (0.1 wt%)/Cr_2O_3 (Cr: 0.05 wt%)/CoOOH (Co: 0.05 wt%)-loaded Al-$SrTiO_3$ (flux)

Wavelength/nm	OD#	Photons / h	Activity / μmol h^{-1}		AQY / %
			H_2	O_2	
350	0	5.26×10^{19}	41.8	20.3	95.7
360	0	1.27×10^{20}	101	54.3	95.9
365	0	1.36×10^{21}	1060	512	93.2
365	0.3	7.49×10^{20}	557	276	89.4
365	0.5	4.84×10^{20}	366	177	91.1
365	1.0	1.70×10^{20}	131	67.3	92.8
370	0	2.54×10^{20}	126	65.2	59.7
380	0	2.06×10^{20}	57.3	25.8	33.6

The AQY value at 365 nm was essentially independent of the light intensity over the range of intensities examined. The average AQY in this series of experiments was 91.6% which was used to generate the plot shown in Figure 3-12. Reaction conditions: photocatalyst, 0.1 g; reaction solution, 100 mL of distilled water; reactor, top-irradiation-type reactor; light source, 300 W Xenon lamp.

#OD, optical density.

Effect of doped various metal ions in $SrTiO_3$ using the flux method on the photocatalytic activity

Inspired by the previous investigations [24,30], the photocatalytic activity of $SrTiO_3$ was improved by adding various metal ions via an impregnation method. Herein, various aliovalent metal ions were introduced into the $SrTiO_3$ lattice through the $SrCl_2$ flux method by adding the corresponding metal oxide under the optimal preparation conditions. The photocatalytic activities of as-prepared samples are shown in Figure 3-9. As shown in Figure 3-9, the Mg-$SrTiO_3$ (flux) sample achieved an outstanding photocatalytic activity among various dopants by the same preparation procedure and condition, suggesting the superiority as an effective dopant of $SrTiO_3$ with lower valance than the other mental ions substituting the Ti^{4+}-site. Therefore, the Mg-$SrTiO_3$ (flux) was taken as a model photocatalyst as an example to further study and confirm the reproducibility of photocatalytic water splitting with a quantum efficiency of almost unity.

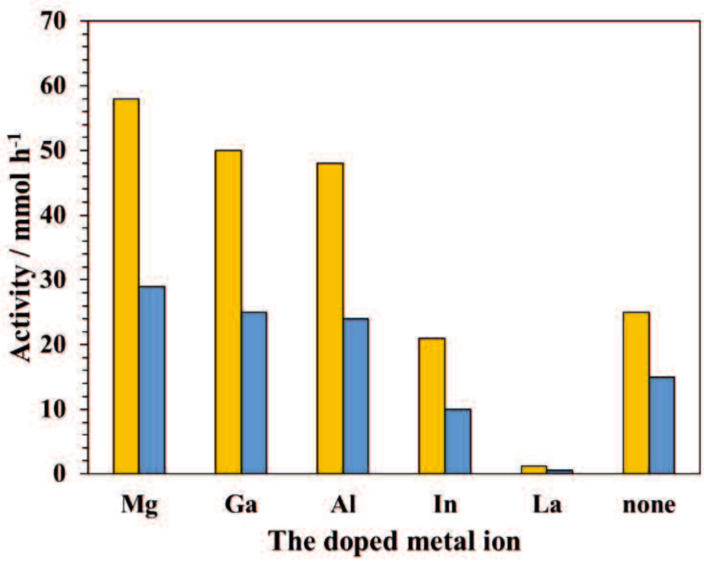

Figure 3-9. The photocatalytic activity of various metal ions doped $SrTiO_3$ prepared by the flux method. Reaction conditions: photocatalyst, 1.0 g; reaction solution, 600 mL of distilled water; reactor, inner-irradiation reactor; light source, 450 W high-pressure Hg-lamp.

Effect of preparation conditions for the Mg-doping into $SrTiO_3$ on the photocatalytic activity

Figure 3-10 shows the photocatalytic activity of Mg-$SrTiO_3$ prepared by the PC method as a function amount of doped Mg ion and photocatalytic activity of Mg(2 mol%)-$SrTiO_3$ as a function of the amount of preparation temperature, respectively. The photocatalytic activity of purity $SrTiO_3$ shows a poor activity for overall H_2O splitting. When a small number of Mg was doped into the $SrTiO_3$, the activity was remarkably improved. As shown in Figure 3-10, the preferable amount of doped Mg was 2 mol%, and the optimal preparation temperature for doping Mg ion into $SrTiO_3$ was 1223 K.

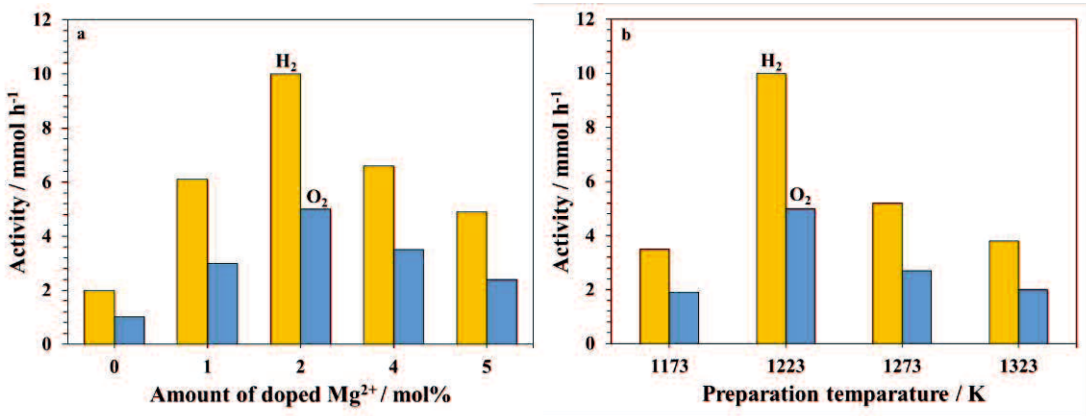

Figure 3-10. (a) Photocatalytic activity of Mg-$SrTiO_3$ (PC) for overall H_2O splitting as a function of the amount of doped Mg^{2+} and (b) photocatalytic activity of Mg(2 mol%)-$SrTiO_3$ (PC) as a function of preparation temperature. Reaction conditions: photocatalyst, 1.0 g; reaction solution, 600 mL of distilled water; reactor, inner-irradiation reactor; light source, 450 W high-pressure Hg-lamp.

The optimal preparation parameter for effective doping Mg used the SSR method was also discussed. Figure 3-11 shows the photocatalytic activity of Mg-$SrTiO_3$ prepared by the SSR method as a function amount of doped Mg ion and photocatalytic activity of Mg(2 mol%)-$SrTiO_3$ (SSR) as a function of the amount of preparation temperature, respectively. The optimal amount of doped Mg and preparation temperature was 0.7 mol% and 1373 K, respectively。

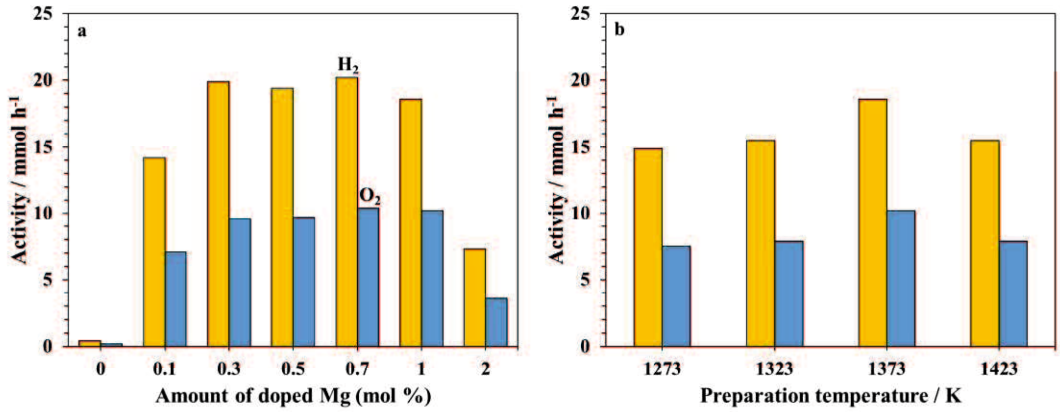

Figure 3-11. (a) Photocatalytic activity of Mg-$SrTiO_3$ (SSR) for overall H_2O splitting as a function of the amount of doped Mg^{2+} and (b) photocatalytic activity of Mg(2 mol%)-$SrTiO_3$ (SSR) as a function of preparation temperature. Reaction conditions: photocatalyst, 1.0 g; reaction solution, 600 mL of distilled water; reactor, inner-irradiation reactor; light source, 450 W high-pressure Hg-lamp.

Figure 3-12 shows the photocatalytic activity of Mg-$SrTiO_3$ (flux) for overall H_2O splitting as a function of the amount of doped Mg and (b) photocatalytic activity of Mg(0.04)-$SrTiO_3$ (flux) as a function of preparation temperature. From the results in Figure 3-3, the optimal molar ratio of MgO powder/$SrTiO_3$ for preparing highly active Mg-$SrTiO_3$ by the $SrCl_2$ flux treatment was 0.04. Herein, the practical preferable content of Mg ion incorporated into the $SrTiO_3$ was around 0.39 mol% calculated from the results of ICP-OES by using the flux method.

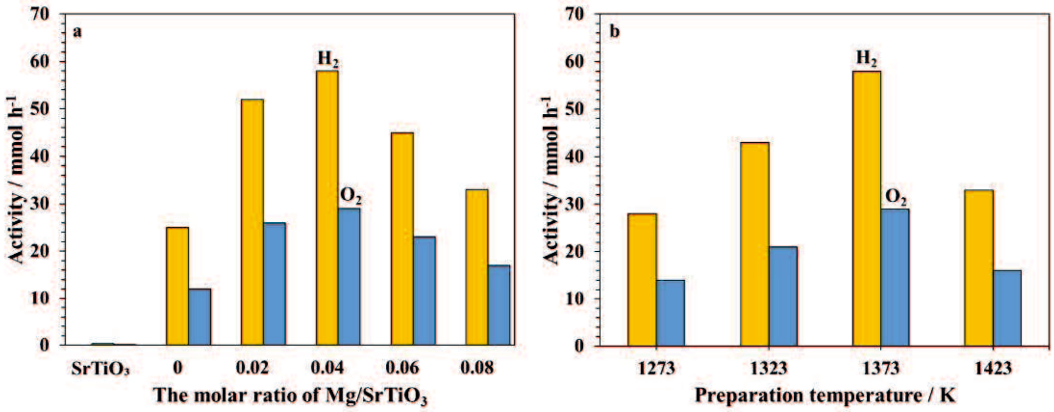

Figure 3-12 (a) Photocatalytic activity of Mg-$SrTiO_3$ (flux) for overall H_2O splitting as a function of the amount of doped Mg^{2+} and (b) photocatalytic activity of Mg(0.04)-$SrTiO_3$ (flux) as a function of preparation temperature. Reaction conditions: photocatalyst, 1.0 g; reaction solution, 600 mL of distilled water; reactor, inner-irradiation reactor; light source, 450 W high-pressure Hg-lamp.

Effect of the preparation methods on the photocatalytic activity

The optimal amount of doped Mg ion for the SSR method and preferable added MgO using the flux method for preparing highly actively Mg-$SrTiO_3$ have been confirmed from Figure 3-10, Figure 3-11, and Figure 3-12. Figure 3-13 shows the photocatalytic activities of pure Mg-$SrTiO_3$ (PC), Mg-$SrTiO_3$ (SSR), Mg(0)-$SrTiO_3$(flux) and Mg(0.04)-$SrTiO_3$ (flux). It can be noticed that the pure $SrTiO_3$ shows a very low photocatalytic activity of nearly 0.4 mmol h^{-1} for H_2 evolution and 0.2 mmol h^{-1} for O_2 evolution, which is attributed to the bulk-rich defects in $SrTiO_3$ as the recombination centers. The introduction of a small amount of aliovalent magnesium ion into the $SrTiO_3$ lattice using the SSR method can decrease the density of the defects, forming a favorable surface-space-charge layer [27] remarkably and thus improved the water-splitting activity of $SrTiO_3$ to 20 mmol h^{-1} for H_2 evolution and 10 mmol h^{-1} for O_2 evolution, respectively. While the Mg ion was incorporated into the $SrTiO_3$ lattice through the $SrCl_2$ flux method by adding a small amount of MgO powder to modify the morphology of the photocatalyst, and the photocatalytic activity was further increased to 58 mmol h^{-1} for hydrogen evolution and 29 mmol h^{-1} for oxygen evolution, respectively. According to the previous report by Ham et al. [25], using the flux method to treat $SrTiO_3$ in the alumina crucible could introduce the Al ion. Therefore, as a comparison, the photocatalytic activity of the pristine $SrTiO_3$ sample that was treated only using an $SrCl_2$ flux in alumina crucible was investigated and achieved an activity of 25 mmol h^{-1} for hydrogen evolution and 15 mmol h^{-1} for oxygen evolution, which is much lower than that of the sample using the $SrCl_2$ flux method with adding a little MgO powder under the same preparation and reaction conditions. The above results suggested that the improvement of photocatalytic activity of Mg-$SrTiO_3$ (flux) is mainly ascribed to the doping of Mg and the polyhedral morphology.

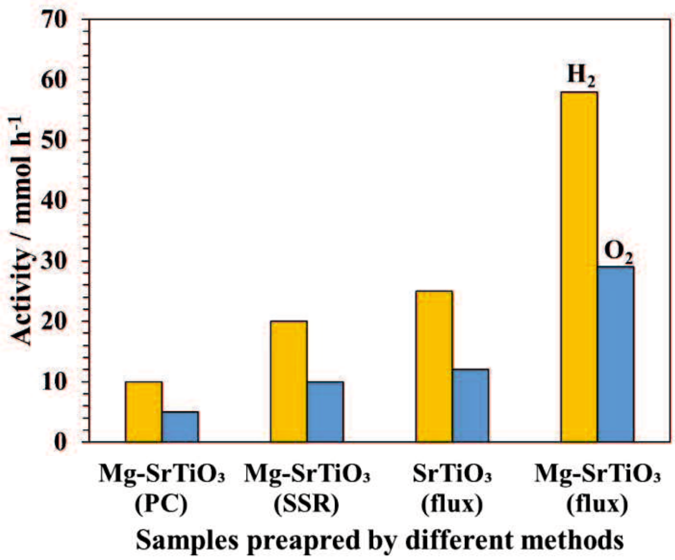

Figure 3-13. Photocatalytic activity of Mg-$SrTiO_3$ as a function of the preparation method for overall H_2O splitting. Reaction conditions: photocatalyst, 1.0 g; reaction solution, 600 mL of distilled water; reactor, inner-irradiation reactor; light source, 450 W high-pressure Hg-lamp.

Effect of the deposition method of cocatalysts on the photocatalytic activity

To further improve the effect of the deposition method for loading cocatalysts on the photocatalytic activity of Mg-$SrTiO_3$ (flux), the deposition methods for loading Rh and Cr species for hydrogen evolution reaction (HER) and Co species for oxygen evolution reaction (OER) were investigated. Figure 3-14 shows the time courses of water-splitting activity of Mg-$SrTiO_3$ (flux) loaded with Rh, Cr, and Co species by the impregnation methods. As seen in Figure 3-14(a), Mg-$SrTiO_3$ (flux) rapidly deactivated with only loading Rh and Cr species by the impregnation methods. When a small amount of Co species was coloaded by the impregnation method, the photocatalytic activity was remarkably improved and maintained stable for a longer time.

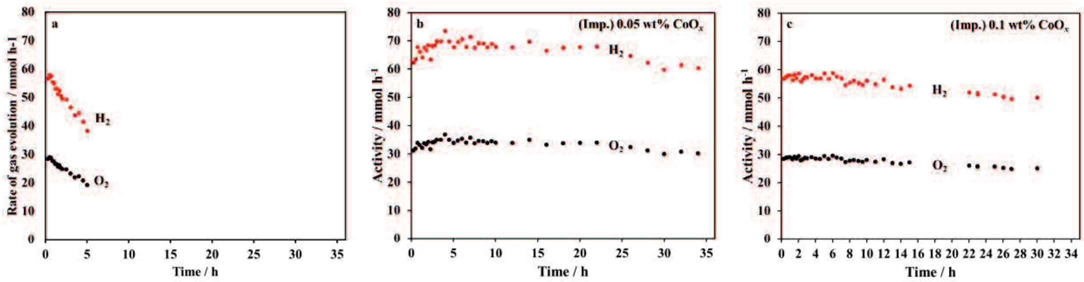

Figure 3-14. Time courses of water-splitting activity of Mg-$SrTiO_3$ (flux) loaded with (a) $Rh_yCr_{2-y}O_3$ (Imp. Rh: 0.1wt%, Cr: 0.1 wt%), (b) $Rh_yCr_{2-y}O_3$ (Imp. Rh: 0.1wt%, Cr: 0.1 wt%) and CoO_x (Imp. Co: 0.05 wt%), and (c) (Imp.) $Rh_yCr_{2-y}O_3$ (Rh: 0.1 wt%, Cr: 0.1wt%), and (Imp.) CoO_x (Co: 0.1 wt%). Reaction conditions: photocatalyst, 1.0 g; reaction solution, 600 mL distilled water; light source, 450 W high-pressure Hg lamp.

Figure 3-15 shows the time courses of water-splitting activity of Mg-$SrTiO_3$ (flux) loaded with Rh and Cr species by the impregnation methods and Co species by the photo-deposition method. The optical sample loaded Co species by the photo-deposition method showed higher activity than that loaded Co species by the impregnation method. The photocatalytic activity also remained stable for a long time.

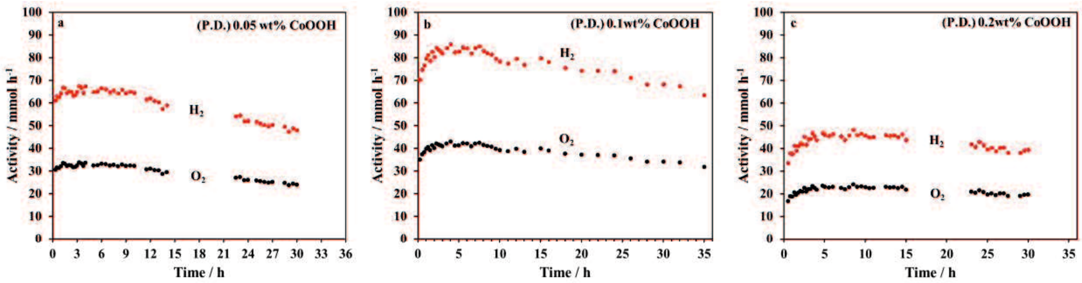

Figure 3-15. Time courses of water-splitting activity of Mg-$SrTiO_3$ (flux) loaded with (a) $Rh_yCr_{2-y}O_3$ (Imp. Rh: 0.1wt%, Cr: 0.1 wt%) and CoOOH at concentrations of Co species (a) 0.05 wt%, (b) 0.1 wt%, and (c) 0.2 wt%. Reaction conditions: photocatalyst, 1.0 g; reaction solution, 600 mL distilled water; light source, 450 W high-pressure Hg lamp.

Figure 3-16 shows the time courses of photocatalytic overall splitting reaction over-optimized the $Rh_{2-y}Cr_yO_3$/Mg-$SrTiO_3$ (Flux), $Rh_{2-y}Cr_yO_3$/Mg-$SrTiO_3$ (flux)/CoO_x, $Rh_{2-y}Cr_yO_3$/Mg-$SrTiO_3$ (flux)/CoOOH, Rh/Cr_2O_3/CoOOH/Mg-$SrTiO_3$ (flux) under irradiation from a 300 W Xenon lamp. Continuous H_2 and O_2 were generated in a stoichiometric ratio of 2/1. All the samples show excellent photocatalytic performance, especially the Rh/Cr_2O_3/CoOOH/Mg-$SrTiO_3$ (flux) sample. After 2.5 hours, the pressure in the system full of evolved gases (hydrogen and oxygen) from the photocatalytic overall water splitting reaction over Rh/Cr_2O_3/CoOOH/Mg-$SrTiO_3$ (flux) arrived quickly at 100 kPa than that over the other samples. Table 3-2 shows the photocatalytic activities and AQY values at 365 nm of Mg-$SrTiO_3$ (flux) loaded HEC and OEC by various methods. The water-splitting activity of H_2 and O_2 is 2.23 and 1.07 mmol h^{-1} over $Rh_{2-y}Cr_yO_3$/Mg-$SrTiO_3$ (flux), respectively. Following co-loading Co species as OEC, the photocatalytic activities are further improved. The Mg-$SrTiO_3$ (flux) loaded with Rh/Cr_2O_3 core-shell structure as HEC and CoOOH as OEC shows the highest activity of 5.05 mmol h^{-1} for H_2 evolution and 2.38 mmol h^{-1} O_2 evolution, while the two photocatalysts Mg-$SrTiO_3$ (flux) loaded $Rh_{2-y}Cr_yO_3$ by the impregnation method and Co species by the impregnation method or in-site photo-deposition method showed similar photocatalytic activity as shown in Table 3-2.

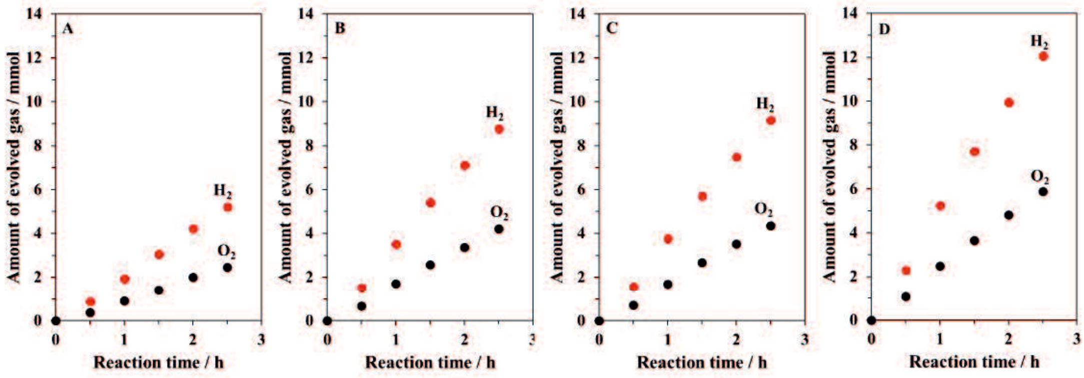

Figure 3-16. Time courses of photocatalytic overall water splitting reaction at background pressures of 10 kPa over Mg-$SrTiO_3$ (flux) loaded with (a) $Rh_yCr_{2-y}O_3$ (Rh: 0.1 wt%), (b) $Rh_yCr_{2-y}O_3$ (Rh: 0.1wt%) and 0.05 wt% CoO_x, and (c) $Rh_yCr_{2-y}O_3$ (Rh: 0.1 wt%), 0.1 wt% CoOOH and (d) Rh (0.1 wt%)/Cr_2O_3 (Cr: 0.05 wt%)/CoOOH (Co: 0.05 wt%). Reaction conditions: photocatalyst, 0.1 g; reaction solution, 100 mL of distilled water; reactor, top-irradiation reactor; light source, 300 W Xenon lamp (full arc).

Table 3-2. Photocatalytic water splitting activities of Mg-$SrTiO_3$ (flux) modified with HEC and OEC by various deposition methods.

Samples	Co-catalyst	Rh	Cr	Co	Activity / mmol h^{-1} (Full arc) H_2	O_2	AQY / % at 365 nm
(a)	$Rh_yCr_{2-y}O_3$	Imp.	Imp.		2.23	1.07	55
(b)	$Rh_yCr_{2-y}O_3/CoO_x$	Imp.	Imp.	Imp.	3.36	1.64	
(c)	$Rh_yCr_{2-y}O_3$/CoOOH	Imp.	Imp.	P.D.	3.50	1.71	68
(d)	Rh/Cr_2O_3/CoOOH	P.D.	P.D.	P.D.	5.05	2.48	88

Imp., Impregnation method; P.D., Photodeposition method

Reaction conditions: photocatalyst, 0.1 g; reaction solution, 100 mL of distilled water; reactor, top-irradiation reactor; light source, 300 W Xenon lamp (full arc).

Effects of light intensity on photocatalytic water splitting and AQY of Mg-$SrTiO_3$ modified with Rh, Cr, and Co species using various deposition methods

To further verify the photocatalytic performances of the photocatalysts, the activity dependence of water splitting over Mg-$SrTiO_3$ (flux) was modified with $Rh_{2-y}Cr_yO_3$, $Rh_{2-y}Cr_yO_3/CoO_x$, and CoOOH, and Rh/Cr_2O_3/CoOOH cocatalysts on the light intensity over the range from 1.0×10^{20} to 1.6×10^{21} photons h^{-1} was carried out using the monochromatic light at 365 nm. The activity dependence and time courses of overall water splitting reaction on light intensity are shown in Figure 3-17 and Figure 3-18. As shown in Figure 3-17 and Figure 3-18, the H_2 and O_2 evolved stoichiometrically during the overall water splitting reaction and the rates were both increasing linearly within the light intensity, suggesting the AQY was effectively unrelated to the light intensity. As shown in Table 3-1, the $Rh_{2-y}Cr_yO_3$/Mg-$SrTiO_3$ (flux) achieved an AQY of 55% at 365 nm, and following co-loading the CoOOH as OEC, the AQY value increased to 68%. When the HEC and OEC were both deposited on the photocatalyst by the photo-deposition method, an AQY value of 88% was achieved.

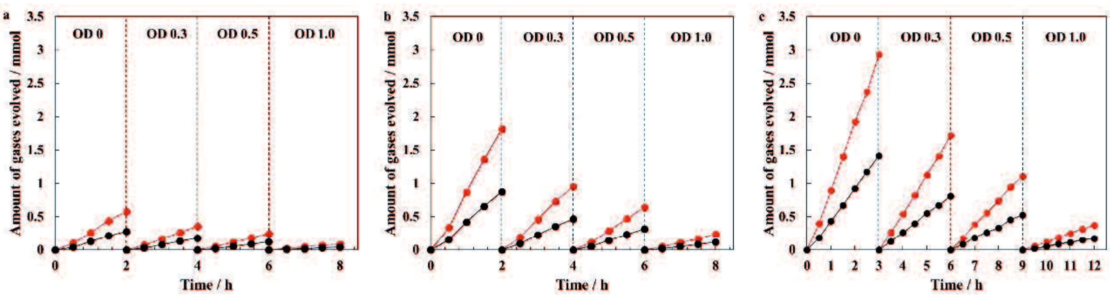

Figure 3-17. Dependence of time courses of photocatalytic overall water splitting reaction at background pressures of 30 kPa on the light intensity over Mg-$SrTiO_3$ (flux) loaded with $Rh_yCr_{2-y}O_3$ (Imp. Rh: 0.1 wt%), and (a) 0 (b) CoOOH, (P.D. Co: 0.1 wt%), and (c) Rh (P.D. 0.1 wt%)/Cr_2O_3 (P.D. Cr: 0.05 wt%)/CoOOH (P.D. Co: 0.05 wt%). Reaction conditions: photocatalyst, 0.2 g; reaction solution, 140 mL of distilled water; reactor, top-irradiation reactor; light source, 500 W Deep UV lamp.

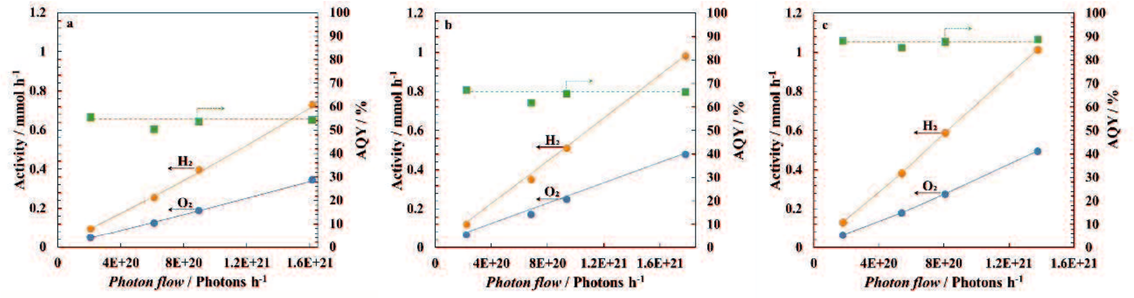

Figure 3-18. Dependence of water-splitting activity and AQY values at background pressures of 30 kPa on the light intensity over Mg-$SrTiO_3$ (flux) loaded with $Rh_yCr_{2-y}O_3$ (Imp. Rh: 0.1 wt%), and (a) 0 (b) CoOOH, (P.D. Co: 0.1 wt%), and (c) Rh (P.D. 0.1 wt%)/Cr_2O_3 (P.D. Cr: 0.05 wt%)/CoOOH (P.D. Co: 0.05 wt%). Reaction conditions: photocatalyst, 0.2 g; reaction solution, 140 mL of distilled water; reactor, top-irradiation reactor; light source, 500 W Deep UV lamp.

3.3.3 AQY dependence of Rh/Cr_2O_3/CoOOH loaded-Al-$SrTiO_3$ photocatalyst on light wavelength

Figure 3-19 gives ultraviolet-visible diffuse reflectance spectrum of (a) bare Mg-$SrTiO_3$ (flux) and wavelength dependence of apparent quantum efficiency (AQY) during water splitting on Rh (0.1 wt%)/Cr_2O_3 (0.05 wt%)/CoOOH (0.05 wt%)-loaded Mg-$SrTiO_3$ (flux). The achieved AQY value at 350 nm and 360 nm is 93.9% and 92.5%, respectively, suggesting almost all the generated electrons and holes were almost fully utilized to overall water splitting applying the current AQY measurement technology regardless of light loss on account of scattering and reflection. The AQY values were similar to that of Rh (0.1 wt%)/Cr_2O_3 (0.05 wt%)/CoOOH (0.05 wt%)-loaded Al-$SrTiO_3$ (flux) [30].

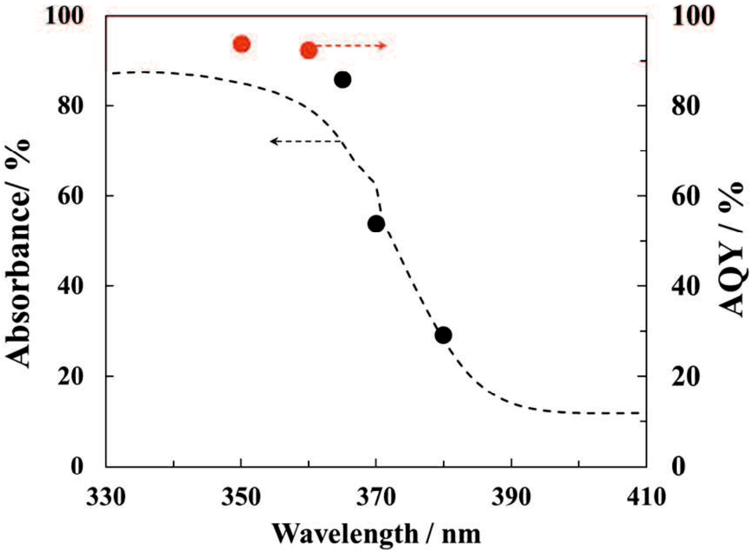

Figure 3-19. UV–vis diffuse reflectance spectrum of (a) bare Mg-$SrTiO_3$ (flux) and wavelength dependence of apparent quantum efficiency (AQY) during overall water splitting on Rh (0.1 wt%)/Cr_2O_3 (0.05 wt%)/CoOOH (0.05 wt%)/Mg-$SrTiO_3$ (flux). Reaction conditions: photocatalyst, 0.1 g; reaction solution, 140 mL of distilled water; reactor, top-irradiation-type reactor; light source, 300 W Xenon lamp.

3.4 Conclusions

The Mg ion-doped $SrTiO_3$ using the $SrCl_2$ flux method was investigated. The successful doping of Mg ion into the $SrTiO_3$ and substituted the Ti^{4+}-site was supported by the detailed structural study. The absence of an Al signal in the EDS spectrum and elemental mapping images indicated negligible Al-doing. The Mg-$SrTiO_3$ (flux) shows cubic and tailoring morphologies suggesting the separated reduction and oxidation facets. The subsequently modified Mg-$SrTiO_3$ (flux) using Rh, Cr, and Co species as HEC and OEC, respectively, achieved high photocatalytic activity and apparent quantum efficiencies. The Rh, Cr, and Co species were selectively deposited on the different surfaces of Mg-$SrTiO_3$ (flux) cubic nanoparticles observed from the TEM-EDS mapping images. The Rh/Cr_2O_3/CoOOH/Mg-$SrTiO_3$ (flux) reproduced again the photocatalytic overall water splitting quantum efficiency of almost unity, which can be attributed to the decreasing defects by Mg-doping and the separated reduction and oxidation facets.

3.5 References

[1] W.-J. Ong, L.-L. Tan, Y.H. Ng, S.-T. Yong, S.-P. Chai, Graphitic carbon nitride ($g-C_3N_4$)-based photocatalysts for artificial photosynthesis and environmental remediation: Are we a step closer to achieving sustainability? Chem. Rev. 116 (2016) 7159–7329.

[2] A.D. Handoko, K. Li, J. Tang, Recent progress in artificial photosynthesis: CO_2 photoreduction to valuable chemicals in a heterogeneous system, Curr. Opin. Chem. Eng. 2 (2013) 200–206.

[3] Y. Zhang, Y.J. Heo, J.W. Lee, J.H. Lee, J. Bajgai, K.J. Lee, S.J. Park, Photocatalytic hydrogen evolution via water splitting: A short review, Catalysts 8 (2018) 655.

[4] H. Ahmad, S.K. Kamarudin, L.J. Minggu, M. Kassim, Hydrogen from photo-catalytic water splitting process: A review, Renew. Sustain. Energy Rev. 43 (2015) 599–610.

[5] S. Ye, C. Ding, M. Liu, A. Wang, Q. Huang, C. Li, Water oxidation catalysts for artificial photosynthesis, Adv. Mater. 31 (2019) 1902069.

[6] D.M. Schultz, T.P. Yoon, Solar synthesis: Prospects in visible light photocatalysis, Science 343 (2014) 1239176.

[7] T. Takata, K. Domen, Particulate photocatalysts for water splitting: Recent advances and future prospects, ACS Energy Lett. 4 (2019) 542–549.

[8] S. Chen, T. Takata, K. Domen, Particulate photocatalysts for overall water splitting, Nat. Rev. Mater. 2 (2017) 1–17.

[9] T. Yamada, K. Domen, Development of sunlight driven water splitting devices towards future artificial photosynthetic industry, ChemEngineering 2 (2018) 36.

[10] Y. Goto, T. Hisatomi, Q. Wang, T. Higashi, K. Ishikiriyama, T. Maeda, Y. Sakata, S. Okunaka, H. Tokudome, M. Katayama, S. Akiyama, H. Nishiyama, Y. Inoue, T. Takewaki, T. Setoyama, T. Minegishi, T. Takata, T. Yamada, K. Domen, A particulate photocatalyst water-splitting panel for large-scale solar hydrogen generation, Joule 2 (2018) 509–520.

[11] J. Low, J. Yu, M. Jaroniec, S. Wageh, A.A. Al-Ghamdi, Heterojunction

photocatalysts, Adv. Mater. 29 (2017) 1601694.

[12] X. Chen, S. Shen, L. Guo, S.S. Mao, Semiconductor-based photocatalytic hydrogen generation, Chem. Rev. 110 (2010) 6503–6570.

[13] A. Kudo, Y. Miseki, Heterogeneous photocatalyst materials for water splitting, Chem. Soc. Rev. 38 (2009) 253–278.

[14] H. Kato, K. Asakura, A. Kudo, Highly efficient water splitting into H_2 and O_2 over lanthanum-doped $NaTaO_3$ photocatalysts with high crystallinity and surface nanostructure, J. Am. Chem. Soc. 125 (2003) 3082–3089.

[15] Y. Sakata, T. Hayashi, R. Yasunaga, N. Yanaga, H. Imamura, Remarkably high apparent quantum yield of the overall photocatalytic H_2O splitting achieved by utilizing Zn ion added Ga_2O_3 prepared using dilute $CaCl_2$ solution, Chem. Commun. 51 (2015) 12935-12938.

[16] E. García-López, G. Marcì, B. Megna, F. Parisi, L. Armelao, A. Trovarelli, M. Boaro, L. Palmisano, $SrTiO_3$-based perovskites: Preparation, characterization and photocatalytic activity in gas-solid regime under simulated solar irradiation, J. Catal. 321 (2015) 13–22.

[17] K. Han, Photocatalytic overall water splitting using modified $SrTiO_3$, University of Twente, (2018) 95-112.

[18] H. Yan, Z. Zhang, S. Wang, K. Jin, Review of photoresponsive properties at $SrTiO_3$-based heterointerfaces, Chinese Phys. B 27 (2018) 117804.

[19] K. Domen, S. Naito, M. Soma, T. Onishi, K. Tamaru, Photocatalytic decomposition of water vapour on a NiO-$SrTiO_3$ catalyst, J. Chem. Soc. Chem. Commun. 227 (1980) 543–544.

[20] K. Domen, S. Naito, T. Onishi, K. Tamaru, M. Soma, Study of the photocatalytic decomposition of water vapor over a nickel(II) oxide-strontium titanate ($SrTiO_3$) catalyst, J. Phys. Chem. 86 (1982) 3657–3661.

[21] K. Domen, S. Naito, T. Onishi, K. Tamaru, Photocatalytic decomposition of liquid water on a NiO-$SrTiO_3$ catalyst, Chem. Phys. Lett. 92 (1982) 433–434.

[22] K. Domen, A. Kudo, T. Onishi, Mechanism of photocatalytic decomposition of water into H_2 and O_2 over NiO-$SrTiO_3$, J. Catal. 102 (1986) 92–98.

[23] T. Takata, K. Domen, Defect engineering of photocatalysts by doping of

aliovalent metal cations for efficient water splitting, J. Phys. Chem. C 113 (2009) 19386–19388.

[24] Y. Sakata, Y. Miyoshi, T. Maeda, K. Ishikiriyama, Y. Yamazaki, H. Imamura, Y. Ham, T. Hisatomi, J. Kubota, A. Yamakata, K. Domen, Photocatalytic property of metal ion added $SrTiO_3$ to overall H_2O splitting, Appl. Catal. A Gen. 521 (2016) 227–232.

[25] Y. Ham, T. Hisatomi, Y. Goto, Y. Moriya, Y. Sakata, A. Yamakata, J. Kubota, K. Domen, Flux-mediated doping of $SrTiO_3$ photocatalysts for efficient overall water splitting, J. Mater. Chem. A 4 (2016) 3027–3033.

[26] J. Jiang, K. Kato, H. Fujimori, A. Yamakata, Y. Sakata, Investigation on the highly active $SrTiO_3$ photocatalyst toward overall H_2O splitting by doping Na ion, J. Catal. 390 (2020) 81–89.

[27] K. Han, Y.C. Lin, C.M. Yang, R. Jong, G. Mul, B. Mei, Promoting photocatalytic overall water splitting by controlled magnesium incorporation in $SrTiO_3$ photocatalysts, ChemSusChem 10 (2017) 4510–4516.

[28] H. Lyu, T. Hisatomi, Y. Goto, M. Yoshida, T. Higashi, M. Katayama, T. Takata, T. Minegishi, H. Nishiyama, T. Yamada, Y. Sakata, K. Asakura, K. Domen, An Al-doped $SrTiO_3$ photocatalyst maintaining sunlight-driven overall water splitting activity for over 1000 h of constant illumination, Chem. Sci. 10 (2019) 3196–3201.

[29] T.H. Chiang, H. Lyu, T. Hisatomi, Y. Goto, T. Takata, M. Katayama, T. Minegishi, K. Domen, Efficient photocatalytic water splitting using Al-Doped $SrTiO_3$ coloaded with molybdenum oxide and rhodium-chromium oxide, ACS Catal. 8 (2018) 2782–2788.

[30] T. Takata, J. Jiang, Y. Sakata, M. Nakabayashi, N. Shibata, V. Nandal, K. Seki, T. Hisatomi, K. Domen, Photocatalytic water splitting with a quantum efficiency of almost unity, Nature 581 (2020) 411–414.

[31] K. Maeda, K. Teramura, D. Lu, N. Saito, Y. Inoue, K. Domen, Noble-metal/Cr_2O_3 core/shell nanoparticles as a cocatalyst for photocatalytic overall water splitting, Angew. Chemie - Int. Ed. 45 (2006) 7806–7809.

[32] K. Maeda, K. Teramura, D. Lu, N. Saito, Y. Inoue, K. Domen, Roles of

Rh/Cr_2O_3 (core/shell) nanoparticles photodeposited on visible-light-responsive $(Ga_{1-x}Zn_x)(N_{1-x}O_x)$ solid solutions in photocatalytic overall water splitting, J. Phys. Chem. C 111 (2007) 7554–7560.

[33] Y. Hiramachi, H. Fujimori, A. Yamakata, Y. Sakata, Achievement of High Photocatalytic Performance to $BaTi_4O_9$ Toward Overall H_2O Splitting, ChemCatChem 11 (2019) 6213–6217.

[34] S. Wang, K. Teramura, T. Hisatomi, K. Domen, H. Asakura, S. Hosokawa, T. Tanaka, Effective driving of Ag-loaded and Al-doped $SrTiO_3$ under irradiation at $\lambda > 300$ nm for the photocatalytic conversion of CO_2 by H_2O, ACS Appl. Energy Mater. 3 (2020) 1468–1475.

[35] K. Maeda, K. Teramura, D. Lu, T. Takata, N. Saito, Y. Inoue, K. Domen, Characterization of Rh-Cr mixed-oxide nanoparticles dispersed on $(Ga_{1-x}Zn_x)(N_{1-x}O_x)$ as a cocatalyst for visible-light-driven overall water splitting Kazuhiko, J. Phys. Chem. B 110 (2006) 13753–13758.

Chapter 4 Fabrication of $SrTiO_3$ Doped Metal Ions Utilizing the $SrCl_2$ Flux as a Medium for Photocatalytic Water Splitting under Visible Light

4.1 Introduction

With the development of the economy and industry, energy crisis and environmental pollution have become the two major themes in the field of science and technology. Photocatalytic technology as a solution to environmental pollution and energy crisis has attracted a great deal of attention because of its high efficiency, easy control, low energy consumption, low cost, and no secondary pollution [1–5].

Since it was discovered that the photoelectrode under sunlight illumination can split water, various photocatalytic semiconductor materials are constantly being explored and developed [6–11]. These photocatalysts are widely applied in environmental and energy fields under the soler energy irradiation, for example, photocatalytic overall H_2O splitting to produce H_2 and O_2 [9,12–15], sewage treatment (photocatalytic degradation of dyes, antibiotics, pesticides, and other organic pollutants) [16–21], photocatalytic reduction of heavy metals to reduce their toxicity and bioavailability, gas purification (degrade NO_x, SO_x, VOCs and other gaseous organic pollutants) [20,22,23], and reduction of CO_2 and organic synthesis [24,25]. However, to fundamentally solve environmental pollution and energy crisis, clean, pollution-free, and recyclable energy should be developed. Hydrogen energy produced via utilizing sunlight-driven overall water splitting is considered as the clean energy with the most development potential. In recent years, a large number of photocatalysts for efficiently decomposing water to produce H_2 and O_2 have been developed [12,13,26–39]. Especially, the Al ion-doped $SrTiO_3$ with loading Rh, Cr, and Co species by an in-situ photo-deposition method achieved an apparent quantum yield (AQY) of almost unity [29,40]. However, these photocatalysts only respond to ultraviolet (UV) light which accounts for 4%~5% of sunlight, which greatly limits the effective utilization of solar energy. Therefore, it is crucial and urgent to tune the bandgap of photocatalysts with broad-spectrum absorption properties to realize the effective utilization of solar energy and promote the conversion of solar energy to hydrogen energy on the road to practical applications.

Strontium titanate ($SrTiO_3$) is a stable and environmentally-friendly photocatalyst. It has been intensively studied for photocatalytic water splitting to produce hydrogen. Nevertheless, the wide bandgap (Eg = 3.2 eV) and high recombination without any modification make it no photocatalytic activity under visible light irradiation. The $SrTiO_3$ photocatalyst could achieve photocatalytic water splitting under visible light irradiation by using surface modification and ion doping techniques [17,18,41–48]. Kudo's group developed numerous effective ion dopants and cocatalysts to modify the $SrTiO_3$ and made great progress in the photocatalytic water splitting reactions [48–56]. Co-doping with Rh ion could significantly enhance the photocatalytic activity of $SrTiO_3$ under visible light irradiation [49,52,57]. Even so, the efficiency of photocatalytic water splitting is still very poor under visible light irradiation.

In this presentation, to further improve the photocatalytic activity of $SrTiO_3$ under visible light irradiation via using morphology modification, the various noble metal ions were doped into $SrTiO_3$ using the $SrCl_2$ flux as a medium. All the as-prepared samples showed a visible-light response implying the successful co-doping of the noble metal ions. The as-prepared samples nanoparticles showed the cubic or tailoring cubic morphology. The photocatalytic sacrificial H_2 and O_2 evolution reactions were examined under visible-light irradiation (λ > 420 nm). The further discussion of the effects of photo-depositing various HECs and OECs on the sacrificial H_2 and O_2 will proceed.

4.2 Experimental section

4.2.1 Preparation of metal ions co-doped $SrTiO_3$ photocatalyst powder

The metal ions were codoped into strontium titanate by a flux method. The raw materials $SrTiO_3$ used for flux treatment were prepared through a conventional solid-state reaction method (SSR). Typically, the raw materials TiO_2 (High purity Chemicals; Rutile, 99.99%), $SrCO_3$ (Wako Pure Chemicals Industries, Ltd, 99.99%) were mixed and calcined at 1373 K for 20 h in alumina crucible under air condition. The as-prepared $SrTiO_3$ sample was fully mixed with Rh_2O_3 powder (Wako Pure Chemicals Industries, Ltd.) and the other noble metal oxides (Ta_2O_5, Sb_2O_3, Nb_2O_3, or La_2O_3) and $SrCl_2$ flux reagent according to the nominally molar ratio of 1: x: y: 10 (x, y represents the molar ratio of the corresponding metal ions in metal oxide and $SrTiO_3$, x/y = 1: 1) in an agate mortar. The molar ratio of $SrTiO_3$ and $SrCl_2$ flux reagent was fixed at 1:10. The fully ground mixtures were calcined at an appropriate temperature (1273 K ~ 1423 K) for 10 h in alumina crucibles in the air. Eventually, the cooled bulk was washed with hot ultrapure water several times to remove the chloride impurities and dried at a high temperature for hours. The as-prepared samples were denoted as $SrTiO_3$ (M_1, M_2)-x (flux) (M_1 and M_2 represent the corresponding metal ions).

4.2.2 Characterization

The absorption spectra of as-prepared samples were acquired by a UV–vis spectrometer (JASCO. V-550DS) equipped with an integrating sphere was applied to obtain. The morphology of as-prepared samples was observed applying the field-emission scanning electron microscopy (SEM, JEOL, JSM 6335F).

4.2.3 Photocatalytic reactions for sacrificial H_2 or O_2 evolution

The photocatalytic reactions were performed in a gas-closed circulation system connected with a top irradiation type photocatalytic reaction cell. The apparatus for the measurement of photocatalytic activity is as shown in Figure 4-1. The as-prepared powder (0.1 g) was dispersed in an aqueous solution containing methanol (10 vol%). The oxygen was produced from an aqueous $AgNO_3$ solution (0.02 mmol h^{-1}). The suspension was illuminated from a 300 W Xenon lamp attached to a cut-off filter (λ > 420 nm) under continuous stirring. The argon gas was used as the carrier gas and brought into the system after degasification makes the system under a background of 10 kPa. Before the photocatalytic reaction, the Pt cocatalyst was deposited on the photocatalyst from an appropriate amount of $H_2PtCl_6 \cdot 6H_2O$ solution ($Na_3[IrCl_6]$ for oxygen evolution) as precursor under full arc irradiation for 30 minutes. The amount of produced H_2 or O_2 was estimated by gas chromatography (Shimadzu GC-8A).

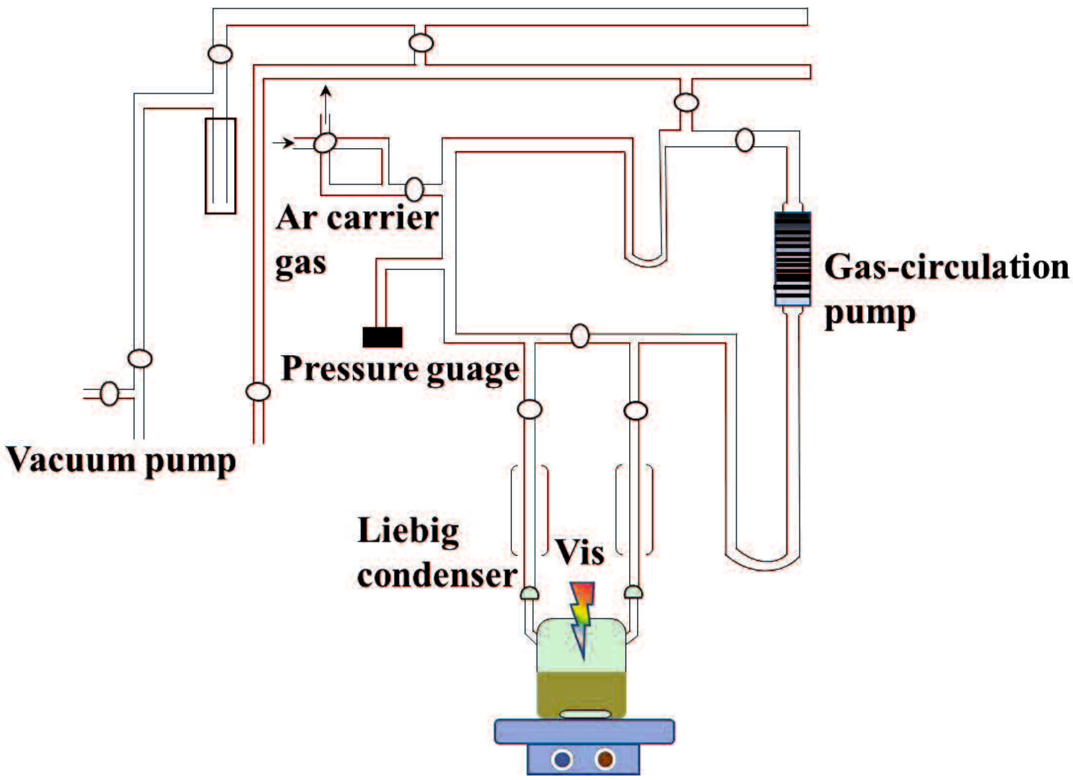

Figure 4-1. Apparatus for photocatalytic reactions.

4.3 Results and discussion

4.3.1 Characterization of photocatalysts

Figure 4-2 shows the SEM images of various noble metal ions co-doped $SrTiO_3$ prepared by the SSR method. In our previous report, the pure $SrTiO_3$ prepared by the SSR method showed irregular particles aggregated nanoparticle morphology [31]. After using $SrCl_2$ treatment, the sample showed rough cubic particles as well as doping a small amount of Al ion. The $SrTiO_3$ using only flux treatment only responded to the UV light. and the size of the particles was very large. The $SrTiO_3$ with $SrCl_2$ flux regent mixed with a small number of noble metal ions showed cubic and tailoring cubic morphology. This morphology was conducive to the separation of reduction surfaces and oxidation surface and then enhanced the photocatalytic activity by selectively depositing oxygen evolution cocatalyst and hydrogen evolution cocatalysts. However, for the (Ce, Rh)-$SrTiO_3$ (flux), there was a spot of large cubic particles, which were a disadvantage of the separation of electrons and holes. Therefore, the H_2 evolution rate was very low. For the (La, Mn, Rh)-SrTiO3, though the sample showed perfect morphology for selectively loading the suitable cocatalysts, too many dopants forming the defects which were as the recombination centers also decreasing the photocatalytic activity.

Figure 4-3 shows the absorbance spectra of various noble metal ions co-doped $SrTiO_3$ photocatalyst. The pure $SrTiO_3$ only responded to UV absorption and the maximum absorption band edge at around 380 nm. After using $SrCl_2$ reagents mixed with a small number of noble metal ions, the absorption was extended to the visible light area. The absorption band edges were around 600 nm, suggesting the successful doping of the noble metal ions during the flux treatment.

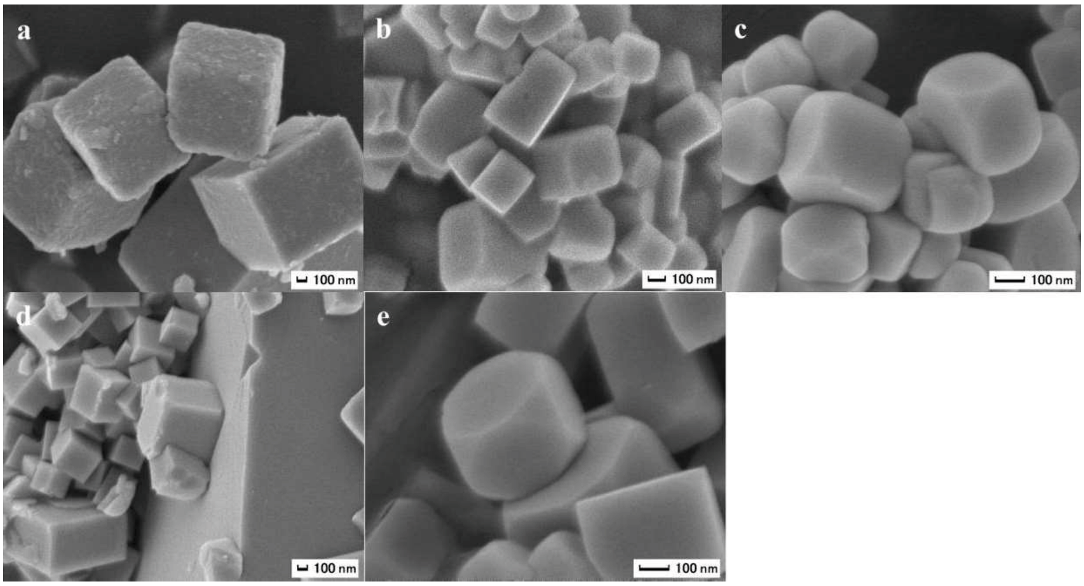

Figure 4-2. SEM images of various noble mental co-doped $SrTiO_3$ prepared by the flux method. (a) $SrTiO_3$ (flux), (b) $SrTiO_3$-(La, Rh)-0.02 (flux), (c) $SrTiO_3$(Ta, Rh)- 0.02 (flux), (d) $SrTiO_3$(Ce, Rh)-0.02 (flux), and (e) $SrTiO_3$ (La, Mn, Rh)-0.02 (flux)

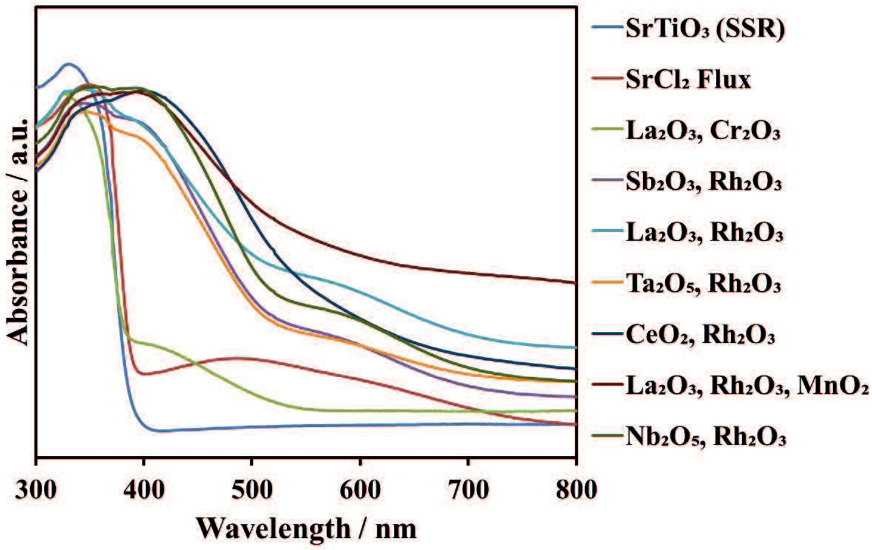

Figure 4-3. Absorbance spectra of various noble mental co-doped $SrTiO_3$ (M_1, M_2)-0.02 prepared by the flux method.

4.3.2 Photocatalytic activity of sacrificial of H_2 or O_2 evolution

Figure 4-4 shows the time courses and activity of photocatalytic H_2 evolution from 10 vol% aqueous methanol solution over Pt (0.1 wt%)/$SrTiO_3$(M_1, M_2)-0.02 (flux) as a function of various noble metal ions co-doped $SrTiO_3$ prepared by the flux method. The results showed that all the samples could split water to produce hydrogen from an aqueous methanol solution under visible light irradiation. The sample using strontium chloride flux mixed with tantalum (five-plus) oxide or lanthanum oxide and rhodium oxide treatment showed a better hydrogen evolution rate for hydrogen evolution reaction. The (Ta, Rh)-codoped $SrTiO_3$ photocatalyst achieved a hydrogen evolution rate of 25.6 μmol h^{-1} in these results under visible light irradiation as shown in Figure 4-2(b).

Figure 4-5 shows time courses activity of photocatalytic O_2 evolution from aqueous $AgNO_3$ (0.02 mol h^{-1}) solution over IrO_2 (1 wt%)/$SrTiO_3$(M_1, M_2)-0.02 (flux) as a function of various noble metal ions co-doped $SrTiO_3$. The (Ta, Rh)-codoped $SrTiO_3$ (flux) photocatalyst achieved a relatively high O_2 evolution rate of 5.64 μmol h^{-1} in the first two hours, and then the activity decreased to 2.21 μmol h^{-1} amount the samples under visible light irradiation as shown in Figure 4-3(b).

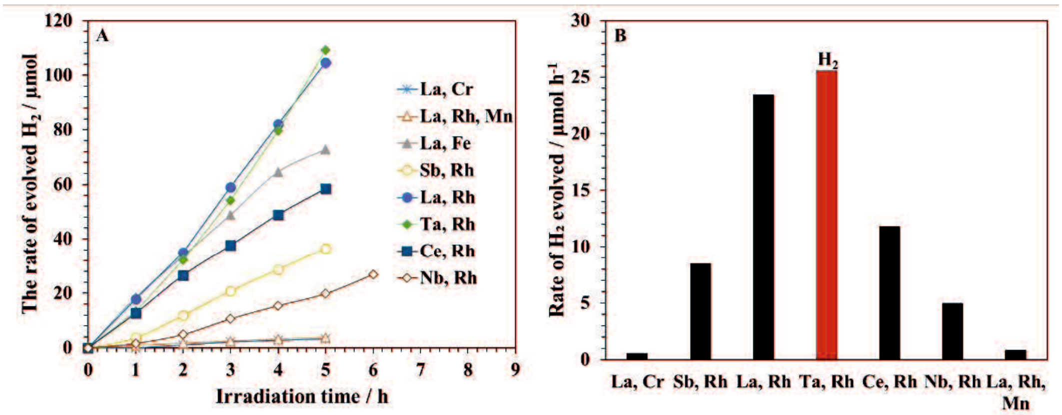

Figure 4-4. (a) Time courses and (b) activity of photocatalytic H_2 evolution from 10 vol% aqueous methanol solution over Pt (0.1 wt%)/$SrTiO_3(M_1, M_2)$-0.02 (flux) as a function of various noble metal ions co-doped $SrTiO_3$. The molar ration of metal ion and $SrTiO_3$, 1:0.02:10; Preparation temperature, 1373 K. Reaction condition: photocatalyst, 0.1 g; co-catalyst, 0.1 wt% Pt (photodeposition method); reaction solution, 100 mL; sacrificial regent, CH_3OH (10 vol%); photocatalytic raction cell, top-type irradiation cell; light source, 300 W Xenon lamp (20 A).

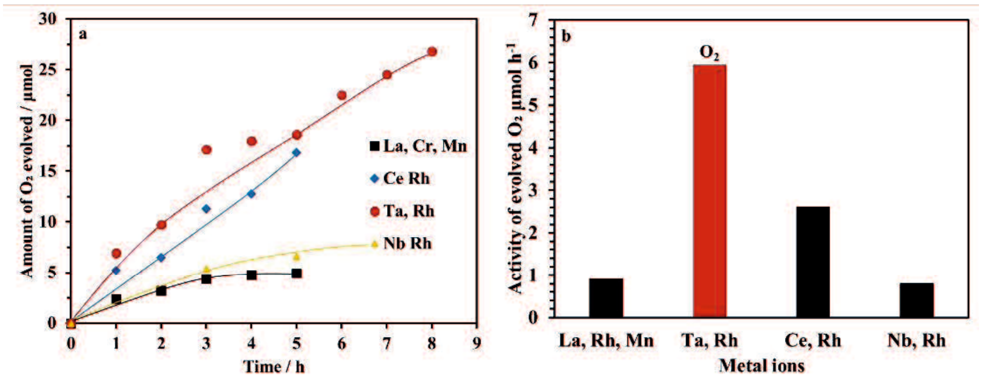

Figure 4-5. (a) Time courses and (b) activity of photocatalytic O_2 evolution from aqueous $AgNO_3$ (0.02 mol h^{-1}) solution over IrO_2 (1 wt%)/$SrTiO_3(M_1, M_2)$-0.02 (flux) as a function of various noble metal ions co-doped $SrTiO_3$. The molar ration of metal ion/$SrTiO_3$, 1:0.02:10; Preparation temperature, 1373 K. Reaction condition: photocatalyst, 0.1 g; co-catalyst, 0.1 wt% IrO_2 (photo-deposition method); reaction solution, 100 mL; sacrificial regent, $AgNO_3$ (0.02 mol h^{-1}); photocatalytic reaction cell, top-type irradiation cell; light source, 300 W Xenon lamp (20 A, $\lambda > 420$ nm);

4.3.3 Effect of the amount of Pt co-catalyst on the H_2 evolution activity

Figure 4-6 shows the photocatalytic activity of sacrificial H_2 evolution activity over Pt/$SrTiO_3$(Ta, Rh)-0.02 from aqueous methanol solution as a function of the amount of loaded Pt nanoparticles. As seen in Figure 4-4, the preferable amount of loaded Pt nanoparticles by the photo-deposition method was 0.3 wt%. The Pt (0.3 wt%)/$SrTiO_3$(Ta, Rh)-0.02 photocatalyst achieved an H_2 evolution activity of 168.98 μ mol h^{-1} from the aqueous methanol solution.

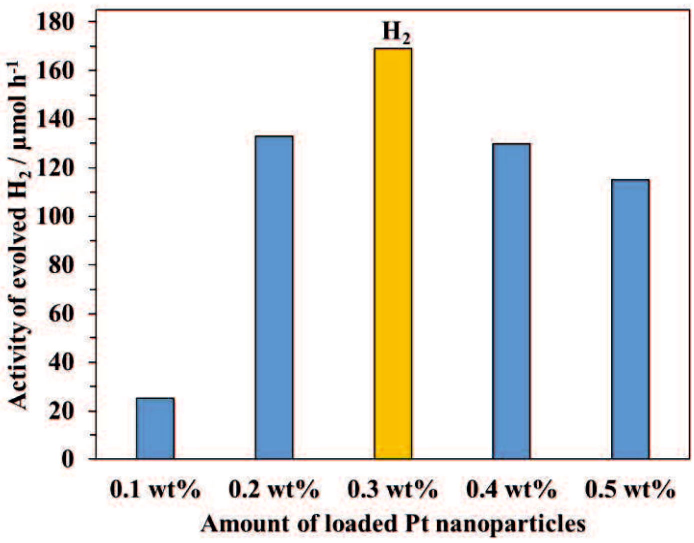

c

Figure 4-6. Photocatalytic activity of sacrificial H_2 evolution from aqueous methanol solution over Pt/$SrTiO_3$(Ta, Rh)-0.02 as a function of the amount of loaded Pt nanoparticles.

Reaction condition: photocatalyst, 0.1 g; co-catalyst, Pt (photo-deposition method); reaction solution, 100 mL; sacrificial regent, $AgNO_3$ (0.02 mol h^{-1}); photocatalytic reaction cell, top-type irradiation cell; light source, 300 W Xenon lamp (20 A, $\lambda > 420$ nm);

Figure 4-7 shows the photocatalytic activity of sacrificial O_2 evolution from aqueous $AgNO_3$ solution IrO_2/$SrTiO_3$(Ta, Rh)-0.02 as a function of the amount of loaded Pt nanoparticles. As seen in Figure 4-5, the preferable amount of loaded IrO_2 nanoparticles by the photo-deposition method was 1 wt%. The IrO_2 (1 wt%)/$SrTiO_3$(Ta, Rh)-0.02 photocatalyst achieved an O_2 evolution activity of 5.64 μ mol h^{-1} from the aqueous methanol solution.

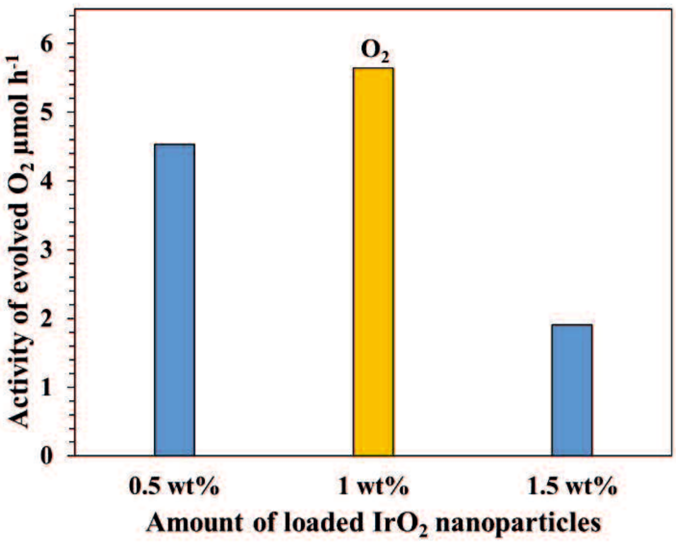

Figure 4-7. Photocatalytic activity of sacrificial O_2 evolution from aqueous $AgNO_3$ solution IrO_2/$SrTiO_3$(Ta, Rh)-0.02 as a function of the amount of loaded Pt nanoparticles.

Reaction condition: photocatalyst, 0.1 g; co-catalyst, IrO_2 (photo-deposition method); reaction solution, 100 mL; sacrificial regent, $AgNO_3$ (0.02 mol h^{-1}); photocatalytic reaction cell, top-type irradiation cell; light source, 300 W Xenon lamp (20 A, $\lambda > 420$ nm);

Figure 4-8 shows the photocatalytic activity of sacrificial O_2 evolution from aqueous $AgNO_3$ solution Pt (0.3 wt%)/$SrTiO_3$(Ta, Rh) as a function of the amount of co-doped Ta and La metal ions. As shown in Figure 4-6, the preferable amount of co-doped Ta and Rh was smaller than 0.02. The maximum photocatalytic activity for sacrificial H_2 evolution achieved over the Pt (0.3 wt%)/$SrTiO_3$(Ta, Rh)-0.06 was 192. 63 μmol h^{-1}.

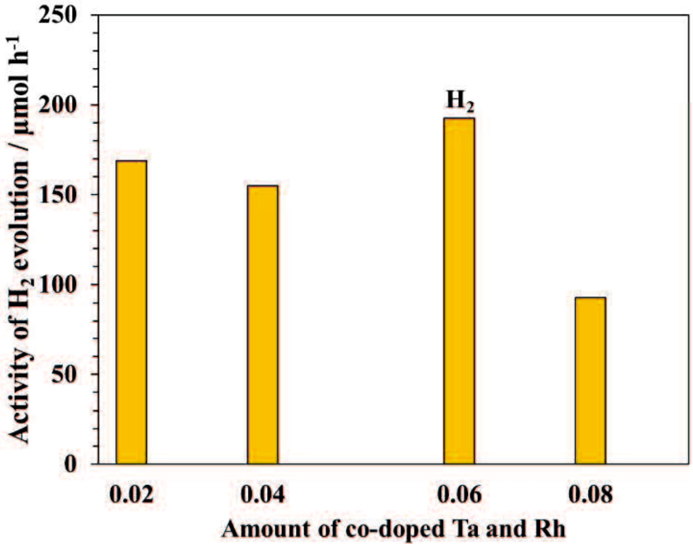

Figure 4-8. Photocatalytic activity of sacrificial O_2 evolution from aqueous $AgNO_3$ solution Pt (0.3 wt%)/$SrTiO_3$(Ta, Rh) as a function of the amount of co-doped Ta and La metal ions.

Reaction condition: photocatalyst, 0.1 g; co-catalyst, Pt (photo-deposition method, 0.3 wt%); reaction solution, 100 mL; sacrificial regent, $AgNO_3$ (0.02 mol h^{-1}); photocatalytic reaction cell, top-type irradiation cell; light source, 300 W Xenon lamp (20 A, $\lambda > 420$ nm);

4.4 Conclusions

Various metal ions co-doped into strontium titanate with cubic nanoparticles were successfully synthesized using the flux method with $SrCl_2$ flux reagents mixed with the corresponding metal oxide. The photocatalyst using flux mixed with metal oxide could respond to visible light up to 600 nm. The photocatalyst $SrTiO_3$(Ta, Rh)-0.02 (flux) using flux treatment modified with 0.3 wt% Pt nanoparticles showed relatively high activity for sacrificial H_2 evolution (168. 98 μmol h^{-1}) from sacrificial aqueous methanol solution, while that modified with 1 wt% IrO_2 nanoparticle achieved an activity of 5.65 mol h^{-1} for O_2 evolution from an aqueous $AgNO_3$ solution under visible light irradiation ($\lambda \geq 420$ nm), respectively, in this presentation.

4.5 References

[1] I.G. Umar, A.A. Halim, Heterogeneous photocatalytic degradation of organic contaminants over titanium dioxide: A review of fundamentals, progress and problems, J. Photochem. Photobiol. C Photochem. Rev. 9 (2007) 1–12.

[2] D. Zhu, Q. Zhou, Action and mechanism of semiconductor photocatalysis on degradation of organic pollutants in water treatment: A review, Environ. Nanotechnology, Monit. Manag. 12 (2019) 100255.

[3] P.A.K. Reddy, P.V.L. Reddy, E. Kwon, K.H. Kim, T. Akter, S. Kalagara, Recent advances in photocatalytic treatment of pollutants in aqueous media, Environ. Int. 91 (2016) 94–103.

[4] M.R.D. Khaki, M.S. Shafeeyan, A.A.A. Raman, W.M.A.W. Daud, Application of doped photocatalysts for organic pollutant degradation - A review, J. Environ. Manage. 198 (2017) 78–94.

[5] Y. Zhang, Y.J. Heo, J.W. Lee, J.H. Lee, J. Bajgai, K.J. Lee, S.J. Park, Photocatalytic hydrogen evolution via water splitting: A short review, Catalysts. 8 (2018) 655.

[6] A. Fujishima, K. Honda, Electrochemical photolysis of water at a semiconductor electrode, Nature 238 (1972) 37–38.

[7] A.A. Ismail, D.W. Bahnemann, Photochemical splitting of water for hydrogen production by photocatalysis: A review, Sol. Energy Mater. Sol. Cells 128 (2014) 85–101.

[8] X. Li, J. Yu, S. Wageh, A.A. Al-Ghamdi, J. Xie, Graphene in photocatalysis: A review, Small 12 (2016) 6640–6696.

[9] A. Kudo, Y. Miseki, Heterogeneous photocatalyst materials for water splitting, Chem. Soc. Rev. 38 (2009) 253–278.

[10] A.J. Bard, Photoelectrochemistry and heterogeneous photo-catalysis at semiconductors, J. Photochem. 10 (1979) 59–75.

[11] J. Low, C. Jiang, B. Cheng, S. Wageh, A.A. Al-Ghamdi, J. Yu, A Review of direct Z-scheme photocatalysts, Small Methods 1 (2017) 1700080.

[12] X. Chen, S. Shen, L. Guo, S.S. Mao, Semiconductor-based photocatalytic

hydrogen generation, Chem. Rev. 110 (2010) 6503–6570.

[13] Y. Goto, T. Hisatomi, Q. Wang, T. Higashi, K. Ishikiriyama, T. Maeda, Y. Sakata, S. Okunaka, H. Tokudome, M. Katayama, S. Akiyama, H. Nishiyama, Y. Inoue, T. Takewaki, T. Setoyama, T. Minegishi, T. Takata, T. Yamada, K. Domen, A particulate photocatalyst water-splitting panel for large-scale solar hydrogen generation, Joule 2 (2018) 509–520.

[14] J. Qi, W. Zhang, R. Cao, Solar-to-hydrogen energy conversion based on water splitting, Adv. Energy Mater. 8 (2018) 1–16.

[15] S. Wang, Y. Wang, S. Zang, X.W. (David) Lou, Hierarchical hollow heterostructures for photocatalytic CO_2 reduction and water splitting, Small Methods 4 (2020) 1900586.

[16] X. Liu, A. Jin, Y. Jia, J. Jiang, N. Hu, X. Chen, Facile synthesis and enhanced visible-light photocatalytic activity of graphitic carbon nitride decorated with ultrafine Fe_2O_3 nanoparticles, RSC Adv. 5 (2015) 92033–92041.

[17] X. Liu, J. Jiang, Y. Jia, J. Qiu, T. Xia, Y. Zhang, Y. Li, X. Chen, Insight into synergistically enhanced adsorption and visible light photocatalytic performance of Z-scheme heterojunction of $SrTiO_3$(La,Cr)-decorated WO_3 nanosheets, Appl. Surf. Sci. 412 (2017) 279–289.

[18] J. Jiang, Y. Jia, Y. Wang, R. Chong, L. Xu, X. Liu, Insight into efficient photocatalytic elimination of tetracycline over $SrTiO_3$(La,Cr)under visible-light irradiation: The relationship of doping and performance, Appl. Surf. Sci. 486 (2019) 93–101.

[19] X. Liu, Y. Zhang, Y. Jia, J. Jiang, Y. Wang, X. Chen, T. Gui, Visible light-responsive carbon-decorated p-type semiconductor $CaFe_2O_4$ nanorod photocatalyst for efficient remediation of organic pollutants,, Chinese J. Catal. 38 (2017) 1770–1779.

[20] G. Huang, Z. Xiao, W. Zhen, Y. Fan, C. Zeng, C. Li, S. Liu, P.K. Wong, Hydrogen production from natural organic matter via cascading oxic-anoxic photocatalytic processes: An energy recovering water purification technology, Water Res. 175 (2020) 115684.

[21] D. Chen, Y. Cheng, N. Zhou, P. Chen, Y. Wang, K. Li, S. Huo, P. Cheng, P.

Peng, R. Zhang, L. Wang, H. Liu, Y. Liu, R. Ruan, Photocatalytic degradation of organic pollutants using TiO_2-based photocatalysts: A review, J. Clean. Prod. 268 (2020) 121725.

[22] Y. Boyjoo, H. Sun, J. Liu, V.K. Pareek, S. Wang, A review on photocatalysis for air treatment: From catalyst development to reactor design, Chem. Eng. J. 310 (2017) 537–559.

[23] H. Park, Y. Park, W. Kim, W. Choi, Surface modification of TiO_2 photocatalyst for environmental applications, J. Photochem. Photobiol. C Photochem. Rev. 15 (2013) 1–20.

[24] C. Peng, G. Reid, H. Wang, P. Hu, Perspective: Photocatalytic reduction of CO_2 to solar fuels over semiconductors, J. Chem. Phys. 147 (2017) 030901.

[25] J. Hong, W. Zhang, J. Ren, R. Xu, Photocatalytic reduction of CO_2: a brief review on product analysis and systematic methods, Anal. Methods 5 (2013) 1086.

[26] S. Chen, T. Takata, K. Domen, Particulate photocatalysts for overall water splitting, Nat. Rev. Mater. 2 (2017) 1–17.

[27] J. Low, J. Yu, M. Jaroniec, S. Wageh, A.A. Al-Ghamdi, Heterojunction photocatalysts, Adv. Mater. 29 (2017) 1601694.

[28] Y. Hiramachi, H. Fujimori, A. Yamakata, Y. Sakata, Achievement of high photocatalytic performance to $BaTi_4O_9$ toward overall H_2O splitting, ChemCatChem 11 (2019) 6213–6217.

[29] H. Lyu, T. Hisatomi, Y. Goto, M. Yoshida, T. Higashi, M. Katayama, T. Takata, T. Minegishi, H. Nishiyama, T. Yamada, Y. Sakata, K. Asakura, K. Domen, An Al-doped $SrTiO_3$ photocatalyst maintaining sunlight-driven overall water splitting activity for over 1000 h of constant illumination, Chem. Sci. 10 (2019) 3196–3201.

[30] T. Takata, J. Jiang, Y. Sakata, M. Nakabayashi, N. Shibata, V. Nandal, K. Seki, T. Hisatomi, K. Domen, Photocatalytic water splitting with a quantum efficiency of almost unity, Nature 581 (2020) 411–414.

[31] J. Jiang, K. Kato, H. Fujimori, A. Yamakata, Y. Sakata, Investigation on the highly active $SrTiO_3$ photocatalyst toward overall H_2O splitting by doping Na ion,

J. Catal. 390 (2020) 81–89.

[32] H. Kato, K. Asakura, A. Kudo, Highly efficient water splitting into H_2 and O_2 over lanthanum-doped $NaTaO_3$ photocatalysts with high crystallinity and surface nanostructure, J. Am. Chem. Soc. 125 (2003) 3082–3089.

[33] K. Maeda, T. Takata, M. Hara, N. Saito, Y. Inoue, H. Kobayashi, K. Domen, GaN:ZnO solid solution as a photocatalyst for visible-light-driven overall water splitting, J. Am. Chem. Soc. 127 (2005) 8286–8287.

[34] K. Maeda, K. Teramura, N. Saito, Y. Inoue, K. Domen, Improvement of photocatalytic activity of $(Ga_{1-x}Zn_x)(N_{1-x}O_x)$ solid solution for overall water splitting by co-loading Cr and another transition metal, J. Catal. 243 (2006) 303–308.

[35] K. Maeda, K. Teramura, H. Masuda, T. Takata, N. Saito, Y. Inoue, K. Domen, Efficient overall water splitting under visible-light irradiation on $(Ga_{1-x}Zn_x)(N_{1-x}O_x)$ dispersed with Rh-Cr mixed-oxide nanoparticles: Effect of reaction conditions on photocatalytic, J. Phys. Chem. B 110 (2006) 13107–13112.

[36] T. Takata, K. Domen, Defect engineering of photocatalysts by doping of aliovalent metal cations for efficient water splitting, J. Phys. Chem. C 113 (2009) 19386–19388.

[37] K. Maeda, K. Domen, Photocatalytic water splitting: Recent progress and future challenges, J. Phys. Chem. Lett. 1 (2010) 2655–2661.

[38] Y. Sakata, T. Hayashi, R. Yasunaga, N. Yanaga, H. Imamura, Remarkably high apparent quantum yield of the overall photocatalytic H_2O splitting achieved by utilizing Zn ion added Ga_2O_3 prepared using dilute $CaCl_2$ solution, Chem. Commun. 51 (2015) 12935–12938.

[39] Y. Ham, T. Hisatomi, Y. Goto, Y. Moriya, Y. Sakata, A. Yamakata, J. Kubota, K. Domen, Flux-mediated doping of $SrTiO_3$ photocatalysts for efficient overall water splitting, J. Mater. Chem. A 4 (2016) 3027–3033.

[40] T. Takata, K. Domen, Particulate photocatalysts for water splitting: Recent advances and future prospects, ACS Energy Lett. 4 (2019) 542–549.

[41] B. Ullah, W. Lei, X.Q. Song, X.H. Wang, W.Z. Lu, Crystal structure, defect chemistry and radio frequency relaxor characteristics of Ce-doped $SrTiO_3$

perovskite, J. Alloys Compd. 728 (2017) 623–630.

[42] M. Yang, X. Jin, Visible light-induced Cr-doped $SrTiO_3$-g-C_3N_4composite for improved photocatalytic performance, J. Wuhan Univ. Technol. Mater. Sci. Ed. 29 (2014) 1111–1116.

[43] H. Yu, J. Wang, S. Yan, T. Yu, Z. Zou, Elements doping to expand the light response of $SrTiO_3$, J. Photochem. Photobiol. A Chem. 275 (2014) 65–71.

[44] S. Fuentes, P. Muñoz, N. Barraza, E. Chávez-Ángel, C.M. Sotomayor Torres, Structural characterization of slightly Fe-doped $SrTiO_3$ grown via a sol–gel hydrothermal synthesis, J. Sol-Gel Sci. Technol. 75 (2015) 593–601.

[45] S. Tonda, S. Kumar, O. Anjaneyulu, V. Shanker, Synthesis of Cr and La-codoped $SrTiO_3$ nanoparticles for enhanced photocatalytic performance under sunlight irradiation, Phys. Chem. Chem. Phys. 16 (2014) 23819–23828.

[46] Y. Yamaguchi, S. Usuki, K. Yamatoya, N. Suzuki, K.I. Katsumata, C. Terashima, A. Fujishima, A. Kudo, K. Nakata, Efficient photocatalytic degradation of gaseous acetaldehyde over ground Rh-Sb co-doped $SrTiO_3$ under visible light irradiation, RSC Adv. 8 (2018) 5331–5337.

[47] D. Wang, J. Ye, T. Kako, T. Kimura, Photophysical and photocatalytic properties of $SrTiO_3$ doped with Cr cations on different sites, J. Phys. Chem. B 2006,. 110 (2010) 15824–15830.

[48] S. Suzuki, A. Iwase, A. Kudo, Long wavelength visible light-responsive $SrTiO_3$ photocatalysts doped with valence-controlled Ru for sacrificial H_2 and O_2 evolution, Catal. Sci. Technol. 10 (2020) 4912–4916.

[49] D.H.K. Murthy, H. Matsuzaki, Q. Wang, Y. Suzuki, K. Seki, T. Hisatomi, T. Yamada, A. Kudo, K. Domen, A. Furube, Revealing the role of the Rh valence state, La doping level and Ru cocatalyst in determining the H_2 evolution efficiency in doped $SrTiO_3$ photocatalysts, Sustain. Energy Fuels 3 (2019) 208–218.

[50] A. Kudo, S. Yoshino, T. Tsuchiya, Y. Udagawa, Y. Takahashi, M. Yamaguchi, I. Ogasawara, H. Matsumoto, A. Iwase, Z-scheme photocatalyst systems employing Rh- and Ir-doped metal oxide materials for water splitting under visible light irradiation, Faraday Discuss 215 (2019) 313–328.

[51] S. Suzuki, H. Matsumoto, A. Iwase, A. Kudo, Enhanced H_2 evolution over an Ir-doped $SrTiO_3$ photocatalyst by loading of an Ir cocatalyst using visible light up to 800 nm, Chem. Commun. 54 (2018) 10606–10609.

[52] R. Asai, H. Nemoto, Q. Jia, K. Saito, A. Iwase, A. Kudo, A visible light responsive rhodium and antimony-codoped $SrTiO_3$ powdered photocatalyst loaded with an IrO_2 cocatalyst for solar water splitting, Chem. Commun. 50 (2014) 2543–2546.

[53] H. Kato, Y. Sasaki, N. Shirakura, A. Kudo, Synthesis of highly active rhodium-doped $SrTiO_3$ powders in Z-scheme systems for visible-light-driven photocatalytic overall water splitting, J. Mater. Chem. A 1 (2013) 12327–12333.

[54] K. Iwashina, A. Kudo, Rh-doped $SrTiO_3$ photocatalyst electrode showing cathodic photocurrent for water splitting under visible-light irradiation, J. Am. Chem. Soc. 133 (2011) 13272–13275.

[55] R. Niishiro, H. Kato, A. Kudo, Nickel and either tantalum or niobium-codoped TiO_2 and $SrTiO_3$ photocatalysts with visible-light response for H_2 or O_2 evolution from aqueous solutions, Phys. Chem. Chem. Phys. 7 (2005) 2241–2245.

[56] T. Ishii, H. Kato, A. Kudo, H_2 evolution from an aqueous methanol solution on $SrTiO_3$ photocatalysts codoped with chromium and tantalum ions under visible light irradiation, J. Photochem. Photobiol. A Chem. 163 (2004) 181–186.

[57] R. Niishiro, S. Tanaka, A. Kudo, Hydrothermal-synthesized $SrTiO_3$ photocatalyst codoped with rhodium and antimony with visible-light response for sacrificial H_2 and O_2 evolution and application to overall water splitting, Appl. Catal. B Environ. 150–151 (2014) 187–196.

Chapter 5 Summary and Outlook

5.1 Summary

In this presentation, the investigations on the development of highly active $SrTiO_3$ photocatalyst for overall H_2O splitting were carried out. Various modification methods were combined to increase the photocatalytic overall H_2O splitting efficiency of $SrTiO_3$ photocatalyst the upper limitation under visible light irradiation. Following, the photocatalytic property of flux-mediated noble metal ions doping of $SrTiO_3$ was studied under visible light irradiation to further enhance the solar-to-hydrogen evolution conversation efficiency. The results are summarized in each chapter as follows.

In chapter 2, the photocatalytic performances of Na-$SrTiO_3$ prepared by the polymerizable complex (PC) method and solid-state reaction (SSR) method were investigated. The purity of starting TiO_2 material for preparing Na-$SrTiO_3$ photocatalyst is also affecting the photocatalytic activity. The optimal $Rh_{0.7}Cr_{1.3}O_3$/Na-$SrTiO_3$/CoO_x photocatalyst achieved an AQY of 30% at 365 nm and this photocatalyst remained stable activity for about 50 hours during photocatalytic overall H_2O splitting reaction. The distortion of the crystal lattice and production of oxygen vacancies in the lattice by Na-doping were the crucial effects on the improvement of $SrTiO_3$ photocatalyst by XRD, Raman spectroscopy, transient absorption spectra. The dependence of H_2O splitting activity on low light intensity confirmed the doped Na acted as hole traps and increase the separation of photogenerated charge carriers.

In chapter 3, Mg ion was doped in the $SrTiO_3$ by the PC, SSR, and the $SrCl_2$ flux treatment. Mg-$SrTiO_3$ photocatalyst by the $SrCl_2$ flux reagent mixed with a small amount of MgO powder treatment showed the highest photocatalytic activity. The photocatalytic properties of the $SrCl_2$ flux-mediated doping of various metal ions (Al, Ga, In, and La) into $SrTiO_3$ were also performed. Among the dopants, Mg, Ga, Al ions were relatively effective dopants that were introduced into $SrTiO_3$ using $SrCl_2$ flux mixed with a small number of corresponding powder treatment modifying with $Rh_yCr_{2-y}O_3$ cocatalyst for the improvement of the photocatalytic property of $SrTiO_3$. The $Rh_{2-y}Cr_yO_3$-loaded Mg-$SrTiO_3$ (flux) sample achieved an AQY value of 53% ± 2% under irradiation of monochromatic light at 365 nm. The various deposition methods of redox co-catalysts were carried out. The optical Mg-$SrTiO_3$ (flux) photocatalyst prepared by the flux method modifying with Rh/Cr_2O_3/CoOOH redox co-catalysts via the in-site photo-deposition method achieved the photocatalytic H_2O splitting quantum efficiency to the upper limitation under UV irradiation. The detailed structure study implied Mg was doped into the $SrTiO_3$ crystal lattice and the as-prepared Mg-$SrTiO_3$ sample by the flux method showed cubic and tailoring cubic morphologies. The absence of an Al signal in the EDS spectrum and elemental mapping images indicated negligible Al-doing. The Rh, Cr, and Co species were selectively deposited on the different surfaces of Mg-$SrTiO_3$ (flux) cubic nanoparticles observed from the TEM-EDS mapping images.

In chapter 4, various noble metal ions co-doped $SrTiO_3$ was prepared using the $SrCl_2$ flux mixed with a small number of corresponding metal oxide powder. The photocatalytic property of flux-mediated various noble metal ions co-doped $SrTiO_3$ photocatalyst for sacrificial H_2 (O_2) evolution from aqueous methanol ($AgNO_3$) solution was performed under visible light ($\lambda > 420$ nm). All the as-prepared samples showed a visible-light response implying the successful co-doping of the noble metal ions. The Pt metal and IrO_2 was photo-deposited onto the photocatalyst used as hydrogen evolution cocatalyst and oxygen evolution cocatalysts during H_2O splitting reaction. The Rh and Ta co-doped $SrTiO_3$ shows the highest sacrificial H_2 evolution and O_2 during evolution among the other samples under the same preparation and reaction conditions. The as-prepared samples nanoparticles showed the cubic and tailoring cubic morphologies. The further discussion of the effects of photo-depositing various HECs and OECs on the sacrificial H_2 and O_2 will proceed.

5.2 Recent prospects and future challenges

Solar-driven artificial photosynthesis to split H_2O into H_2 and O_2 is an ideal method to realize the conversion of solar energy to clean and renewable hydrogen energy, and it is also one of the ways to solve the problem of the energy crisis.

At present, the most widely reported materials capable of H_2O splitting are mainly wide bandgap semiconductors loaded with cocatalysts and most of them only responded to UV irradiation. Even though, we have accomplished photocatalytic H_2O splitting with the ultimate quantum efficiency under UV irradiation. The solar-to-hydrogen conversation was still very low and could not satisfy the application in practical production.

The process of photocatalytic overall H_2O splitting is complex multi-electron and multi-step reactions. The requirements for photocatalytic materials are very high. The photocatalyst must have a suitable energy level structure to absorb enough visible light and stable hydrogen and oxygen production active sites. The photogenerated charge carriers must be effectively separated and transferred to the redox-active sites. Therefore, the improvement of a new novel efficient, stable, and low-cost photocatalyst responding to visible light still exists great challenges.

List of publications

[Chapter 2]

1. **Junzhe Jiang**, Kosaku Kato, Hirotaka Fujimori, Akira Yamakata, Yoshihisa Sakata, Investigation on the highly active $SrTiO_3$ photocatalyst toward overall H_2O splitting by doping Na ion, Journal of Catalysis 390 (2020) 81-89.
2. Kosaku Kato, **Junzhe Jiang**, Yoshihisa Sakata, Akira Yamakata, Effect of Na-Doping on Electron Decay Kinetics in $SrTiO_3$ Photocatalyst, ChemCatChem 11 (2019) 6349–6354.

[Chapter 3]

3. Tsuyoshi Takata, Junzhe Jiang, Yoshihisa Sakata, Mamiko Nakabayashi, Naoya Shibata, Vikas Nandal, Kazuhiko Seki, Takashi Hisatomi & Kazunari Domen, Photocatalytic water splitting with a quantum efficiency of almost unity, Nature, 581 (2020) 411-414.
4. **Junzhe Jiang**, Yoshihisa Sakata, ,Akira, Yamakata, , et al. Controllable modification of Mg-$SrTiO_3$ for overall H_2O splitting to almost the ultimate quantum efficiency

[Others]

5. 高田 剛, **姜 君哲**, 酒多喜久, 中林麻美子, 柴田直哉, Nandal Vikas, 関 和彦, 久富隆史, 堂免一成, 量子収率約 100％で水を分解する微粒子光触媒, 61 （2020） 2-4。

[Not included in this thesis]

6. Junzhe Jiang, Yushuai Jiaa, Yabin Wang, Ruifeng Chong, Liping Xu, Xin Liu, Insight into efficient photocatalytic elimination of tetracycline over $SrTiO_3$(La,Cr) under visible- light irradiation: The relationship of doping and performance, Applied Surface Science 486 (2019) 93–101.
7. Xin Liu, Junzhe Jiang, Yushuai Jia, Jinmin Qiu, Tonglin Xia, Yuhong Zhang, Yuqin Li, Xiangshu Chen, Insight into synergistically enhanced adsorption and visible-light photocatalytic performance of Z-scheme heterojunction of $SrTiO_3$(La,Cr)-decorated WO_3 nanosheets, Applied Surface Science 412 (2017) 279–289.
8. Xin Liu, Junzhe Jiang, Yushuai Jia, Ailing Jin, Xiangshu Chen, Fei Zhang, Hongxian Han, p-Type $CaFe_2O_4$ semiconductor nanorods controllably synthesized by molten salt method, Journal of Energy Chemistry 25 (2016) 381–386.
9. Xin Liu, Ailing Jin, Yushuai Jia, Junzhe Jiang, Na Hu, Xiangshu Chen, Facile synthesis and enhanced visible-light photocatalytic activity of graphitic carbon nitride decorated with ultrafine Fe_2O_3 nanoparticles, RSC Advance 5 (2015) 92033–92041.
10. Ailing Jin, Yushuai Jia, Changfeng Chen, Xin Liu, Junzhe Jiang, Xiangshu Chen, Fei Zhang, Efficient photocatalytic hydrogen evolution on band structure tuned polytriazine/heptazine based carbon nitride heterojunctions with ordered needle-like morphology achieved by an in situ molten salt method, The Journal of Physical Chemistry C 121 (2017) 21497−21509.
11. Xin Liu, Yuhong Zhang, Yushuai Jia, Junzhe Jiang, Yabin Wang, Xiangshu Chen, Tian Gui, Visible light-responsive carbon-decorated p-type semiconductor $CaFe_2O_4$ nanorod photocatalyst for efficient remediation of organic pollutants, Chinese Journal of Catalysis 38 (2017) 1770–1779.

Acknowledgment

On the occasion of the completion of this thesis, with deep feelings, I would like to express my sincere respect and cordial appreciation to my supervisor, Professor Yoshihisa Sakata. This article was completed under his careful and patient guidance. I admire Professor Sakata's rigorous academic attitude, broad and profound academic level, demonstrative work style, and tireless teaching spirit, which has also benefited me a lot. In three years of studying for a doctoral degree, Professor Sakata has given me strict, serious, and meticulous guidance on my studies. All the achievements I have achieved include the careful guidance of Professor Sakata.

I am deeply grateful to Professor Akira Yamakata and Doctor Kosaku Kato of Toyota Technological Institute for their support on Transient Absorption Spectroscopy analysis.

I am also grateful to Professor Kazunari Domen and Professor Tsuyoshi Takata of Shinshu University for their help on my research.

Professor Hidetoshi Kita is greatly appreciated for introducing me to study in the laboratory of Yoshihisa Sakata and providing the devices of characterization.

Thank Dr. Yoshida Masaaki for the discussion on research work and life in Japan. At the same time, I would like to thank every member in this research group for their help and support during my three-year studies.

Finally, I would like to sincerely thank my family for their multi-faceted spiritual encouragement and help in life over the years. Thank my husband, Mr. LIU YONGSHENG, for his continuous care, accompany, and support in work and life.

Thanks again to all those who care and help me.